



TU Clausthal  
Clausthal University of Technology

# Coating of gasborne nanoparticles with silica and silica-organic shells in a post-plasma CVD process

Cumulative Dissertation

to be awarded the degree  
*Doctor of Engineering (Dr.-Ing.)*

submitted by  
Patrick Post  
from Emden

approved by the  
Faculty of Mathematics/Computer Science and Mechanical Engineering,  
Clausthal University of Technology

Date of oral examination: 22.02.2019

---

Dean: Prof. Dr.-Ing. Volker Wesling

Chairperson of the Board of Examiners: Prof. Dr.-Ing. Thomas Turek

Supervising tutor: Prof. Dr. rer. nat. Alfred P. Weber

Reviewer: apl. Prof. Dr. rer. nat. Wolfgang Maus-Friedrichs

Reviewer: PD Dr.-Ing. habil. Martin Seipenbusch

---

## Abstract

---

In many applications using nanoparticles, the particles require a defined coating to achieve the desired product properties, such as a reduced photocatalytic activity or a controlled drug delivery. Especially silica shells are interesting, because silica is an inert and stable material. There are multiple methods to produce such core-shell structures, many of which use liquid phase sol-gel processes. However, gas phase processes have many advantages over liquid phase ones, such as a reduced complexity and the possibility of continuous core-shell particle production. There are different methods to apply coatings to nanoparticles in the gas phase. Most of these processes are chemical vapor deposition methods, where a precursor reacts to the desired coating material. The initiation of these reactions can be done in a multitude of ways, but the use of a non-thermal plasma discharge requires no high temperatures, which opens up interesting material combinations. Such a plasma was used here in the form of a dielectric barrier discharge to coat particles with silica-like coatings. The coating took place in the post-discharge environment outside of the plasma itself, which has significant advantages regarding the process stability. The process had two basic modes of operation, defined by the temperature during coating, which was either room temperature or between 100 and 300 °C. The particles were introduced continuously and coated in-flight at atmospheric pressure. Two precursors were used, tetraethyl orthosilicate for the production of inorganic silica shells and hexamethyldisiloxane for silica-organic coatings. The coatings produced in the process were quite homogeneous and the coating thickness could be controlled well. An important factor for a successful coating was found to be the species in the post-discharge environment, primarily defined by the discharge characteristics. The coating thickness could be controlled by the precursor concentration, the residence time in the system, the core particle surface area and the temperature during coating. Some changes in the core particle concentration were observed during the residence time, which seemed primarily related to agglomeration and less to actual losses by deposition on walls. The process was used to produce different combinations of core and shell materials and seemed very flexible in this regard. In fact, no core material was found that could not be coated. The connection between core and shell seemed to be mostly physical, but in the case of titania core particles,

---

evidence for chemical bonds was found. The silica coatings were hydrophilic, while the silica-organic coatings were very hydrophobic. The hydrophobic property was preserved even after outgassing of the samples or tempering. Some applications for the core-shell particles were studied, such as the improvement of the mechanical and thermal stability of metals and the control of the photocatalytic behavior of titania. For the measurement of the mechanical stability, the coating process was combined with a low pressure impactor, where agglomerates were impacted on a TEM sample grid and the size of the resulting fragments was determined. Both the mechanical and the thermal stability were found to be improved even by thin coatings. The photocatalytic activity could either be reduced or improved depending on the process parameters.

---

## Acknowledgments

---

As is the case with basically all projects above a certain size, this thesis would not have been possible without the support of many different people. First and foremost I want to thank Prof. Dr. rer. nat. Alfred P. Weber for the supervision of my PhD thesis and his support in all its phases. This would not have been possible without him. I very much thank apl. Prof. Dr. rer. nat. Wolfgang Maus-Friedrichs and PD Dr.-Ing. habil. Martin Seipenbusch for the review of my thesis. A special thanks also to PD Dr. habil. Jean-Pascal Borra from CNRS in Gif-sur-Yvette (France) for co-supervising the thesis. On one hand, his expertise in aerosol-plasma interaction was especially valuable for realizing the proof of concept of the post-DBD coating process and for the identification/confirmation of the regulation parameters controlling the coating thickness. On the other hand, with his experience and profound knowledge of DBD plasma physics and chemistry, he guided the work along the main route without getting lost in the complexity of the topic. I am grateful for the good cooperation with Lisa Wurlitzer, Dr. rer. nat. Sebastian Dahle and apl. Prof. Dr. rer. nat. Wolfgang Maus-Friedrichs from the Institute of Energy Research and Physical Technology of the Clausthal University of Technology within the DFG project. Furthermore, I thank all my colleagues from the IMVT for their support and the nice work environment. Special mention deserve Peggy Knospe for the support with the sample analysis, Malte Bierwirth for the good cooperation during the work on the fourth paper and Henning Dunemann and the rest of the workshop for building important parts of the experimental setups. I also thank Dr. rer. nat. Nicolas Jidenko from CNRS for his help in characterizing the first DBD reactor and understanding DBDs a bit more. Finally, I want to thank the Deutsche Forschungsgemeinschaft (DFG) for the financial support of the project under grant number WE 2331/18-1 and the Clausthal University of Technology for employing me and giving me the opportunity to write this thesis.

---

# Contents

---

<b>1</b>	<b>Introduction</b>	<b>1</b>
1.1	Overview and objectives . . . . .	1
1.2	State of the art . . . . .	4
1.2.1	Coating of particles in the liquid phase . . . . .	4
1.2.2	Coating of particles in the gas phase (excl. plasma) . . . . .	5
1.2.3	Coating with plasma-assisted processes . . . . .	9
<b>2</b>	<b>Overview of the publications</b>	<b>17</b>
2.1	Publication 1 . . . . .	17
2.2	Publication 2 . . . . .	18
2.3	Publication 3 . . . . .	18
2.4	Publication 4 . . . . .	19
<b>3</b>	<b>Experimental</b>	<b>21</b>
3.1	Overview of the coating process . . . . .	21
3.2	Production of core particles . . . . .	22
3.2.1	Spark discharge generator . . . . .	22
3.2.2	Atomizer . . . . .	24
3.3	DBD reactors . . . . .	25
3.3.1	Cylindrical DBD reactor . . . . .	25
3.3.2	Plate-to-plate DBD reactor . . . . .	27
3.4	Coating precursors . . . . .	29
3.5	Characterization methods . . . . .	30
<b>4</b>	<b>Process control</b>	<b>33</b>
4.1	General considerations . . . . .	33
4.2	Formation of coatings in the post-discharge environment . . . . .	34
4.3	Control of the coating thickness . . . . .	39
4.3.1	By TEOS concentration and aerosol residence time . . . . .	39
4.3.2	By available particle surface area . . . . .	41

---

4.3.3	By post-process temperature . . . . .	43
4.4	Coating thickness homogeneity . . . . .	44
4.5	Losses and agglomeration of particles . . . . .	45
<b>5</b>	<b>Core-shell material combinations</b>	<b>48</b>
5.1	Silica coatings with TEOS . . . . .	48
5.1.1	Metals and metal oxides produced in a SDG . . . . .	48
5.1.2	AEROXIDE P25 titania . . . . .	53
5.1.3	Salts and others . . . . .	55
5.2	Silica-organic coatings with HMDSO . . . . .	57
<b>6</b>	<b>Applications of the coated particles</b>	<b>61</b>
6.1	Improvement of the mechanical stability of metal agglomerates . . . . .	61
6.2	Improvement of the thermal stability of metal agglomerates . . . . .	65
6.3	Photocatalysis effects of coated titania . . . . .	66
<b>7</b>	<b>Summary and outlook</b>	<b>69</b>
	<b>References</b>	<b>72</b>



# CHAPTER 1

---

## Introduction

---

### 1.1 Overview and objectives

The term nanoparticle generally refers to ultrafine particles with a diameter between 1 and 100 nm that are especially interesting because of their properties in the transition regime between molecules and bulk materials. These particles are used in increasingly complex applications, which often entail special requirements for the particle surfaces, for example to improve the contacts between the particles and the matrix in composite materials. This resulted in the development of a multitude of surface modifications, such as the change of specific particle surface groups, hydrophobic polymer coatings or inert silica films. This thesis will focus on so-called core-shell structures, which are combinations of two materials into a new particle, consisting of an inner core particle and an outer shell (coating) around it.

The properties of the resulting structure depend significantly on the shell. A hermetic shell prevents the core particle from participating in chemical reactions, since it is no longer in direct contact with the environment. However, the inner particle might still interact with its surroundings through other ways, such as electromagnetic radiation or magnetic fields. A classic example is the use of titania ( $\text{TiO}_2$ ) nanoparticles in sun screens. These particles are characterized by good UV absorbing properties as well as colorlessness in visible light. However, titania is also a photocatalyst, which can result in the destruction of the organic crème medium [1, 2]. Furthermore, titania has cytotoxic properties and can permeate into the skin [3]. These unwanted properties can be suppressed by a silica ( $\text{SiO}_2$ ) coating on the particles if this coating is complete and hermetically covers all of the particles' surfaces. Complete silica coatings are also used to improve the dispersibility of particles in liquids, e.g. pigments in paints. Here, the change of the surface groups on the particles through the coating plays an important role [1]. Finally, completely covered core-shell particles increasingly find applications in the medical field, for example

for controlled drug delivery, bioimaging, cell labeling, biosensors and in tissue engineering applications [4].

In other applications a hermetic coating is not desired, since the chemical and physical properties of the core material need to be preserved. For example, silica coatings might be interesting for the modification of aerosol catalysts. The particles used here are often made up of small primary particles in fractal agglomerate structures [5]. The coating with a material with a higher melting point could improve the resistance of these structures against sintering and restructuring at elevated temperatures by mechanically stabilizing the agglomerates. However, if all the particle surface area were covered, a loss of catalytic activity would result in most cases. Hence, a more localized silica coating is preferred that covers only the parts relevant for the stability of the structure.

The production of core-shell particles can be accomplished with many different methods, some of which will be presented in the following sections. Especially interesting are plasma-based processes at atmospheric pressure, since they provide a high flexibility in regard to the material combinations and particle sources. In this thesis, the coating of nanoparticles with a silica ( $\text{SiO}_x$ ) or silica-organic ( $\text{SiO}_x\text{C}_y\text{H}_z$ ) shell is achieved in a continuous gas phase process using a dielectric barrier discharge (DBD). The process is a chemical vapor deposition (CVD) using two precursors, tetraethyl orthosilicate (TEOS) and hexamethyldisiloxane (HMDSO), which require somewhat different coating environments as will be shown later. A DBD is a popular choice for film deposition and can be constructed in many different ways [6, 7, 8, 9]. Two of the main advantages of DBDs are the simple setup, with a relatively low constructive complexity and simple cooling requirements. Two electrodes are separated by at least one dielectric barrier, such as a ceramic plate, and a gap of a few mm with the discharge gas (Fig. 1.1). Depending on the used discharge gas, the pressure and other parameters, a DBD results in either a filamentary discharge with individual discharge filaments or a homogeneous discharge. Filamentary discharges are more common at atmospheric pressure. DBDs have a long history in industrial applications, such as the ozone production, and are scalable by parallelization [10]. The physics of plasmas are highly complex and cannot be adequately covered in this thesis. However, there are multiple books available about this topic, such as the ones by Becker et al. [11] and Meichsner et al. [12].

A DBD is used here to provide reactive species to the coating system. The coating itself is done in the post-discharge environment after the discharge. This means that neither the particles nor the precursor come in direct contact with the plasma. This has significant advantages for a continuous particle coating process, since material losses are reduced and the long-term stability of the process is improved. If particles are introduced directly into the discharge, which is the more common method for particle coating, a significant portion of the particles and the precursor is lost to the walls of the reactor, due

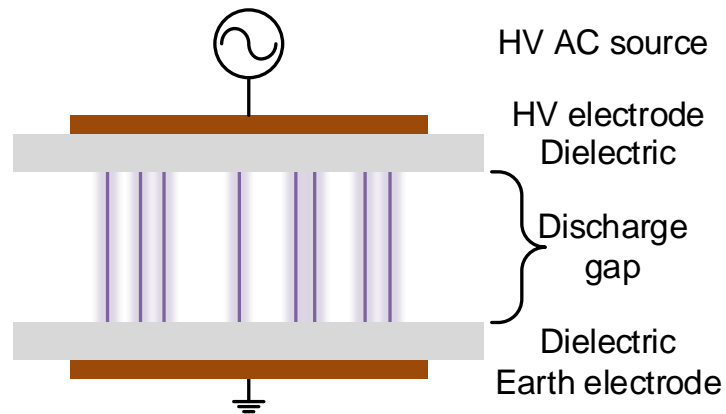


**Fig. 1.1:** Basic dielectric barrier discharge (DBD) setup with two dielectrics. It is also possible to use only one dielectric. The discharge gap is typically a few mm.

to the strong electric fields. This restricts the long-term stability of the discharge, due to the buildup of material on the dielectric surfaces, which changes the electrical properties of the reactor. It also causes an unnecessary reduction in the process efficiency. While these problems can be somewhat mitigated by optimization of the reactor design (e.g., higher discharge frequencies), the decoupling of the discharge from the coating process, as done in this thesis, avoids them completely. However, the chemical environment in the post-discharge differs from that in the discharge zone itself and is often characterized by less reactive species. Since this thesis focuses on the engineering aspects of the coating process, only some reasonable assumptions concerning the basics of the mechanisms are made, but for the most part the mechanisms are considered as a black box. Chemical reactions involving plasma discharges are typically highly complex and would require a lot of specialized and dedicated research, which is beyond the scope of this thesis.

The general structure of this cumulative dissertation is as follows: The next section of this introduction gives an overview of the state of the art of different coating techniques with a focus on particles. The two subsequent chapters contain information about the four publications which are part of this cumulative thesis (chapter 2), and the papers themselves (chapter ??). The following chapters provide an overview of all important results in context. That part starts with the description of the experimental setup in chapter 3. The subsequent chapters focus on the engineering aspects of the post-discharge coating process such as the proof of concept, which shows that the formation of coatings and their control is possible (chapter 4), specific combinations of core and shell materials (chapter 5) and examples for applications of particles coated in the process (chapter 6). Finally, the results are summarized in chapter 7.

## 1.2 State of the art

### 1.2.1 Coating of particles in the liquid phase

In many cases, particles are coated in liquid phase batch processes. There are multiple processes for the coating of particles with silica in the liquid phase, with modified Stöber processes among the most common. The Stöber process is a type of sol-gel process, in which a precursor, typically TEOS, reacts with water in an alcoholic solution and forms continuously larger structures through the cross-linking of molecules in the presence of a catalyst (e.g., base or acid). The process is well-studied due to its many applications, such as the formation of silica particles, special materials, such as aerogels, and coatings on bulk substrates or particles [13, 14, 15]. However, this hydrolysis reaction of TEOS and water to silica is slow (hours).

Hence, some research focused on ways to speed up the reactions, such as the work by Siddiquey et al. [16], who used a microwave for this purpose. They slowly mixed ZnO nanoparticles with a mixture of TEOS, ethanol, water and  $\text{NH}_3$ , which caused the hydrolysis and condensation of  $\text{SiO}_2$ . Conventionally, this process is stirred for about 6 h, but with the microwave irradiation they could reduce the reaction time to a few minutes. However, afterwards the particles still needed to be collected by centrifugation, washed three times with ethanol and dried in a vacuum oven for 2 h.

As the most common process, silica coatings produced in the liquid phase have been used for many applications, such as the inhibition of the photocatalytic activity of titania [17] or the production of active and sinter-resistant catalysts [18]. Silica and silica-organic coatings from sol-gel processes are interesting for biomedical applications [19]. One of the main advantages of the coating in the liquid phase is the possibility to coat individual particles even at relatively high particle concentrations, by stabilizing the suspension against agglomeration.

While liquid phase processes generally allow a good control of the coating formation, they have several disadvantages compared to gas phase methods. First, the majority of them are batch processes and do not allow a continuous production of the powder. While this might be acceptable in industries where batch processes are traditionally used, such as the pharmaceutical industry, it becomes a problem in high volume markets. Commercial nanoparticles, such as carbon black, silica and titania, are often produced in gas phase processes such as flame synthesis [20, 21]. These kinds of particles would need to be collected from the continuous gas phase production and then introduced into liquid phase batch processes, which additionally require long reaction times. Furthermore, liquid phase processes require additional steps to obtain the dry powder, which include separation, washing and drying, and often have a high amount of by-product contamination on the

particles [22]. Hence, there is a lot of interest in gas phase processes for particle coating.

### 1.2.2 Coating of particles in the gas phase (excl. plasma)

The coating of nanoparticles in the gas phase can be achieved with different methods. The most common group of techniques are CVD processes, where a precursor reacts to the desired coating material. The term chemical vapor deposition includes a multitude of gas phase processes. All of them use chemical reactions of a precursor in the gas phase to form structures, such as particles, films on bulk substrates or coatings on particles. A lot of subcategories can be created, depending, for example, on the operating conditions (e.g., atmospheric pressure CVD) or the applied technique to initiate the reactions (e.g., combustion CVD, photo-initiated CVD or plasma-enhanced CVD). This can sometimes cause uncertainty which technique was actually used by a given group, since many methods can be assigned to multiple categories. Often, the assignment depends on the background of the researchers. In this thesis, the coating is facilitated by a plasma discharge at atmospheric pressure and could hence be called both atmospheric pressure CVD (APCVD) or plasma-enhanced CVD (PECVD). However, to emphasize the more indirect role of the plasma as a supplier of reactive species into a post-discharge environment, a more fitting description might be "plasma-assisted CVD". Besides plasma CVD processes, which will be discussed in more detail in section 1.2.3, aerosol coating processes in the literature commonly include flame synthesis, atomic layer deposition, hot-wall CVD and photo CVD.

**Flame synthesis (thermal CVD)** An especially interesting technique is the direct coating during flame synthesis, because many high volume particles are produced in flame synthesis processes and a direct combination of particle production and coating would greatly reduce the complexity of the setup. As shown in Fig. 1.2, the coating precursor is introduced in a certain distance above the burner outlet. The hot aerosol reacts with the precursor and forms silica coatings on the particles.

Teleki et al. coupled a flame spray pyrolysis (FSP) reactor for the production of titania particles with a silica coating [23, 24]. They found that the position of the coating precursor injection had a significant influence on the coating homogeneity with patchy and poorly coated structures forming if the injection was done too early. Furthermore, the geometry of the injection ring was found to be important for the formation of homogeneous coatings. A similar, but somewhat simpler setup was used by Qi et al. [25]. They produced titania particles in a premixed flame burner from the reaction of  $\text{TiCl}_4$  with  $\text{O}_2$  and added  $\text{SiCl}_4$  directly into the flame above the burner. They reported the formation of silica coatings on the titania particles that improved the photocatalytic activity of the samples after heat-treatment.

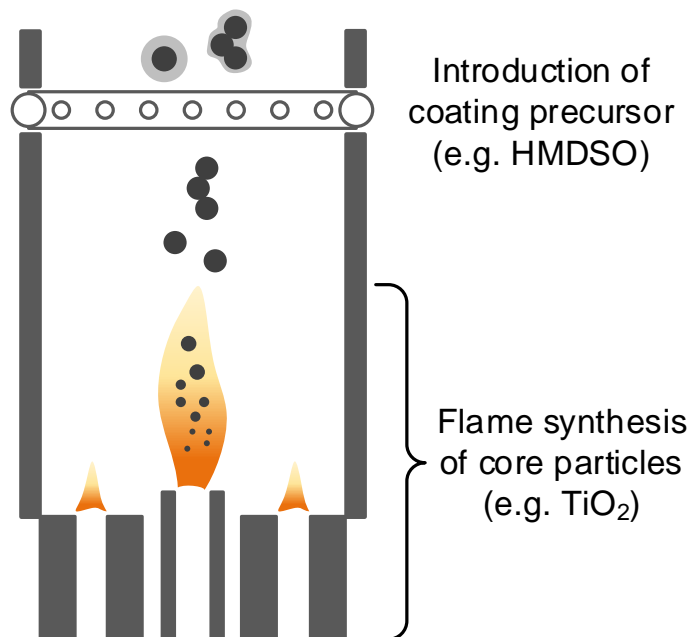


**Fig. 1.2:** Particle production and coating with flame spray pyrolysis.

Due to the industrial relevance of the flame synthesis for nanoparticle production, the coating of particles by this method is one of the most promising and hence most studied for the in-flight coating of aerosols, with a lot of attention given to the modeling of reactions and flow simulations [26, 27]. However, while the direct coating during flame synthesis is a good way to coat particles produced in the flame, it is necessarily coupled with this synthesis method and cannot easily be combined with other techniques.

**Hot-wall or thermal CVD without flame** The particle coating with hot-wall CVD is similar to flame synthesis, since both use thermal energy to allow the particle formation and coating with CVD. However, while flame synthesis methods use an open flame, the reactions in a hot-wall reactor take place in a furnace, where the reaction mixture is heated from the outside (the hot wall). This is often achieved in fluidized beds, where a powder is placed in a batch reactor and mixed with the reactants at higher temperatures [28]. However, hot-wall reactors can also be used for the continuous coating of aerosols. A very basic setup is shown in Fig. 1.3, where both particles and precursor are introduced together into a tube furnace.

As the flame synthesis, the hot-wall CVD allows the combination of continuous particle production and coating in one step, when the coating precursor is added into the reactor after the core particle formation is finished. Powell et al. [29] demonstrated this for the

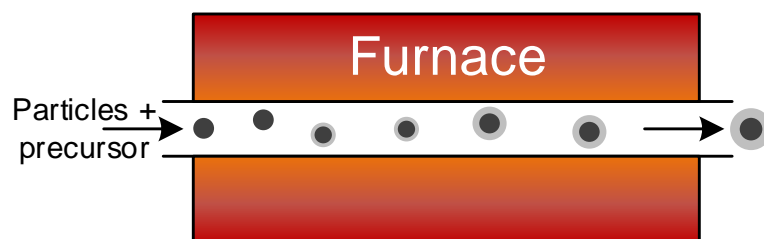


**Fig. 1.3:** Continuous particle coating with thermal (hot-wall) CVD. Actual coating setups are more complex in regard to the flow control and mixing conditions.

production of silica coated titania particles at temperatures between 1300 and 1500 °C using  $\text{SiCl}_4$ . While they reached fast film deposition rates, the coatings were often rough and inhomogeneous. To acquire smoother coatings, they had to control the temperature, water concentration and dilution gas in the reactor. Fotou and Kodas [30] used a very similar setup to produce and coat titania particles with a multilayer film of alumina and silica. Simpson et al. [31] were able to reduce the required temperatures for silica coating to about 1000 °C. Their setup also allowed the coating of particles produced in a separate setup and was hence more flexible in regard to the core material. However, the main disadvantage of thermal CVD is the high required temperature, which significantly reduces the selection of core materials that can be coated without structural or chemical changes.

**Atomic layer deposition** The atomic layer deposition (ALD) is a method for the deposition of very thin, but very homogeneous films on surfaces. Due to the interactions between the precursors and the surface, the film formation is self-limiting and allows the control of the coating in the monolayer range. Most ALD processes use reaction sequences of two or more different precursors that are deposited in cycles. A first precursor forms a thin layer until all available surface sites are covered and produces new sites for the reactions with the second precursor and so on until the desired thickness is reached. The direct interaction between surface sites and precursor allows the complete coverage of surfaces, without special regard to the precursor supply design. Due to the very defined film formation, ALD processes are used especially in semiconductor processing [32]. While there are low temperature ALD variants, most reactions require higher temperatures of a few hundred °C.

ALD can also be used for the coating of particles. King et al. [2] used a fluidized bed reactor to coat titania powder with silica and alumina by ALD. They used an aminosilane

precursor with  $\text{H}_2\text{O}_2$  in  $\text{H}_2\text{O}$  at  $500\text{ }^\circ\text{C}$  and pressures between 0.3 and 0.4 kPa. They were able to produce conformal and pinhole-free films of a few nm thickness. They showed that the 2 nm thick films inhibited the photocatalytic activity of the titania and improved the acid resistance. However, due to the low growth rates of approx.  $0.4\text{ \AA}/\text{cycle}$ , the formation of sufficient films took multiple hours in the batch reactor. Hence, the main disadvantages of ALD are its slow film growth rate and the necessity of a batch setup.

**Photoinduced CVD** An interesting method to coat nanoparticles independent of the synthesis method is the use of the photoinduced CVD. An example is the work by Boies et al. [33, 34]. The core particles were introduced into a tube furnace, where they were mixed with the precursor TEOS. A UV excimer lamp radiated the aerosol mixture and resulted in the formation of silica coatings on the particles, through the formation of oxygen radicals. The basic setup of this photoinduced CVD process is shown in Fig. 1.4. Due to the generation of a more reactive environment by the UV radiation, the required furnace temperature is significantly lower than during the classical thermal CVD. While this method is similar to PECVD processes in the post-discharge environment, the instrumental complexity is somewhat higher, due to the UV radiation required in the coating chamber.

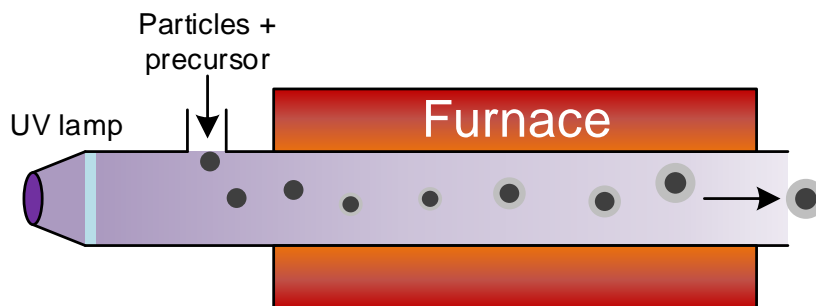


**Fig. 1.4:** Setup for continuous particle coating with photoinduced CVD.

**Other** Besides these more common particle coating methods, there are a few others, which are used only by a small number of researchers. An example is a technique demonstrated by Kim and Ehrmann [35] to coat titania agglomerates with silica. The core particles were placed in a chamber and this chamber saturated with TEOS vapor, which caused the precursor to condense on the particles. Afterwards, the chamber was opened to the atmosphere and the ambient moisture caused the formation of silica in a kind of localized sol-gel process. This allowed the formation of very small and defined coatings in the areas between particles, where TEOS was collected, due to capillary forces. However,

while interesting, this technique is an exclusively lab scale experiment with only enough powder for TEM analysis and it required very long reaction times (hours, overnight), due to the slow reaction of TEOS with water.

A similar idea of transferring traditional liquid phase processes to the gas phase was shown by Zhu et al. [36]. They coupled the formation of iron oxide particles by the dehydrolysis of  $\alpha$ -FeOOH particles in a fluidized bed reactor (FBR) with the simultaneous formation of silica coatings by using TEOS-saturated nitrogen for the bed fluidization and an ammonia-saturated gas flow from the top of the reactor. The reactor was heated to 250 - 500 °C and after a few hours the coated iron oxide particles were removed and studied. They found that the dehydrolysis of the core particles promoted the formation of homogeneous coatings on the particles over the formation of silica particles.

### 1.2.3 Coating with plasma-assisted processes

**Bulk substrates** The coating of bulk substrates with silica coatings using plasma processes has been extensively researched in the last decades, mainly due to many applications in electronics. It can be assumed that many of the observations of the interactions of coating precursor and plasma species will be at least similar for particle coatings. To reduce the number of publications, only the most relevant plasma-assisted processes working at ambient pressure and utilizing the same precursors used in this thesis will be discussed for bulk films.

The increasing demand in Very-large-scale integration (VLSI) processes for the production of microchips and other microelectronic devices at the end of the last century resulted in an increased interest in coating processes that could help in the modification of wafers. While many early substrate coating processes used CVD reactions at reduced pressures, the reduced instrumental complexity of APCVD resulted in a number of publications combining silica precursors with post-discharge environments in the 1990s. In these applications, silica coatings are interesting for the formation of interlayer dielectrics on Si wafers. Important requirements for these films include good gap-filling properties and a low deposition temperature to prevent damage to the wafers [37]. Among the different systems studied for these applications was the combination of TEOS with ozone, which provides a much better step coverage than the silane ( $\text{SiH}_4$ ) based processes used earlier. A common method was to place the Si wafer in a chamber, where it was heated to around 300 to 400 °C, while TEOS was continuously supplied from a bubbler and mixed with ozone produced in a so-called ozonizer using oxygen [38, 39]. These ozonizers are commercially available devices that continuously produce ozone in a plasma discharge. Different types of ozonizer are available using a corona discharge, a surface discharge, a dielectric barrier discharge or a combination of those. Sadly, most publications did not supply additional information about the used discharge type. However, regardless

of the exact type of discharge, the chemical environment during film formation was always at least similar, since the ozone was decomposed into oxygen radicals at the utilized temperatures and enabled the polymerization of the precursor.

Work on TEOS-based silica coatings in the post-discharge environment was published by Adachi et al. and Okuyama et al. They focused both on the film formation on substrates and the particle formation in the gas phase. Their early publications described the formation of films and the particle generation by TEOS in He heated above 700 °C without a discharge [40]. However, they soon moved to the TEOS/oxygen [41, 42] and TEOS/ozone system [41, 43, 37], because this allowed the film formation at lower temperatures of around 600 and 100 °C, respectively. Adachi et al. produced the ozone with a commercial ozonizer, using a surface discharge in oxygen. The discharge gas was diluted with He and introduced into a furnace, where it was mixed with TEOS supplied from a bubbler with He. Depending on the conditions (furnace temperature, precursor concentration etc.), this resulted in the film formation on a Si wafer in the middle of the furnace and the production of silica particles in the gas phase, which either got integrated into the film or left the furnace with the gases.

Fueled by the increasing demand for microelectronics, the TEOS/ozone process continued to garner a lot of interest in later publications that focused on different aspects of the process such as the influence of the substrate surface [44], the chemical reactions and their kinetics [45, 46, 47, 48, 49] as well as new applications [50].

HMDSO has been used as precursor in similar coating setups as well. For example, Alexandrov et al. [51] used remote AP-PECVD for the deposition of  $\text{SiO}_x$  coatings on a heated sample (300 - 550 °C). A DBD was fed with a mixture of Ar and  $\text{O}_2$  to produce metastables and ozone at atmospheric pressure. The reactive species were transported to the sample, where they were mixed with HMDSO and the coating was deposited. Between the discharge and the substrate was a residence time of a few seconds. They were able to control the coating thickness and the film density by changing the electrical power, the substrate temperature, the precursor concentration, the discharge gas composition and the distance between discharge and substrate. In general, the use of HMDSO in PECVD systems seemed to result more often in silica-organic coatings than the use of TEOS as the precursor [52, 53, 54].

**Particles** Additional challenges arise when particles are coated with plasma processes that rely on the particles and precursor being present in the discharge area. On the one hand, the discharge characteristics can change significantly with higher particle concentrations, resulting in a much more complex discharge behavior ("dusty plasma"). On the other hand, certain types of discharges (e.g., DBD) will be less stable in continuous operation, due to the deposition of particles and coating material on the dielectric or electrode

surfaces, which can influence electrical properties of the system such as the resistance. For aerosol coating methods, these losses also affect the economic viability of the process, since particles following the electric fields to surfaces are in most cases lost from the process. Additionally, filamentary discharges produce unwanted nanoparticles that might leave the DBD together with the coated particles [55, 56]. Since fewer publications are available for particle coatings with plasmas than for bulk substrate films, some relevant examples using other precursors will be discussed here as well.

One approach to reduce particle losses in dielectric barrier discharges is the increase of the applied discharge frequency. Since a higher frequency of an AC discharge means faster reverses in polarity, the particles have less time to travel to the electrode before the electric field changes and moves them in the opposite direction. Depending on the frequency and the distances of the particles from surfaces, this can result in an oscillation of particles around their flight path without deposition. A similar approach is the use of a pulsed discharge that periodically interrupts the applied voltage and hence the discharge and electric fields. This results in short (e.g., ms) times when particles in the discharge zone are less likely to be lost by electrostatic deposition. Obviously, this will drastically change the discharge characteristics and the chemical environment, since the discharge becomes much less homogeneous. The third approach to coat particles in plasma processes is the introduction of the particles and coating precursor after the discharge. This circumvents the aforementioned problems since the particles do not come into contact with the electric fields. However, the post-discharge environment chemistry is often significantly different from the discharge itself with longer living and mostly neutral species and their decomposition products dominating the reactions instead of radicals and ions in the discharge. Two different forms of post-discharge environment need to be distinguished: the post-discharge environment in a significant temporal distance of the discharge that contains only relatively stable species, such as ozone, and the plasma afterglow region. The afterglow is the radiation originating from a plasma after the removal of its ionization source, for example by interrupting (pulsing) the discharge or by transport of the charge carriers from the discharge zone by a gas flow. Compared to the distant post-discharge environment, the afterglow region is chemically more similar to the discharge itself. In this thesis, the coating is accomplished in a distant post-discharge environment, but the other scenarios are more common in the literature and will be discussed here as well.

Aside from the location of the particle and precursor injection, different kinds of powder feed can be employed. In continuous systems, such as the one shown in this thesis, the particles are steadily supplied from a source and fed directly into the coating setup, where the coating continues for as long as additional particles keep entering the system. In contrast, batch processes contain a limited amount of powder that needs to be exchanged between the coating charges. A semi-batch process is a combination of both

and either introduces or removes the particles continuously.

The by far most common method to coat particles in plasmas (especially  $\mu\text{m}$  to  $\text{mm}$  sized powders) is the use of batch processes. In fact, there are hundreds of publications available about this topic, but in view of the limited space in this thesis and the similarities between most of these methods, only a handful will be discussed here exemplarily. However, multiple review articles are available, such as the one from Vahlas et al. [28].

Often, the discharge is generated directly around the powder, e.g. in a fluidized bed, which is often accomplished in low pressure environments. Microwave (MW) or radio frequency (RF) discharges are especially suitable for this purpose since the discharge energy is induced from outside the powder vessel (e.g., with a coil) and hence no direct contact exists between the electrode and the particles. Some examples include the work by Bayer et al., who coated NaCl particles (0.5  $\mu\text{m}$ ) with a silica-like hydrophobic coating using HMDSO in a MW plasma in a fluidized bed [57]. Hody et al. [58] coated silicon carbide particles with silica-organic coatings in a low-pressure system. Here, the powder was kept in a container inside the coil used to produce the RF plasma. Through magnetic stirring, the powder was moved inside the discharge to expose all surfaces to the discharge. Hexamethyldisilazane (HMDSN) was used as the precursor with oxygen at 40 Pa chamber pressure. They were able to coat powder with a few nm thick coatings and functionalize them with carboxylic groups, but did not accomplish complete coverage of all surfaces. Other groups used similar setups: Tsugeki et al. [59] coated AlN powder with silica in a low pressure RF process with TEOS. Shi et al. coated  $\text{Al}_2\text{O}_3$  nanoparticles [60] and carbon nanotubes [61] with polymers from pyrrole in low-pressure RF plasmas. Titania particles were coated by Oksuz et al. [62] with a conductive polymer in a rotating capacitively coupled RF plasma reactor.

In multiple other publications, plasmas were coupled with batch processes that supply the powder from a reservoir into the plasma zone by different kinds of dispersion methods instead of keeping the particles in the plasma for the whole process duration. Due to the batch nature of the setups, the same particles can be introduced into the discharge multiple times and hence long coating times can be realized. A main advantage of this method are comparatively low temperatures and hence a low thermal stress on the particles. There are multiple methods how the circulation can be accomplished. A generalized example is shown in Fig. 1.5.

Such a setup was used by Mori et al. [63] to coat  $\text{Fe}_3\text{O}_4$ , FeOOH and Lithol Rubine BCA (a red pigment) powder with silica, using a mixture of the carrier gas He, TEOS and  $\text{N}_2\text{O}$  at atmospheric pressure. The powder was placed in a reservoir below the discharge zone and transported together with the gaseous precursors to the top of the device by a carrier gas, where it fell down through the plasma discharge. The plasma was an atmospheric pressure glow discharge (APGD), using an RF source and treatment times

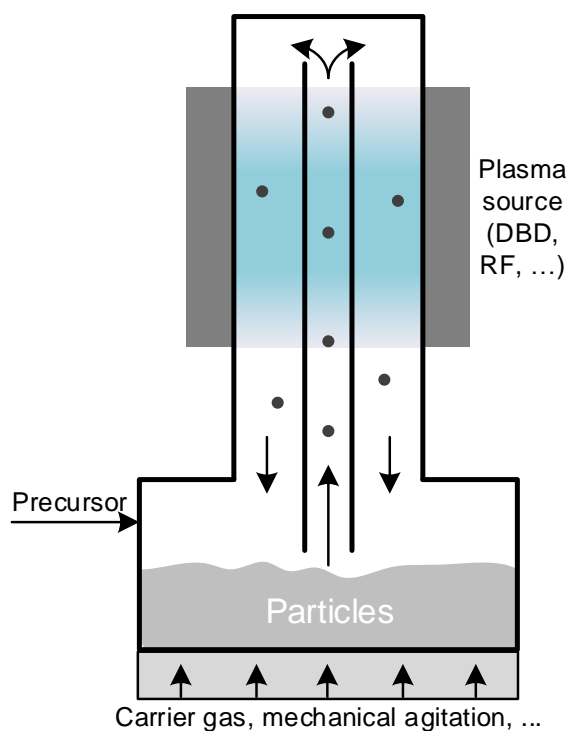


**Fig. 1.5:** Setup for powder coating with a circulating plasma batch reactor. Different combinations of powder agitation method and plasma source are possible.

between 15 and 60 min. However, the method required an adequate fluidity of the powder to allow the circulation through the discharge. To improve the fluidity of  $\text{Fe}_3\text{O}_4$ , they pretreated the powder with TEOS in a liquid phase process for 7 days and then oxidized undecomposed TEOS in the reactor. This method was later refined by Kogoma et al. [64], who developed a device where the powder falls from a storage onto an ultrasonic horn and is then blown into the discharge area of an RF APGD plasma and subsequently collected. They used TEOS as the precursor to coat titania and iron doped titania with silica. In their so-called adsorb and dry method, TEOS was adsorbed on the particle surfaces in ethanol, before the coating formation was initiated in the plasma. It is also possible to combine a APGD with a circulating fluidized bed reactor [65]. MW discharges can also be used in combination with a fluidized bed, as shown by Karches et al. [66].

Some groups developed setups for the coating of particles in the post-discharge environment, sometimes referred to as remote plasma, to solve problems with the coating of very temperature-sensitive powders and particle-plasma interactions. Caquineau et al. [67] used such a setup to coat polyethylene particle ( $260 \mu\text{m}$ ) with silica at 10 Torr. The particles were placed in a reactor and fluidized with a mixture of nitrogen and oxygen

that previously (47 cm distance) passed through a microwave discharge.  $\text{SiH}_4$  was added to the particle bed and formed the coatings on the particles.

Another approach to batch processes is the coating of particles placed on a bulk substrate. He et al. [68] scattered zirconia powder on a glass substrate and placed this in the plasma zone, generated with an inductively coupled RF source. A mixture of  $\text{C}_2\text{H}_4$  and  $\text{N}_2$  was introduced into the chamber kept at 150 Pa and resulted in polymer coatings on the particles. Brüser et al. [69] used a similar process to coat NaCl and KBr particles in a surface DBD setup. The particles were placed on a circuit board that constituted the DBD electrode and dielectric setup. The whole setup could be mechanically agitated to move the powder through the plasma zones. When the precursors (HMDSO, TEOS) were introduced with  $\text{O}_2$  and Ar into the atmospheric pressure discharge, silica-organic coatings formed on the particles. A particles-on-substrate setup was also used by Dahle et al. [70] to coat titania particles in a DBD with monosilane ( $\text{SiH}_4$ ). They used a novel two-step method, where a silicon nitride film is first produced on the particles before it is converted to silicon dioxide in a second DBD plasma. Shearer et al. [71] used an inductively coupled RF plasma to coat deposited titania particles with different materials.

A semi-batch process was employed by Kouprine et al. [72] to coat silica powder with polymer-like hydrocarbon layers. This was accomplished in a capacitively coupled RF discharge in either pure methane or ethane and reduced pressure. While the powder was supplied from outside the coating reactor (fluidized bed), the powder was collected in corners and walls of the setup. Another semi-batch process was used by Tavares et al. [73]. They produced Cu particles in an arc discharge, which was surrounded by a low-pressure RF plasma. With the addition of ethane or ethylene glycol into the discharge, polymeric coatings could be applied to the particles, which were then collected in the reactor. However, the coatings seemed to exhibit a low degree of homogeneity and a high amount of homogeneous nucleation of polymer.

While batch coating methods are very interesting for the follow-up treatment of independently produced powders, a direct and continuous coating of particles after their production in a gas phase process would be advantageous for large scale applications. Hence, some groups tried to design continuous in-flight methods for the particle coating. Marino et al. [74] used different DBD setups to coat copper oxide nanoparticles with different kinds of organic precursors to control their reactivity by covering the surfaces. Here, both the particles and the monomer were introduced into the discharge zone to form the coating. They were able to achieve a higher percentage of coverage on the particles by increasing the residence time in the plasma. Lei et al. [75] used a similar process to coat copper particles. Again, both particles and polymer precursor ( $\text{CH}_4$ ,  $\text{H}_2$ ) were introduced into the discharge to facilitate the coating. While the authors were able to coat particles, they had problems with silica contamination from the dielectrics.

Vons et al. [76] coated nanoparticles that they produced in a first DBD plasma with silica in a subsequent second plasma, by introducing the particles and the precursor HMDSO into the second discharge zone. Such a setup is schematically shown in Fig. 1.6. They were able to coat particles, but did not reach high coating homogeneities and had problems with the formation of silica particles, due to homogeneous nucleation. Vollath and Szabó [77, 78] used a similar combination of particle production and coating in two separate plasma discharges within the same setup. However, instead of a DBD, they used a microwave plasma process. They were able to combine a multitude of materials, such as ceramic cores with polymer coatings. The coating was done in a low-pressure environment and involved temperatures of a few hundred °C. Another combined process for the production and coating of particles was used by Münzer et al. [79]. They used a microwave plasma to produce Si-nanoparticles from  $\text{SiH}_4$  and added  $\text{C}_2\text{H}_4$  at different distances from the plasma discharge (215 - 465 mm). Due to the high temperatures of the microwave plasma, polyethylene coatings could be formed on the particles.

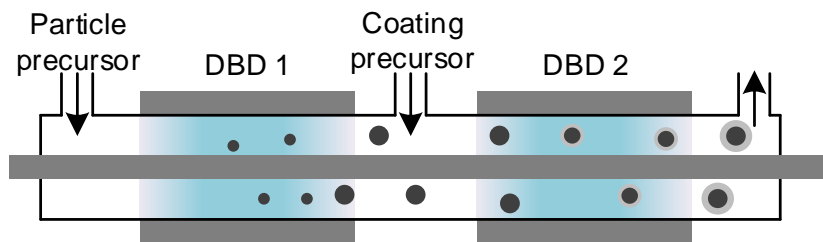


**Fig. 1.6:** Setup for continuous particle production and coating in a setup with two DBDs.

Nessim et al. [80, 81] used two different kinds of DBD setups: One was a shell design with multiple plasma zones that the particles passed together with the precursor. The other was a coaxial torch, where particle and precursor could be added into the discharge or into the afterglow region. Different powder feeders were used to introduce silica or Al particles into the system. The coating was done with different precursors such as ethylene, butadiene, pyrrole, acetylene for polymer coatings or TEOS and HMDSO for silica and silica-organic ones. The system worked at atmospheric pressure with different plasma gases.

In conclusion, the coating of particles with a second material is certainly not a new concept and while traditionally most methods use the liquid phase, multiple techniques are known to accomplish coating in gas phase processes. However, each aerosol process has its own challenges and no versatile process for the coating of arbitrary core particle materials seems to exist. In contrast, plasma CVD processes are very flexible and can be

used for a plethora of material combinations. However, the focus of previous research in this area has been on batch processes with only a few groups seeming to be interested in the continuous in-flight coating at atmospheric pressure and low temperatures. The present thesis aims to demonstrate that such a method is relatively easy to set up (at least at lab scale) and allows the controlled coating of multiple materials.

# CHAPTER 2

---

## Overview of the publications

---

The central aspects of this cumulative thesis were the development of a continuous aerosol process for the surface modification of gasborne nanoparticles with silica-like coatings and its uses for different applications. As described before, this was achieved with a post-plasma coating process at ambient or elevated temperatures. Much of the work was published in the following four peer-reviewed research papers, which cover essential parts of this project.

### 2.1 Publication 1

Post, P.; Jidenko, N.; Weber, A. P.; Borra, J.-P. Post-Plasma SiO<sub>x</sub> Coatings of Metal and Metal Oxide Nanoparticles for Enhanced Thermal Stability and Tunable Photoactivity Applications. *Nanomaterials* 2016, 6, 91, doi:[10.3390/nano6050091](https://doi.org/10.3390/nano6050091).

This publication was the first study published by the author about this process. It demonstrated the general feasibility of the silica coating process with TEOS at ambient temperature as a proof of concept. This was done by first describing species produced with the DBD reactor at different discharge conditions to characterize the chemical environment during coating (section 3.1 in the publication). In the next section, the formation of coatings at certain extreme conditions was demonstrated and a possible reaction pathway discussed. In section 3.3, the parameters influencing the coating formation on spherical particles were studied in more details. Especially the initial TEOS concentration and the residence time in the system were found to influence the coating thickness significantly. Furthermore, a discrepancy between the coating thickness measured in-situ in the gas phase and that obtained from TEM micrographs was found, which was explained with the formation of a liquid film on the particles, which slowly solidified to the finished silica coating. In section 3.4, the coating of highly agglomerated particles was discussed. It

was found that very thin coatings seemed to be focused in interparticle spaces between primary particles. This was corroborated by photoemission measurements that indicated only a slow loss of accessible core particle surface for the agglomerates with increasing precursor concentration, but a nearly instant loss of accessibility for the homogeneous coating on spherical particles. As an example for a possible application of this coating behavior on agglomerates, metal agglomerates were coated with a thin coating that seemed to cover primarily inner parts of the structures and hence left most of the core particles surface available, which is important for catalysts. It was found that this thin coating already improved the thermal stability of the particles.

The thesis author was directly involved in the planning of the experiments and conducted all the experimental work and sample analyses, excluding the plasma characterization. The author did most of the evaluation of the experiments and wrote most parts of the manuscript.

## 2.2 Publication 2

Post, P.; Weber, A. P. Beschichtung von gasgetragenen Nanopartikeln mit SiO<sub>2</sub> mithilfe eines plasma-unterstützten CVD-Prozesses bei Umgebungsbedingungen. *Chemie Ingenieur Technik* 2018, 90, 443–450, doi:[10.1002/cite.201700109](https://doi.org/10.1002/cite.201700109).

The second publication can be viewed as an extension of the first. It also covered the TEOS process at ambient temperature, but focused on questions that remained open after the first paper. One of those was the influence of the available surface area of the core material on the coating thickness (described in section 3.1 of Publication 2). It could be confirmed that a higher surface area reduced the coating thickness if all other parameters were constant, which shows the importance of this aspect for a controlled coating. Furthermore, more particle materials were demonstrated as possible core materials such as salts or polymer, in addition to the metal particles used in the first publication (section 3.2). Additionally, some information about the chemical coating composition was provided (3.3), which was later done in more detail (Publication 3). Last but not least, Publication 2 showed important process features by quantifying the agglomeration and diffusion losses occurring in the coating chamber (3.4).

The author did all the planning, execution and analysis of the experiments. He also wrote the manuscript for the most part.

## 2.3 Publication 3

Post, P; Wurlitzer, L; Maus-Friedrichs, W; Weber, A. P. Characterization and Applications of Nanoparticles Modified in-Flight with Silica or Silica-Organic Coatings.

Nanomaterials 2018, 8, 530, doi:[10.3390/nano8070530](https://doi.org/10.3390/nano8070530).

The third paper extended the published coating parameters by a new coating precursor (HMDSO) and a new temperature range (above 100 °C). In section 3.1 of the publication, the coating morphology differences between these parameters on multiple core particles were demonstrated, which showed a reduced homogeneity of HMDSO-based coatings on spherical metal particles as well as differences in the TEOS-based coating on titania particles at ambient and elevated temperatures. The next section (3.2) focused on the coating composition acquired with different coating parameters, analyzed with Fourier-transform infrared spectroscopy as well as X-ray photoelectron spectroscopy (XPS). It showed clear differences between the TEOS-based and HMDSO-based coatings, with the HMDSO ones containing more organic compounds. Furthermore, chemical bonding between the silica coating and titania particles was indicated by XPS. The findings were used to demonstrate possible applications for the different coatings in section 3.3. The more organic HMDSO coatings could be used to produce hydrophobic particle surfaces and the silica coating could be used to control the photoactivity of titania catalyst particles.

The author planned and conducted the coating experiments and did the sample analyses, apart from the XPS measurements. He also did the evaluation of the work, apart from XPS. He wrote most of the manuscript, but not the parts about XPS.

## 2.4 Publication 4

Post, P.; Bierwirth M.; Weber, A. P. Mechanical stability measurements of surface modified nanoparticle agglomerates. *Journal of Aerosol Science* 2018, 126, 33-46, doi:[10.1016/j.jaerosci.2018.08.007](https://doi.org/10.1016/j.jaerosci.2018.08.007).

The final paper described an application of the coating process with TEOS and HMDSO by demonstrating the improvement of the mechanical stability of metal agglomerates during inertial impaction. It showed a method to acquire information about the fragmentation degree of impacted agglomerates from TEM measurements, which was described in section 2 of the paper. The results start with the description of the structure of the model particles and how the coating behaved on these particles (3.1). The next section (3.2) showed the deposition and rebound behavior of the different agglomerates (coated/uncoated etc.) in the low pressure impactor. Section 3.3 showed the results for the fragmentation studies for silica-coated particles at ambient temperature. It was found that the uncoated particles seemed to increase in size with increasing impaction velocity before showing the expected fragmentation behavior. This was explained with a flattening of branches onto the TEM sample grid. The coatings reduced both this flattening as well as the later fragmentation and so improved the mechanical stability. A similar effect

was found for HMDSO-coated particles in section 3.4, where the coating also improved the stability. Furthermore, however, it was found that the coating also seemed to reduce sinter effects occurring during the coating formation at 200 °C.

The author was directly involved in the planning of the experiments and participated with about 50 % on the experimental work. The author also did about 50 % of the analyses and evaluation of the experiments, but was only indirectly involved in the image analysis and impaction velocity calculations. The manuscript was written by the author for the most part.

# CHAPTER 3

---

## Experimental

---

### 3.1 Overview of the coating process

The particle coating process studied in this thesis is a CVD using a DBD plasma as a source of a chemically reactive environment. It is a post-discharge process, where neither the precursor nor the particles need to be in direct contact with the discharge itself, which has significant advantages for the continuous in-flight coating. The process takes place at atmospheric pressure and low temperatures. Since it works continuously and completely in the gas phase, the particles are synthesized and coated in the same system without being deposited in the interim. This section gives a brief overview of the coating setup, before the individual parts are discussed in more detail in the following sections.

The coating setup consisted of three main gas pathways, which were mixed to start the particle coating (Fig. 3.1). These were the particle production, the precursor dosing and the production of plasma species. A spark discharge generator (SDG) and an atomizer were used as particle sources. Different precursors were used, depending on the desired coating material. Silica coatings were produced with TEOS and silica-organic ones with HMDSO. The plasma species were produced in one of two self-built DBD reactors.

After mixing, a variable part of the total gas flow was pumped through the coating chamber. The coating chamber was one of several quartz glass tubes, which acted as a vessel to provide the required combination of temperature and residence time. Two process variations can be distinguished depending on the temperature in the chamber. One proceeded at ambient temperature (24 °C) and required residence times in the range of minutes. The most used coating chamber at 24 °C had a volume of 4.2 L. In the second, the aerosol mixture was heated in a small tube furnace ( $V = 0.1$  L) to 100 - 300 °C, which reduced the required residence times significantly (to seconds). The residence time of the coating mixture in the system was controlled by the volume of the respective tube and the volume flow through it. Since reactive species such as ozone and nitrous oxides

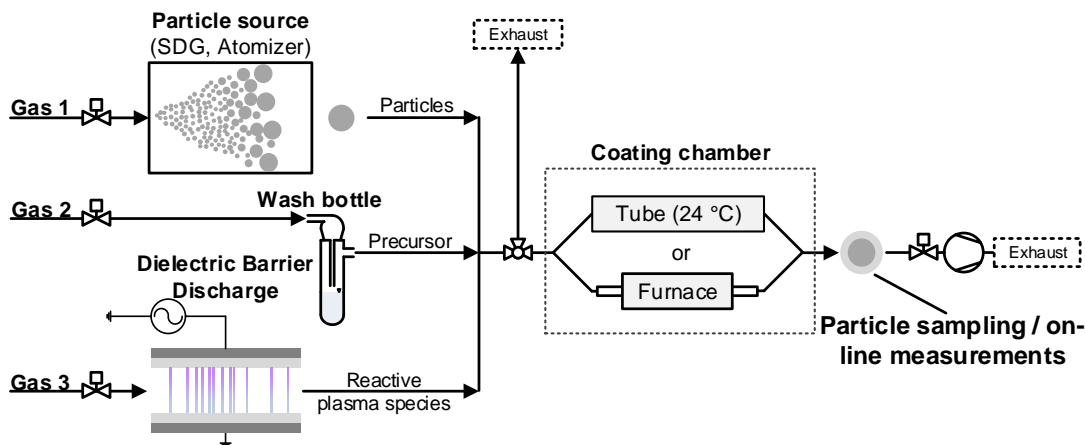


**Fig. 3.1:** Overview of the coating process with the pathways for the particles, the precursor and the plasma species. After mixing, the aerosol was introduced into the coating chamber, which was either a glass tube at 24 °C, a tube furnace with up to 300 °C or a combination of both.

were present in the process, a chemically resistant pump (KNF Laboport) was used. To prevent pulsation in the pumped gas flow, a vacuum tank was used as a buffer between coating chamber and pump.

For most of the experiments, filtered, pressurized air was chosen as carrier and discharge gas, because of its low price and availability, which makes it interesting for a potential scale up at a later stage. Other gases used included synthetic air as well as mixtures of  $N_2$  (99.999 %), He, Ar and  $O_2$ . If a spark discharge generator was used as the particle source, nitrogen was used mostly as particle carrier gas to prevent oxidation of the SDG electrodes. The volume flows were chosen to be within the common range of lab scale experiments. The particle carrier gas flow (Fig. 3.1, Gas 1) was typically 1 L/min, the precursor carrier gas flow (Gas 2) between 7 and 125 mL/min, and the discharge gas flow (Gas 3) 2 L/min.

## 3.2 Production of core particles

### 3.2.1 Spark discharge generator

A SDG is a simple solution for the lab-scale production of aerosol nanoparticles. Fig. 3.2 illustrates the used device. In a SDG, two electrodes with a gap of a few mm between them are connected to a high voltage DC power supply with a capacitor connected in parallel. The capacitor is charged by the power supply and when the voltage threshold for gas breakdown is reached, the energy is discharged in the form of a spark between

the electrodes. This discharge voltage is primarily dependent on the discharge gap, the gas composition and the gas pressure. The discharge frequency (number of discharges per time interval) is dependent on the capacity of the capacitor and the applied electrical current.

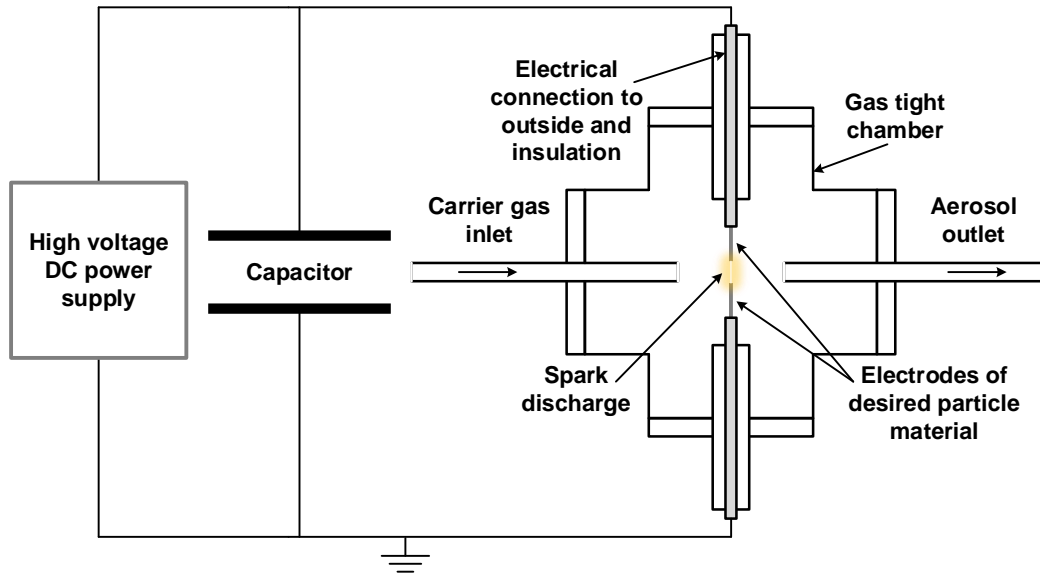


**Fig. 3.2:** Schematic of the spark discharge generator setup (not to scale).

The particle formation in a SDG is a purely physical process, which allows the production of aerosols without any by-products in the gas [82, 83]. The high energy and high local temperatures of the spark – a form of a thermal plasma – vaporize material from the electrode surfaces. The vapor forms droplets in the gas by nucleation and subsequent condensation, which then solidify to particles. The size of these primary particles is typically around 5 nm and depends on the material and discharge parameters. Due to the high local particle concentration, these particles agglomerate rapidly and form large agglomerates, when this is not prevented, e.g. by a fast dilution. The material of the particles can be controlled easily by the choice of the electrodes. Typically, metal electrodes are used, but other electrically conductive materials are also possible. The produced mass of the aerosol is generally limited to a few  $\mu\text{g/h}$  to  $\text{mg/h}$ .

For this thesis, a SDG was used for the production of metal and metal oxide particles. Platinum (Pt), Gold (Au), Silver (Ag), Copper (Cu), Nickel (Ni), Iron (Fe), Titanium (Ti) and Zinc (Zn) were used as electrode materials. Due to the increased oxidation tendency of small nanoparticles in comparison to bulk materials, only Pt and Au showed no oxidation. A capacitor of 24 nF and a discharge gap of about 2 mm were used for the experiments. The current was often around 1 mA (about 2 to 3 Hz discharge frequency), but could be changed to control the concentration and size of the produced particles.

### 3.2.2 Atomizer

An atomizer was used for the production of aerosols from particle suspensions or salt solutions. There are different types of atomizers, such as pressure, pneumatic, ultrasonic or electrostatic atomizers, defined by their type of operation [84]. A simple pneumatic atomizer was used here (Topas ATM 220), where a liquid was sprayed into small droplets with a two-substance nozzle. The droplets were subsequently dried in a silica gel dryer, leaving the solid aerosol particles in the carrier gas (Fig. 3.3).

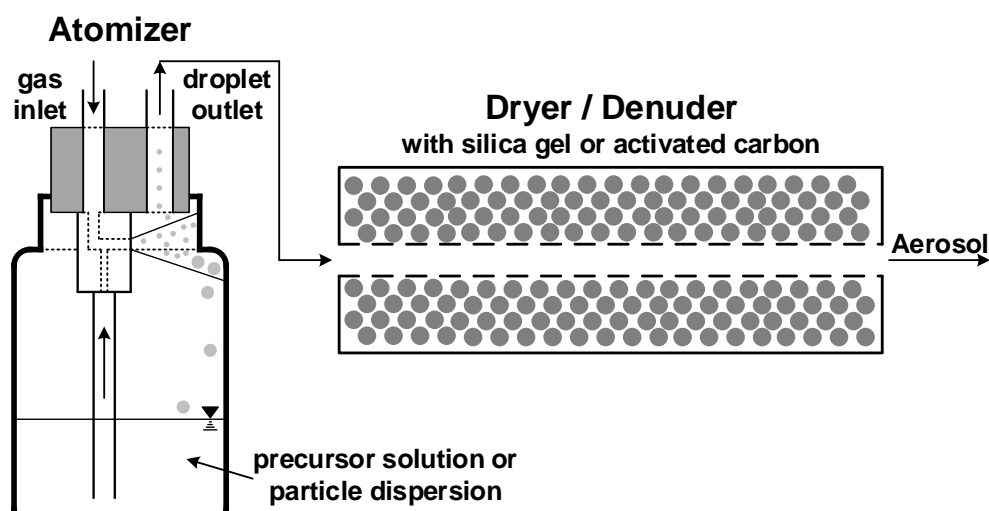


Fig. 3.3: Schematic of the atomizer setup (not to scale).

The liquid suspension or solution was kept in a 100 mL glass bottle. A two-substance nozzle was used, which consisted of a carrier gas inlet, where pressurized gas (1.5 bar) passed a small orifice and thus accelerated to high velocities before exiting the nozzle. This resulted in a reduced pressure because of the Bernoulli Effect. Another drill hole connected a tube from the liquid reservoir to this part, which caused the liquid to be sucked upwards and to be sprayed out of the nozzle in the form of droplets. The produced droplets followed a certain size distribution depending on atomizer geometry and gas velocity. The droplet outlet from the device was in the cap above the spray. Due to their inertia, bigger droplets hit the side of the glass and fell back down into the liquid, while small droplets followed the carrier gas out of the device. These droplets contained the particles or solution. In a subsequent step after the atomizer, the liquid was removed in a denuder, which consisted of a penetrable tube through a packed bed of either silica gel to remove water or activated carbon to remove organic liquids. In most experiments the atomizer was operated with 1.5 bar pressurized air, which resulted in an aerosol gas flow of 1 L/min.

## 3.3 DBD reactors

### 3.3.1 Cylindrical DBD reactor

A dielectric barrier discharge is used to provide reactive species to the system. On a basic level, a DBD reactor consists of two electrodes connected to a high voltage AC power supply with at least one dielectric and a small gap with the discharge gas between them. Many different geometries are possible as long as these requirements are fulfilled. A cylindrical DBD reactor was used in Publication 1 (Fig. 3.4). Here, the discharge area was between two concentric electrodes with a difference in electrode surface area between the inner and outer electrodes. Hence, the discharge was asymmetric, which means that the ion avalanches leading to the discharge were somewhat different for each reverse of polarity. However, this should make no significant difference in the chemical composition in the post-discharge environment, since the time scales are very short.

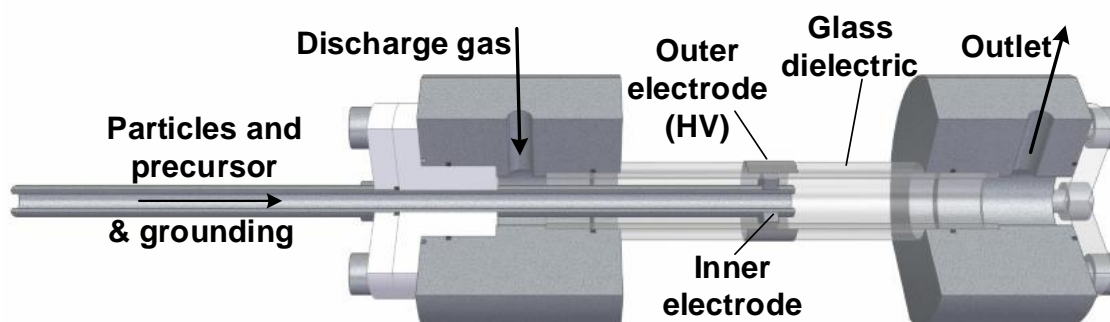


**Fig. 3.4:** CAD drawing of the cylindrical DBD reactor (partial cross section).

A quartz glass tube was used as both the dielectric and as gas tubing. Two stainless steel parts held a quartz glass tube with an inner diameter of 13 mm and a thickness of 1.5 mm that acted as the dielectric. These steel parts also contained all gas connectors and the right one contained a window that allowed the direct observation of the discharge. The total length of the reactor from the outsides of the steel parts was about 13 cm. The electrode on the outside of the glass tube was made of copper adhesive tape and connected to the high voltage AC power supply. A stainless steel disc with a diameter of 12 mm and a length of 2 mm was attached to the grounded central stainless steel tube. The edges of this disc were slightly smoothed to reduce their influence on the discharge characteristics. The discharge occurred in the 0.5 mm ring-shaped gap between the metal disc and the dielectric glass tube. The inner tube could be moved in all directions with the help of a modified lens mounting from outside the reactor, which allowed the central alignment of

the disc (not shown, left of the reactor in Fig. 3.4). The reactor had two separate gas inlets for the aerosol and precursor mixture and the discharge gas. The gases were mixed directly after the disc electrode to start the coating. For the experiments in Publication 1, the discharge was run with 2 L/min of a 1:1 mixture of air and nitrogen.

A Kalwar power generator was used to supply the high voltage to the outer electrode. The device produced a sinusoidal voltage with a frequency of 41 kHz. The electrical characteristics for these conditions were studied with an oscilloscope (Rhode & Schwarz HMO2024). To characterize the electrical behavior of a DBD reactor, the temporal voltage and current curves and the discharge power in dependence on the applied voltage are especially interesting. The applied voltage is directly controlled by the power supply and needs to be measured with a high voltage probe, since voltages in the range of a few kV are typically required to start the discharge. A Tektronix P6015A 1000x voltage probe was used for this purpose. In contrast, the currents observed in lab-scale DBDs are comparatively low and can be measured directly without an attenuator probe. Since an oscilloscope can only measure voltages, the current is recorded indirectly over a resistor. A BNC coaxial cable with a length of about 0.9 m with two 50  $\Omega$  resistors on the end caps was used. According to Ohm's law, the measured voltage can be converted to the current with  $I = U/R$ . Fig. 3.5 (left) shows the voltage and current signals for the cylindrical reactor with the expected phase shift between them. The current exhibits pulses indicating the microdischarge activity of the air plasma [10]. The negative pulses of filaments going from the inner electrode to the surface area are slightly larger than the positive ones going in reverse, which is typical for an asymmetrical DBD with only one dielectric (mono-DBD).

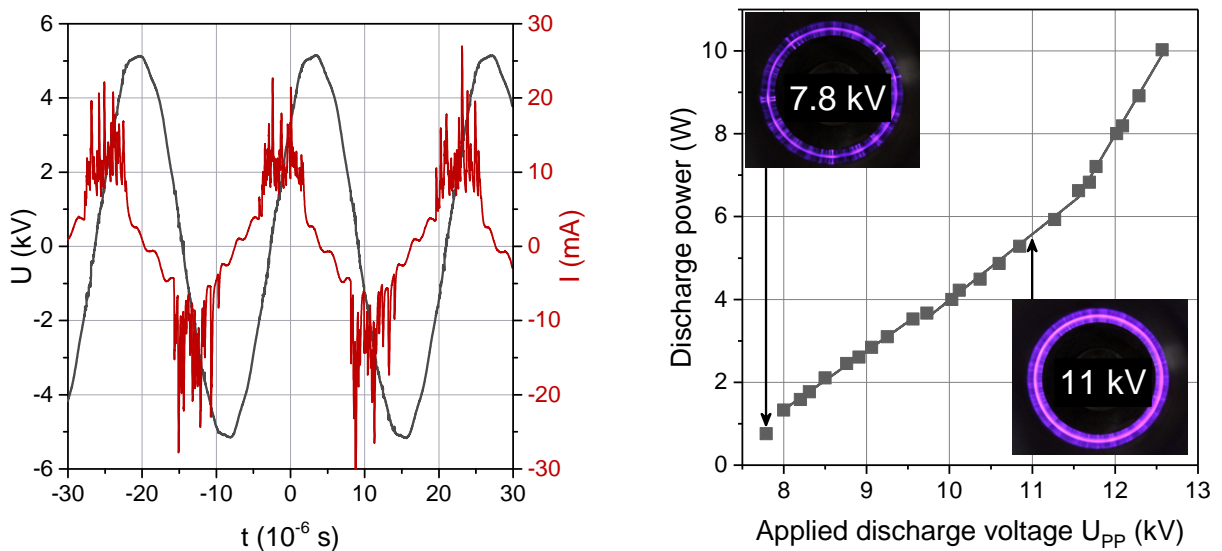


**Fig. 3.5:** Electrical behavior of the cylindrical DBD reactor with a 1:1 mixture of filtered air and nitrogen.

The measurement of the exact discharge power of a DBD is quite difficult, since it is

distributed over many short-lived microdischarges. However, in many cases the knowledge of the average discharge power is sufficient. It can be determined by different methods. An easy and common one is the use of so-called Lissajous figures. They allow the measurement of the discharge power by calculating the area of the parallelogram of the applied voltage and the capacitive charge and multiplying this by the frequency. The charge can be acquired by measuring the voltage over a capacitor of known capacity in series with the discharge. Here, a capacitor of 10 nF was used. Another option is the calculation of the power from the voltage and current according to:

$$P = \frac{1}{n \cdot t_P} \cdot \int_{n \cdot t_P} u(t) \cdot i(t) dt$$

which was used for this reactor. As shown in Fig. 3.5 (right), the discharge power in this reactor followed up to three different linear behaviors in the measured voltage range. This seems related to the different states of discharge ignition on the inner disc electrode. First, the filaments originate only from the edges of the electrode, since this is where the electric fields are highest, before they get distributed over the whole surface area at higher voltages. The pictures of the discharges shown in the figure visualize two different discharge conditions.

### 3.3.2 Plate-to-plate DBD reactor

The second DBD reactor had a symmetrical plate-to-plate geometry, which is shown in Fig. 3.6. This setup was used in Publications 2, 3 and 4. The mixing of the plasma species with the particles and precursor took place after the reactor, instead of the direct mixing in the cylindrical reactor, which reduced the necessary cleaning. The main advantages of this reactor in contrast to the cylindrical one were the symmetrical discharge and easier discharge gap alignment, which should result in a more uniform discharge. Furthermore, the reactor used two dielectrics and hence should produce less particles by corrosion of the electrodes. The dielectrics were alumina plates with a size of  $70 \times 57 \times 2$  mm. The electrodes consisted of self-adhering copper tape on the outsides of these dielectrics, with a size of  $27 \times 27$  mm. The electrode connected to the high voltage power supply was electrically insulated with silicone adhesive to prevent discharges on the outside of the reactor. The two alumina plates were mounted in an aluminum frame that contained the gas connections. The reactor was sealed with PTFE sheets placed between the two frames, into which the flow canal for the discharge gas was cut. Hence, the discharge gap was the total thickness of these compressed sheets of 1 mm. For most experiments, the discharge was operated in 2 L/min pressurized air. A Redline G2000 was used as the high voltage power supply for the experiments with the plate-to-plate DBD reactor. For this device, a sinusoidal voltage was found at a frequency of 106.8 kHz, which was hence used

for the experiments.

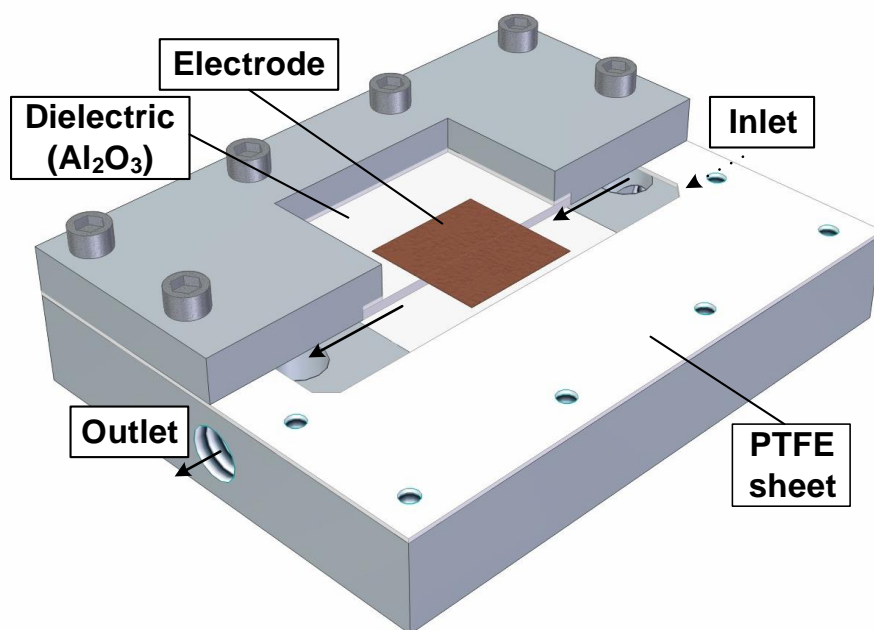


**Fig. 3.6:** CAD drawing of the plate-to-plate DBD reactor (partial cross section).

Analogous to the characterization of the cylindrical DBD, Fig. 3.7 shows the voltage, current and power behavior of the plate-to-plate DBD. The left figure represents the behavior for the lowest stable discharge voltage of 10.6 kV, which was used for most experiments. It is apparent that the supplied voltage was not perfectly sinusoidal with slight differences in the positive and negative parts. However, it was constant even over long time periods. In contrast to the cylindrical DBD, the microdischarges in the plate-to-plate DBD caused much larger current peaks. It is important to note that this reactor was operated with air in contrast to the air/nitrogen mixture, which changes the discharge environment. Furthermore, large peaks do not necessarily indicate a higher power of individual discharges, but could rather be multiple discharges taking place simultaneously, due to the about ten times larger surface area of the electrodes. As expected in a symmetrical DBD with two dielectrics, the positive and negative discharges were similar on average.

The discharge power was measured with the Lissajous figure method described earlier. In the voltage range measured, the power increased linearly with the applied voltage (Fig. 3.7, right). This indicates that there were no discernible differences in the discharge distribution on the surfaces. In comparison to the cylindrical DBD, the total discharge power was higher. For the lowest possible discharge voltage around 10.6 kV, the outside electrode temperature was about 50 °C and increased to up to 95 °C at 12.09 kV.



tube was not immersed into the liquid to prevent the formation of droplets and reduce the concentrations. A carrier gas flow in the range of mL/min was saturated in the wash bottle and introduced into the coating system. Air was used most of the time. Since HMDSO has a higher vapor pressure (Tab. 3.1), it was necessary to cool the liquid with an ice bath to reduce the introduced concentration to a usable amount. During experiments, the precursor concentration in the system was controlled by the carrier gas flow. The temperature and fill level were kept constant. Since the precursor masses used in the experiments were very small (too small to easily weight), additional precursor practically only needed to be refilled during long experiments (6-8 h) with HMDSO.

### 3.5 Characterization methods

Multiple methods were used to analyze the process and the particles. However, since these were mostly techniques common in aerosol research, this section will only give a brief overview of aspects especially relevant for this thesis.

**Transmission electron microscopy (TEM)** The transmission electron microscopy is an established technique for the analysis of small particles. It allows the imaging of particles deposited on a specialized sampling device, the so called TEM grid. These TEM grids are a few mm in diameter and consist primarily of a metal mesh (e.g., copper or nickel) that gives the grid some stability. The mesh is covered with a thin carbon film, on which the particles are deposited and which does not significantly hinder the electron transmission. Different kinds of grids were deployed for this thesis. The classical grid, where the mesh is completely coated requires sampling from a powder sample such as a filter or some force to deposit the particles from a gas (e.g., inertia force), while the incompletely coated Lacey grid allows the direct sampling from a gas flow due to its porosity. The TEM used was a JEOL JEM 2100. In most cases, the coatings had very sharp and defined edges and were clearly distinguishable from the background. However, in some samples they exhibited blurry and less defined edges in the micrographs. This was typically observed for conditions where a complete solidification of the coatings was not guaranteed (i.e. high precursor concentrations combined with short residence times). Hence, this was interpreted as a sign for shells, which solidified on the sample grid and not in the gas phase. Fig. 3.8 illustrates both scenarios.

An energy-dispersive X-ray spectroscopy sensor (EDX, OXFORD Instruments X-Max<sup>N</sup> 80 T) was integrated into the TEM and allowed the analysis of the atomic composition of the TEM sample. Since the resolution of the device was limited, it provided an average value over a few particles, but could not characterize individual particles or particle parts.

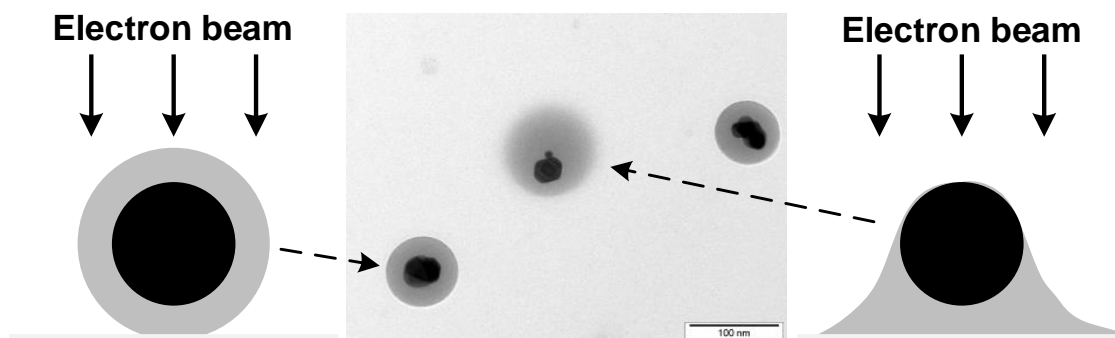


**Fig. 3.8:** Possible interpretation of differences observed in coated particles in the TEM. The coating might either solidify in the gas phase or on the TEM grid.

**Fourier-transform infrared (FTIR) spectroscopy** The Fourier-transform infrared spectroscopy is a common technique to identify chemical compounds. It is based on the absorption of electromagnetic radiation in the form of infrared light by the sample, which results in different forms of atomic excitation such as bending or stretching. The device used here was a Bruker Tensor 27. Powder samples were pressed into small discs, while a 22 cm long cell was used for gases.

FTIR spectroscopy can be used both for qualitative analysis as well as quantitative measurements. The challenge of the qualitative analysis lies in the assignment of the vibration bands, especially when unknown compounds or a mixture of different compounds are present in the sample. Relevant bands for coatings were acquired from the literature, such as [87, 88] for common organic groups and [8, 89, 90, 52] for silica and silica-organic bands.

Quantitative analysis is possible with FTIR, but requires knowledge of the absorption coefficient of the material. The relationship between the analyte concentration and the IR signal is given by the Lambert-Beer law:

$$\log \frac{I_0}{I} = A = a \cdot b \cdot C \quad (3.1)$$

with  $I_0$  the incident light,  $I$  the light after the sample,  $A$  the absorbance (peak height),  $a$  the absorption coefficient,  $b$  the sample thickness or length of the sampling chamber and  $C$  the analyte concentration. For common substances, absorption coefficients can sometimes be acquired from the literature. However, for rarer analytes a calibration is required. This was done for TEOS, where the gas cell was filled with the precursor until the liquid level was directly below the measurement beam. This allowed the measurement of the absorbance of the saturated gas, which had a known concentration (vapor pressure). However, even without a calibration, different concentrations of the same substance can

be compared to each other in the same measurement setup, due to the linear dependence of concentration and absorbance.

**X-ray photoelectron spectroscopy (XPS)** X-ray photoelectron spectroscopy, sometimes called electron spectroscopy for chemical analysis (ESCA), is a spectroscopy technique that measures the elemental composition of samples. One of its main advantages is the small penetration depth of typically less than 10 nm, which allows detailed information about the surface of the samples. XPS uses the photoelectric effect that describes the emission of electrons when a material is irradiated with electromagnetic radiation. The measurements were done by the Institute of Energy Research and Physical Technologies (TU Clausthal) and the device is described in Publication 3.

**Scanning mobility particle sizer (SMPS)** A scanning mobility particle sizer was used for the measurement of particle number distributions. The commercial device consisted of a Grimm 5.403 CPC (condensation particle counter) and a Grimm 55-40-26-Uni DMA (differential mobility analyzer). Alternatively, some experiments were conducted with an IMVT-built SMPS setup, consisting of a radial DMA (RDMA) and a faraday cup electrometer (FCE). This setup was much more robust concerning the gas environment, but also less sensitive, requiring higher particle number concentrations. For coated nanoparticles, an SMPS allows the monitoring of changes in particle sizes in dependence on the process parameters and one should hence be able to determine the coating thickness from the change in diameter. This requires spherical particles for meaningful results. Furthermore, the method requires a stable particle source in regard to the produced particle sizes and their number concentration. A common method to monitor particle distribution changes is the so-called tandem DMA setup. Here, a DMA is used directly before introduction of the particles into the coating setup. This ensures a constant size of the introduced particles and simplifies the interpretation of the data. However, a classification by a DMA always results in a significant reduction in the number concentration, since only a part of the distribution and only charged particles pass the device.

**Low pressure impactor (LPI)** In Publication 4, a low pressure impactor was used for the measurement of the fragmentation behavior of particles and their rebound from a surface. As the name suggests, an LPI is an impactor being operated in a low pressure environment. This allows high particle velocities and hence the inertial deposition of nanoparticles onto a target. The degree of fragmentation of particles on the target can be related to their mechanical stability and the ratio of initial to remaining particle concentration to the rebound. The setup is explained in detail in Publication 4.

# CHAPTER 4

---

## Process control

---

### 4.1 General considerations

As shown in section 1.2.3, the most common way to achieve coatings in plasma processes is the introduction of the particles and precursor directly into the discharge zone to utilize the high reactivity of the plasma environment. In this work, due to the problems this poses for a continuous coating process, particles and precursor were instead mixed with the plasma species after the discharge. However, even though the environment downstream of a dielectric barrier discharge is still characterized by much higher concentrations of reactive species than those found in ambient gases, it is in many regards less reactive than the plasma itself. Hence, one of the first questions was whether such a process can be used for the coating of particles and which parameters influence the coating.

A successful particle coating process is characterized by requirements such as the formation of coatings at all, a controllable coating thickness, a good homogeneity of the coatings and the desired chemical composition of the coatings. It is also important to have information about the efficiency of the process, e.g. the amount of particles lost during the process. These characteristics might be influenced by different process parameters, such as the discharge properties (e.g., applied power or gas composition), the chosen precursor and its concentration in the system, the residence time of the particles in the system, the core particle properties (e.g., material, surface area, morphology) and the temperature and pressure in the system. Since the process was developed for the coating of particles from different continuous synthesis methods, most of which work at atmospheric pressure, the pressure was kept constant at atmospheric conditions. However, as discussed in the literature overview, plasma discharges can be operated at low pressures, which should also be possible here.

The experimental results in this chapter will first demonstrate the general feasibility of the presented process with the example of the coating of particles with silica, which

is described in Publications 1 and 2. The chemical composition and the influence of the core material will be discussed separately in chapter 5, which covers the different material combinations studied in this thesis.

## 4.2 Formation of coatings in the post-discharge environment

The first and most important requirement of a particle coating process is the actual formation of coatings on particles. In this post-plasma CVD process, this depended very much on the chemical environment provided by the discharge. Hence, it is important to first characterize the chemical environment in the coating chamber. Many of the short living species present in the discharge do not participate in the coating reactions in the post-discharge. This affects for example the radicals, which are only stable in the ns to  $\mu\text{s}$  range [9]. However, new radicals and other very reactive species might be produced by consecutive reactions, such as decomposition reactions of more stable species.

The detection of these very short-lived species requires specialized methods [12], which were outside the scope of this thesis. However, information about some of the more stable species present in the post-discharge coating environment can be acquired with an FTIR spectrometer by analyzing the gas composition during different process conditions. In the air plasma of the plate-to-plate reactor,  $\text{O}_3$ ,  $\text{N}_2\text{O}$ ,  $\text{HNO}_3$  and  $\text{N}_2\text{O}_5$  were found in the gas a few seconds after the discharge with the standard discharge voltage of 10.6 kV. The absence of  $\text{NO}_2$  and the presence of  $\text{O}_3$  indicate a comparatively cold discharge, which is confirmed by the low electrode temperatures (measured on the outside) of  $< 50^\circ\text{C}$ . The composition of the species in the exhaust was dependent on the residence time in the system since their individual stabilities vary. The concentrations of the plasma species can be calculated with the Lambert-Beer law, as described in section 3.5. This was done for different residence times for the four plasma species found, as shown in Fig. 4.1 (left). The data points show the average concentrations from three different experiments that were conducted on different days, up to 2.5 months apart. The error bars denote the standard deviation. The first data point (0 min) corresponds to the measurement of the plasma exhaust before the residence time tube. It was found that ozone had the highest concentration (243 ppmv), with dinitrogen pentoxide, nitric acid and nitrous oxide significantly lower at 41, 36 and 8 ppmv, respectively. The data points for the longer residence times were acquired in the exhaust after the glass tube with varying volume flows. With increasing residence time, the  $\text{N}_2\text{O}_5$  concentration decreased to zero between 3 and 4 min, while the amount of  $\text{HNO}_3$  increased to around 60 ppmv in the same time. This is probably due to the reaction of  $\text{N}_2\text{O}_5$  with water vapor according to

[91]:



that is known to take place homogeneously in the gas phase and heterogeneously on particles or other surfaces. Since pressurized air was used, some water vapor was present in the system.  $\text{N}_2\text{O}$  showed no significant time dependent change in concentration, which indicates that it was stable in this time scale.  $\text{O}_3$  fell by about 20 ppmv ( $< 10\%$ ) in the studied time frame.

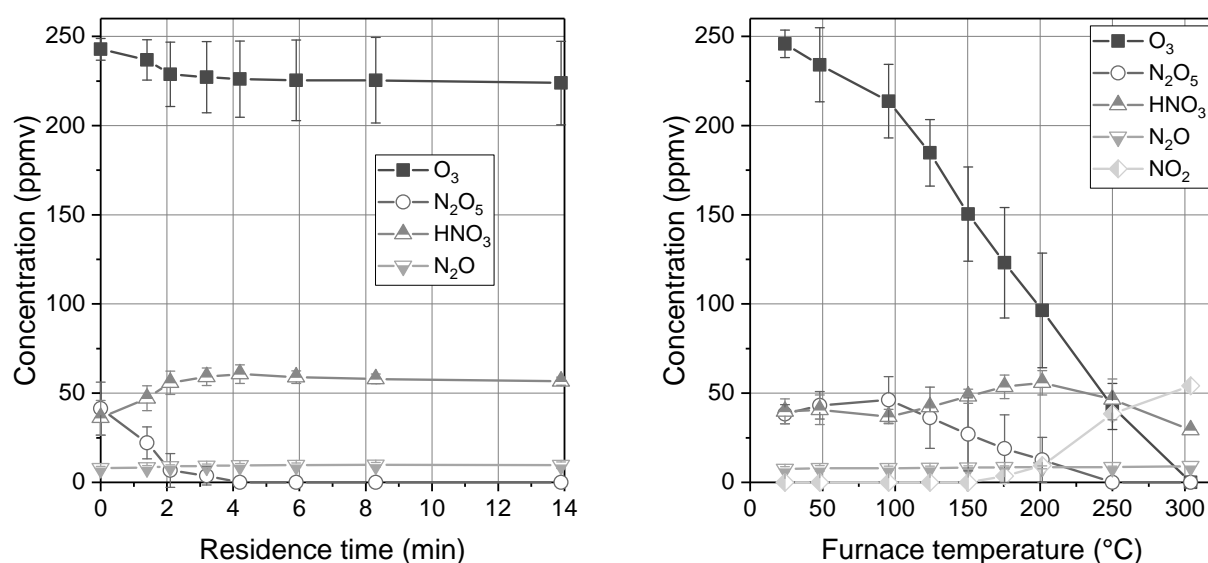
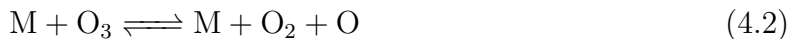


**Fig. 4.1:** Time and temperature dependent concentrations of the plasma species in the post-discharge environment of the plate-to-plate DBD reactor (10.6 kV). Left: at ambient temperature, right: with a residence time of 3 s (24 °C).

Furthermore, the influence of the temperature in the coating chamber on the gas composition was studied. The species concentrations for different furnace temperatures are shown in Fig. 4.1 (right). It was found that the  $\text{HNO}_3$  concentration showed a small increase before decreasing above 200 °C.  $\text{N}_2\text{O}_5$  showed a similar trend, but already decreased above 100 °C.  $\text{N}_2\text{O}$  showed no significant temperature dependent change.  $\text{NO}_2$  was observed at temperatures above 175 °C, presumably as a product of the depletion of the other nitric oxides and ozone. However, the biggest change was observed in the ozone concentration, which showed a significant temperature dependent decrease starting above ambient temperature and a complete disappearance at 300 °C. It is believed to

decompose according to the following reaction schemes [92]:



where M denotes a third party molecule. The rate of decomposition is very dependent on the temperature. As shown, the decomposition involves the formation of an oxygen radical. This radical is not stable and will quickly react to form more stable species. However, within the gas volume where the radical formation takes place (i.e. the tube furnace), a chemically very reactive environment is produced for a short time. If other molecules, such as a coating precursor, are present in the direct vicinity of the ozone decomposition, the radicals react with these molecules and start the coating formation [48, 37]. Since this chemical environment is much more reactive than the post-discharge environment at ambient temperature, the coating formation is significantly faster. In fact, the higher temperatures were required to obtain coatings with HMDSO. The disadvantage of these higher temperatures is the thermal strain on the aerosol particles. Experiments showed that it is not sufficient to mix the precursor and particles directly after the heated plasma exhaust, due to the very short life time of the radicals. While theoretically only the precursor and not the particles need to be present in the heated gas, the reactions were too quick to form homogeneous coatings if the activated precursor and the particles were mixed after the furnace. Without the addition of the plasma species, thermal decomposition of TEOS in the system was not observed below about 500 °C after 8 s residence time.

Obviously, the plasma discharge has a significant influence on the post-discharge environment and hence the possibility of coating formation. In the case of coatings with TEOS at ambient temperature using the cylindrical DBD reactor, it was found that no coatings were formed when a high discharge voltage was applied. Fig. 4.2 shows this for sintered Pt particles and three different applied voltages of 8, 10 and 12 kV (peak-to-peak). While for 8 and 10 kV similar coatings were observed on the particles, no coating was formed on the sample with 12 kV discharge voltage.

This seems related to the different discharge temperatures and the resulting produced species. Tab. 4.1 shows the electrode (outside) temperatures and the observed concentrations of species at these conditions. The main differences between the first two conditions, where coating formation was observed, and the condition without formation were the temperatures in the discharge zone. This resulted in changes of the composition of the post-discharge gas with different plasma species, due to their individual thermal stabilities. In particular, the concentrations of O<sub>3</sub> and N<sub>2</sub>O<sub>5</sub> fell to zero at 12 kV. This might indicate an importance of these species for the coating mechanisms at 24 °C.

A similar observation was found for the plate-to-plate reactor with air. Here, the

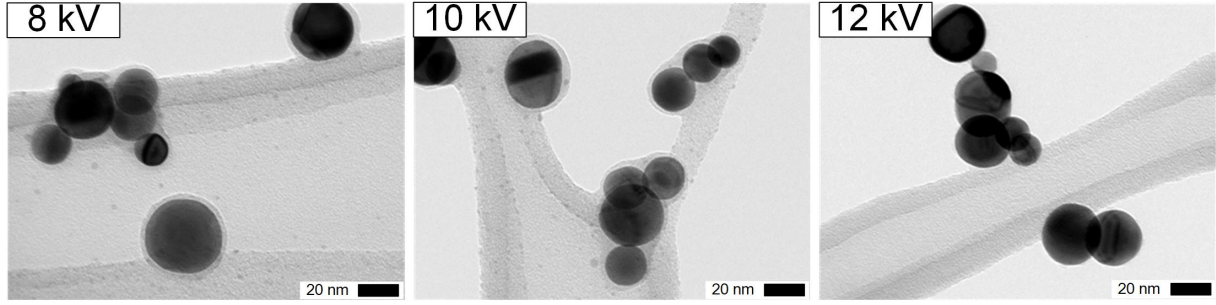


**Fig. 4.2:** Dependence of the coating formation on sintered Pt particles with TEOS and the cylindrical DBD reactor on the applied discharge voltage. Homogeneous coatings were found with  $U_{PP} = 8$  and 10 kV, but not 12 kV.

**Tab. 4.1:** Electrode and reaction temperatures and ozone and  $\text{NO}_x$  concentrations (in ppmv) for three DBD voltages with the cylindrical DBD reactor run with a 1:1 mixture of air and nitrogen.  $\text{HNO}_3$  could not be quantified, due to significant interference.

$U_{\text{DBD,PP}}$ (kV)	$T_{\text{electrode}}$ ( $^{\circ}\text{C}$ )	$\text{O}_3$	$\text{NO}_2$	$\text{N}_2\text{O}$	$\text{N}_2\text{O}_5$	NO
8	33	296	23	2	10	0
10	46	301	20	20	24	0
12	120	0	76	38	0	0

influence of the plasma gas volume flow was studied by changing the flow through the discharge zone between 0.5 and 2 L/min and measuring the exhaust with the FTIR. The other volume flows in the system were changed to keep the total volume flow during measurement constant, preventing dilution. It was observed that this had a significant influence on the plasma species found after the discharge. A reduction in the gas flow resulted in a decrease of the concentrations of  $\text{O}_3$  and  $\text{HNO}_3$  and an increase in the NO concentration at 0.5 L/min. This is very similar to the influence of the applied voltage and might also be related to the discharge temperatures. TEM micrographs of the powders coated with the different volume flows showed that with decreasing volume flow the coating thickness decreased and became less homogeneous. From a product design standpoint, the results indicate that the discharge needs to be kept within a certain temperature range, with higher temperatures decreasing the coating homogeneity until no coating can be acquired.

To study which plasma species might be especially important for the coating, different gas mixtures were used as discharge gas. The TEOS concentration was monitored with the FTIR as an indicator for the reaction. The original TEOS concentration (without plasma) was used as the reference and compared with the concentration with plasma at post-discharge temperatures of 24 or 300  $^{\circ}\text{C}$  (Tab. 4.2).

It was found that both air and synthetic mixtures of oxygen and nitrogen resulted

**Tab. 4.2:** TEOS depletion in the post-discharge with different plasma gas mixtures measured with FTIR (✓ shows depletion). Each measured both after 8.3 min at ambient temperature and after 4 s at 300 °C.

Gas mixture	Species found (24 °C)	24 °C	300 °C
Air or air + N <sub>2</sub>	O <sub>3</sub> ,N <sub>2</sub> O,N <sub>2</sub> O <sub>5</sub> ,HNO <sub>3</sub>	✓	✓
N <sub>2</sub> + 20 vol.-% O <sub>2</sub>	O <sub>3</sub> ,N <sub>2</sub> O,N <sub>2</sub> O <sub>5</sub> ,HNO <sub>3</sub>	✓	✓
Ar + 20 vol.-% O <sub>2</sub>	O <sub>3</sub>	x	✓
He + 20 vol.-% O <sub>2</sub>	O <sub>3</sub>	x	✓
N <sub>2</sub>	small amount of N <sub>2</sub> O	x	x

in the production of similar species and a reduction of the TEOS concentration at both temperatures. In this process with air, TEOS and also chemically similar compounds, such as Triethoxymethylsilane, can be used to coat particles at ambient temperature. Reactions were observed with pressurized air or a mixture of nitrogen and oxygen (synthetic air). However, with synthetic air the conversion at 24 °C was somewhat lower for long residence times with about 75 % conversion of TEOS after 14 min vs. 94 % with pressurized air (up to 6 min both were similar). When only nitrogen 5.0 was used, small amounts of N<sub>2</sub>O were found, which was possibly due to small oxygen impurities in the gas or desorption from walls. However, this could not enable the reaction and no TEOS reduction was observed at either temperature. The presence or absence of core particle also made no difference on whether TEOS could be depleted during the measurements, indicating gas phase reactions. It would be obvious to assume that the same reactions take place at both temperatures with the slower rate at 24 °C being a purely kinetic effect. However, this seems not to be the case. Experiments with an Ar or He/O<sub>2</sub> mixture as the plasma gas showed that ozone alone (as observable species) was sufficient to cause a clear reduction of the TEOS concentration at 300 °C. This indicates ozone and the resulting oxygen radicals as an essential part of the reactions, which fits with models developed for a similar substrate coating process [48, 37]. However, when argon or helium were used together with oxygen to produce ozone without nitric oxides at 24 °C, no change in the TEOS concentration could be observed. This shows that ozone alone might not be responsible for the start of the reactions at ambient temperatures. Further experiments indicated that the concentration of H<sub>2</sub>O has an influence on the reaction kinetic at 24 °C and hence seems to be involved directly or indirectly with the reactions. However, the use of H<sub>2</sub>O without the plasma or even a mixture of H<sub>2</sub>O and HNO<sub>3</sub> with similar concentrations as in the plasma process, to check whether similar reactions as known from the liquid phase take place, showed no depletion of TEOS in the experimental time frames. In conclusion, the experiments preliminarily indicate that only ozone or rather oxygen radicals need to be present for a successful coating with TEOS or HMDSO at elevated temperatures.

However, the reactions of TEOS at 24 °C seem to involve more reactants that are exclusive to air discharges.

## 4.3 Control of the coating thickness

### 4.3.1 By TEOS concentration and aerosol residence time

The coating thickness is one of the most important product parameters of core-shell particles since it can define important product properties such as the permeability. The most straightforward way to control the coating thickness on the particles is the control of the initial precursor concentration added into the system and the aerosol residence time between mixing and sampling. The precursor concentration controls the amount of total mass available for the shell, while the aerosol residence time corresponds to the degree of overall conversion of the precursor to the finished product. Fig. 4.3 (left) shows the dependence of the average coating thickness on the particles as a function of the TEOS concentration at 24 °C. The particles were size classified with an RDMA prior to the coating and measured with an SMPS and TEM after 1.4 min in the coating chamber. The coating thickness was determined from the shift of the SMPS-measured particle size distributions and by image analysis from the TEM micrographs. It was found that no coating was formed in the system without the species from the plasma discharge, as neither the SMPS nor TEM measured sizes changed. With the plasma present, a significant increase of the particle size was measured with the SMPS and the TEM micrographs showed coatings. However, there was a significant difference in the coating thickness observed with the SMPS and with TEM, with the SMPS showing much thicker coatings. This can be explained with a difference in the measurement conditions. While the SMPS measures in-situ in the system after the sheet air has been saturated with the system gas, the TEM sample needed to be removed from the system and was then introduced into the vacuum of the microscope. The low pressure causes liquid compounds to evaporate from the sample, leaving only solidified material behind when the micrographs are obtained. If parts of the shells are not hardened, these parts are removed in TEM, while they are still measurable in-situ by the SMPS. Here, this indicates that a liquid intermediate is formed that covers the particles and causes the increase in the SMPS-measured size. This cannot have been caused by condensed TEOS or a change in particle size, since without the discharge no shift was observed. The diagram also seems to indicate that the hardening rate of the shells limits the coating thickness more than the formation of liquid intermediates on the core particles, since an increase in the TEOS concentration resulted in an increase in the SMPS measured thickness, but the TEM measured one became constant.

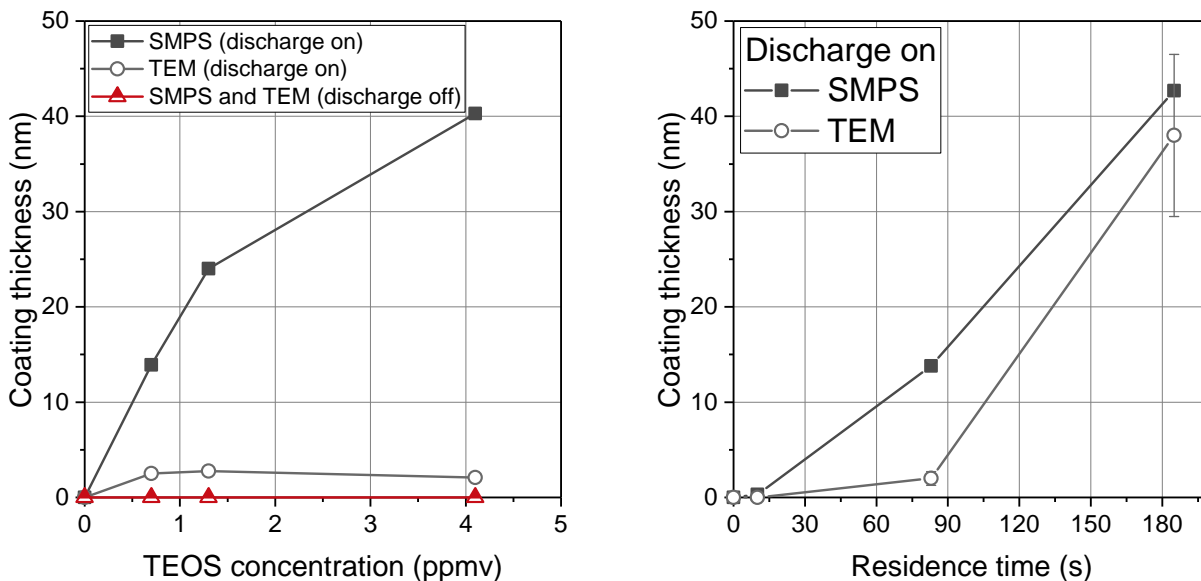


**Fig. 4.3:** Coating thickness of size classified sintered Pt particles measured with SMPS and TEM in dependence on the TEOS concentration (24 °C, cylindrical DBD) for 83 s aerosol residence time (left) and as a function of the reaction time for 0.7 ppmv TEOS (right).

The big influence of the aerosol residence time on the coating thickness is evident in Fig. 4.3 (right). Here, the initial TEOS concentration was constant while the residence time was changed. The coating thickness increased significantly with increasing residence time, both in the SMPS and the TEM measurements. This shows that the conversion to the coating in this residence time range was quite low, but increased with increasing residence time. This seemed to include both the formation of the liquid intermediate as well as the solidification of the silica shell.

The liquid intermediates might be silanol oligomers of varying length that continuously polymerize until a solid coating is formed, as known from processes at elevated temperatures [48, 41] and indicated by Si–OH groups in the coatings (see section 5.1). A basic model of the process that can explain most results shown in this thesis would include two important steps: The formation of liquid intermediates and the solidification to the silica coatings. The liquid intermediates are formed by gas phase or surface reactions on the particles, both of which seem to take place simultaneously. Gas phase reactions are indicated by the formation of silica particles, if no core particles are present and surface reactions might help explain the homogeneity of thin coatings. The ratio of the influence of both reaction pathways on the finished coatings is unknown and might even change with the process parameters, such as the initial TEOS concentration. For gas phase reactions, these intermediates need to condense on the particles. The final step is the solidification of the intermediates to the silica network on the particle surfaces, which can proceed in parallel to the formation of new liquid intermediates.

To produce core-shell particles with a defined coating thickness of hardened silica, both the TEOS concentration and the aerosol residence time need to be controlled simultaneously. If a very short residence time is chosen in conjunction with a high TEOS concentration, the conversion will be low and coatings might not be completely hardened when they are collected from the system. An example for this is shown in Fig. 4.4a. The blurry edges of the coating indicate that the shell was not completely hardened before deposition on the sample grid and only solidified there (section 3.5), due to the insufficient residence time. This behavior might be interesting for applications, where a strong bond between coated particle and surface is desired, but is unwanted in most core-shell powder applications. On the other hand, if both the residence time and the TEOS concentration are high (Fig. 4.4c), then a significant portion of the coating material might form silica particles without core particles (homogeneous nucleation). The combined control of concentration and time allows the formation of completely hardened shells in the desired thickness (Fig. 4.4b). In comparison to earlier experiments with other plasma processes (e.g., the use of silane or the direct introduction into the discharge), this window of controllable coating thickness is quite big and allows the formation of hardened coatings from a few nm to many tens of nm thickness without homogeneous nucleation.

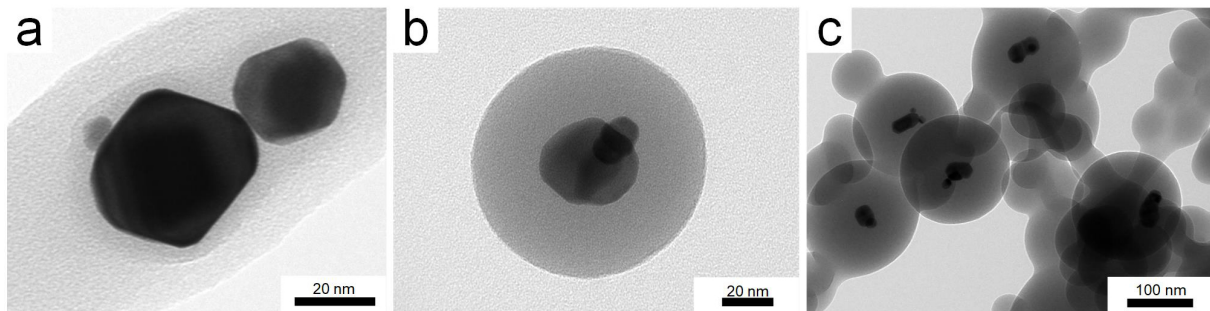


**Fig. 4.4:** Qualitative examples of sintered Pt particles coated with different combinations of initial TEOS concentration and aerosol residence time to show the interplay of the two parameters. (a) medium concentration and low residence time, (b) low concentration and medium residence time, (c) high concentration and long residence time.

### 4.3.2 By available particle surface area

For a given mass of silica coating, the total surface area of the core particles should have an influence on the coating thickness with thicker coatings expected when less surface area needs to be covered. To study this influence of the core particle surface area, Au particles were sintered in a tube furnace at 900 °C to create well defined spherical particles. The spherical particles were coated with an initial TEOS concentration of 3 ppmv, an aerosol residence time of 4.2 min at ambient temperature and a discharge voltage of 10.6 kV

in the plate DBD. The surface area of the aerosol could be controlled by changing the discharge current in the SDG, which controlled the spark discharge frequency. Since this simultaneously changed both the particle size and the number concentration, the initial number distribution of the core particles needed to be measured with an SMPS. From these distributions, the total available surface area could be estimated by multiplying the total number concentration with the mean surface area per particle based on the surface area weighted size distribution. The particles micrographed in TEM were analyzed with ImageJ. To reduce the influence of other parameter changes on the results, the four data points were measured in a random sequence. Fig. 4.5 shows the results of the experiments.

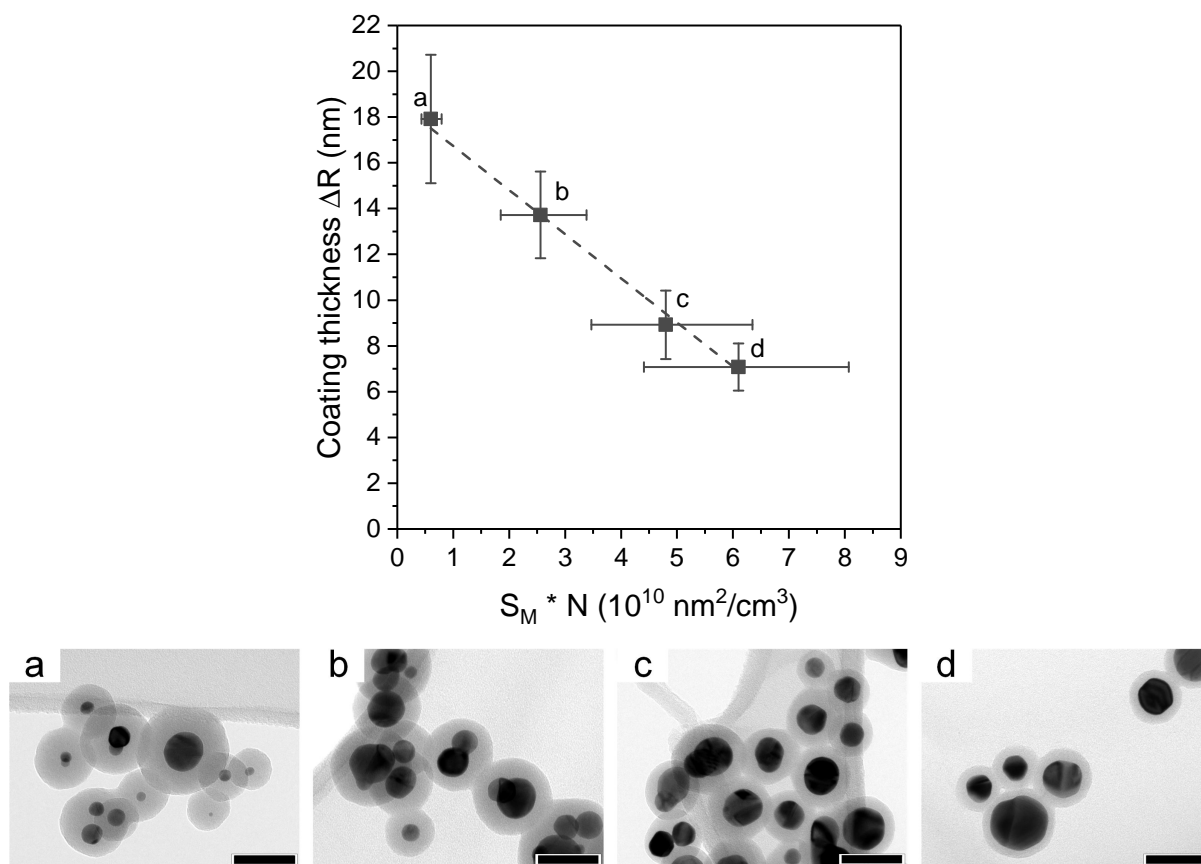


**Fig. 4.5:** Top: dependence of the coating thickness on the particle surface area of spherical Au particles. Bottom: TEM micrographs of the coated particles for the four data points. The black bars in the micrographs correspond to 50 nm.

As expected, the coating thickness decreased with increasing surface area of the core particles. However, the detailed explanation of the linear curve is difficult without a complete understanding of the reaction mechanism. It could be related to different reaction pathways in the gas phase and on particle surfaces. Other effects such as the loss of coating material to the reactor walls and the continuous change of the particle cross sectional area due to the growing shell might also have an influence. Nevertheless, it is

clear that the surface area has a significant influence on the coating thickness. While this is not a practical way to control the shell thickness on particles, it becomes relevant if core particles from an unstable source need to be coated.

### 4.3.3 By post-process temperature

Instead of keeping the post-discharge environment at ambient temperature, the mixture of particles, TEOS and plasma species can also be heated in a tube furnace. This allows the coating of particles within a few seconds instead of minutes for comparable coating thicknesses, when temperatures between 100 and 200 °C are used. As discussed in section 4.2, this seems to cause changes in the reacting species in the process. While the finished coatings showed no significant differences in their composition (see section 5.1), the use of higher temperatures restricted the particle materials to more thermally stable ones. Nevertheless, besides precursor concentration and residence time, the temperature adds a third option to control the coating thickness in the post-discharge process. Fig. 4.6 shows the influence of the temperature on the amount of silica on the particles. Instead of showing the coating thickness as before, the coating amount was defined here as the ratio of at.% Si to at.% core material. This method was used, since some of the coatings were very thin (single digit nm) and not always perfectly homogeneous around the particles. Nine different combinations of the aerosol residence time in the tube furnace, the initial TEOS concentration, the particle material and the temperature are shown. The residence times provided in the diagram were calculated for ambient temperature. Since the volume flow through the furnace was controlled by a pump after the furnace, the actual residence time in the furnace changed with the temperature, due to the increase in gas volume. At ambient temperature, no coating formation was observed with a residence time of a few seconds. However, when the small tube furnace with a volume of 0.1 L was used, the particles were coated even with these low residence times, which seems to be due to the formation of oxygen radicals as shown in section 4.2.

As expected, the samples showed a dependence of the coating amount on both the aerosol residence time and the initial TEOS concentration and the thickness could be increased with either of those parameters as shown before (see section 4.3.1). Moreover, the temperature as additional process parameter showed a big influence. Temperatures above 100 °C were sufficient to form visible coatings on the particles even within 3 s, which was much faster than at ambient temperature. For higher temperatures, the heating of the aerosol mixture exponentially increased the amount of silica on the particles. This is probably related to the formation of oxygen radicals through the thermal decomposition of ozone. As shown in section 4.2, a higher furnace temperature resulted in a lower ozone concentration. A faster ozone decomposition should result in a faster formation of oxygen radicals that are then able to react with the precursor. Furthermore, the temperatures

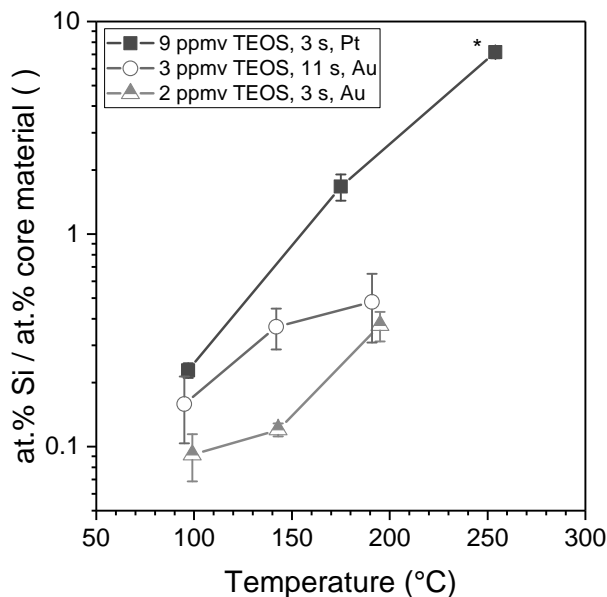


**Fig. 4.6:** Influence of the post-discharge temperature on the coating thickness (defined as the atomic ratio of Si to the core material) for different TEOS concentrations and furnace residence times. \* indicates that the formation of homogeneously nucleated  $\text{SiO}_2$  was observed.

will presumably also influence the reaction kinetics of the coating formation (Arrhenius equation).

## 4.4 Coating thickness homogeneity

Another property that influences the quality of core-shell products is the homogeneity of the coatings. The coating homogeneity describes two things: The distribution of the coating material over all particles and the coating thickness distribution on individual core particles. Since the coating thickness can influence particle properties such as the barrier effectiveness, similar thicknesses around all particles are required in many applications. It was observed in most experiments that all particles showed coating material in TEM. In particular, there were never simultaneously particles without any coating and others with very thick coatings in successful samples.

This is demonstrated in Fig. 4.7 for different samples, where the coating thickness was measured together with the particle size of the core particles by TEM. An average thickness was determined for the respective sample and the relative deviation of every individual particle to this average identified. The results were sorted into different core diameter classes. It is clear that the thickness is not perfectly homogeneous over all particles, but seems relatively symmetrically distributed around the average. Furthermore, no dependence of the coating thickness on the core particle size was found, which fits with studies by Wu and Biswas [93] for the condensation in vapor limited systems. How-

ever, as discussed before, the mechanisms involve probably more pathways than only a condensation of gaseous species.

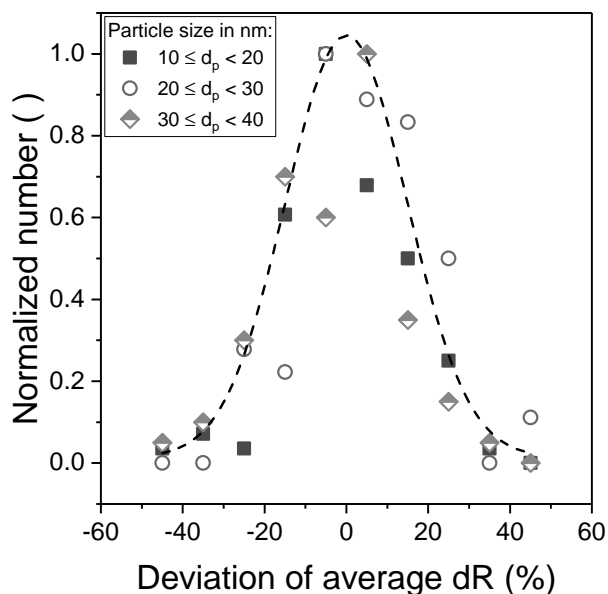


**Fig. 4.7:** Number of particles with different deviations of their coating thicknesses from the sample average for different particle size ranges (TEOS, 24 °C).

The homogeneity around individual particles can be influenced by different factors, such as the wettability of the coating intermediates on the core particles and the reaction rate of the solidification. The wettability of the core particles with the coating material (or rather the intermediates) depends very much on the combination of materials used. This will be discussed in more detail in chapter 5, but in general, the use of TEOS resulted in the formation of homogeneous coatings on most hydrophilic particles, while HMDSO often resulted in inhomogeneous coatings on such materials. The question of the reaction rate becomes especially relevant for the comparison between the TEOS coating at ambient and elevated temperatures. While the ambient temperature reactions are comparatively slow and give the intermediates time to move around the particle surfaces, higher temperatures reduce this time considerably. As an example, it was found that the coatings moved into inner parts of TiO<sub>2</sub> aggregates at 24 °C, but not at elevated temperatures (section 5.1.2).

## 4.5 Losses and agglomeration of particles

Since the coating process with TEOS at ambient temperature requires relatively long aerosol residence times, particle losses are to be expected. To quantify them, particle number concentrations of spark discharge generated Pt agglomerates were measured with the condensation particle counter (CPC) for different residence times, controlled by the

volume flow through the reaction chamber. Fig. 4.8 (left) shows the number concentration changes in dependence on the residence time. The concentration is given relative to the original particle concentration, measured directly before the residence time tube. First, Pt agglomerates with an original concentration of  $3 \cdot 10^6$   $1/\text{cm}^3$  were introduced into the system with the plasma discharge turned off and without TEOS (squares). The number concentration was reduced quickly and was at about 12 % of the original concentration after a residence time of 13 min. However, the addition of the plasma species (circles) or the presence of the coating reaction after addition of TEOS (triangles) caused no further significant changes.

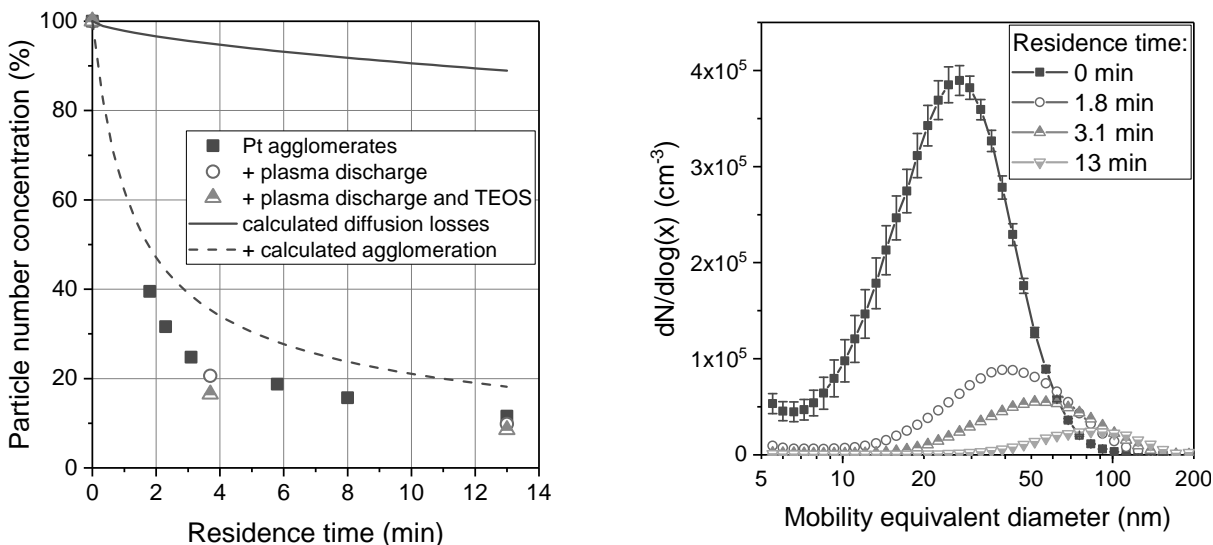


**Fig. 4.8:** Particle number concentration relative to the original concentration in dependence on the aerosol residence time in the system at ambient temperature (left) and the corresponding changes of the particle size distributions without discharge (right).

Different mechanisms can cause losses in aerosol processes. Charged particles follow electric fields that might lead them to walls (electrophoresis), particles move to colder regions if thermal gradients are present (thermophoresis), they follow the gas flow, which might impact them unto surfaces and they move mostly randomly due to Brownian motion. If nanoparticles come into contact with surfaces such as tube walls, they have a very high probability to adhere to them, resulting in a reduction in the aerosol particle concentration. However, no significant thermal gradients are expected during the residence time in this process, since the whole setup stays at ambient temperature. In contrast, thermal gradients become important if the coating is done at elevated temperatures. However, measurements of the losses in the tube furnace showed only very small changes for the short residence times that were smaller than the variations in the particle source. No electric fields are expected in the particle path, since the particles do not pass the plasma discharge. Hence, losses due to thermophoresis or electrophoresis of particles to the tube

walls should be negligible at 24 °C. Another possible source of particle losses to reactor walls are turbulent flows. The level of turbulence of the air flowing through the cylindrical residence time tube can be described with the Reynolds number, which was about 70 for the highest used volume flow of 3 L/min. Since the Re number for the given conditions is much lower than the typical transition range from laminar to turbulent flow in tubes of around 2300, a laminar flow can be assumed and turbulent particle losses should play no significant role during the residence time. However, losses of particles due to diffusion to walls will basically always happen in aerosols and especially those in the nanometer range, since the diffusion constant increases with decreasing particle size. The deposition of particles onto the walls of a cylindrical tube by diffusion from a fully developed laminar flow was calculated with the model by Gormley and Kennedy [94]. The expected diffusion losses in the residence time tube with the experimental particle size distribution (shown in Fig. 4.8, right, 0 min) were calculated. However, as shown in Fig. 4.8 (left, solid line), the theoretical diffusion losses are much smaller and follow a different trend than the experimental data. This indicates that other effects significantly influence the particle number concentration. The main suspect for this is the agglomeration of the particles to larger agglomerates. The influence of the agglomeration on the number concentration can be calculated with the Smoluchowski equation. However, since the agglomeration rate of an aerosol is very dependent on the particle number concentration, it needs to be calculated coupled with the particle losses due to diffusion. To accomplish this, the residence time was divided into small time steps and for each step both calculations applied to the aerosol. As shown in Fig. 4.8 (dashed line), this describes the experimental results better, indicating that much of the concentration change is caused by agglomeration. The big influence of the agglomeration is also apparent in the particle number distributions shown in the right diagram of Fig. 4.8, where not only the particle number decreased but also the whole distribution moved to bigger particle sizes for increasing residence times. Diffusion losses alone might move the mode of the distribution to bigger particle sizes, since the smaller particles diffuse faster, but bigger sizes than originally present are not possible. It is important to note that, while the agglomeration did cause a big change in particle number concentration, only the particle mass of the particles diffusing to the tube walls was actually lost. However, because of the dependence of the agglomeration on the particle number concentration, the coating of individual particles is only possible at low number concentrations. At higher concentrations, agglomerated particles will mostly be coated instead, since the agglomeration proceeds faster than the coating formation. While these limitations apply to all aerosol-based coating processes with any significant particle concentrations and are not specific to this process, the long residence times reinforce the effect.

# CHAPTER 5

---

## Core-shell material combinations

---

### 5.1 Silica coatings with TEOS

#### 5.1.1 Metals and metal oxides produced in a SDG

Having shown in the last chapter that coatings can be produced and controlled with the post-discharge process, different combinations of precursor and core material were produced and analyzed. Metal particles, especially Platinum and Gold, were the most used core materials in this thesis, due to their high contrast in TEM micrographs, which simplified the observation of coatings. They were produced with the spark discharge generator (section 3.2.1). Both materials are noble metals and as such resistant to oxidation. Pure metal surfaces are generally considered hydrophilic [95] and should hence exhibit a good wettability with hydrophilic coatings or coating intermediates. The particles produced in the SDG were highly agglomerated in dendritic structures of primary particles in the single digit nm range. They could be sintered to more compact and more spherical geometries in a tube furnace at around 750 °C (Au) and 1000 °C (Pt). Fig. 5.1 shows silica-coated agglomerates with different coating thicknesses (TEOS, 24 °C).

In most cases, the silica coatings based on TEOS were homogeneously distributed on these types of particles (e.g., Fig. 5.1, right). Even small coating thicknesses covered the complex agglomerate structures quite well. This indicates an influence of surface reactions, since pure gas phase reactions would probably not lead to such homogeneous coatings. However, if the applied silica amount was very small, the coatings tended to be focused in the interparticle spaces or between branches (Fig. 5.1, left). This effect was also hinted at by photoemission measurements that showed a slowly increasing surface coverage with increasing coating amount (see Publication 1). This indicates capillary forces acting on the coating and might be related to the liquid coating intermediates discussed earlier (section 4.3.1), which can move on the particle surfaces before they solidify to silica. For

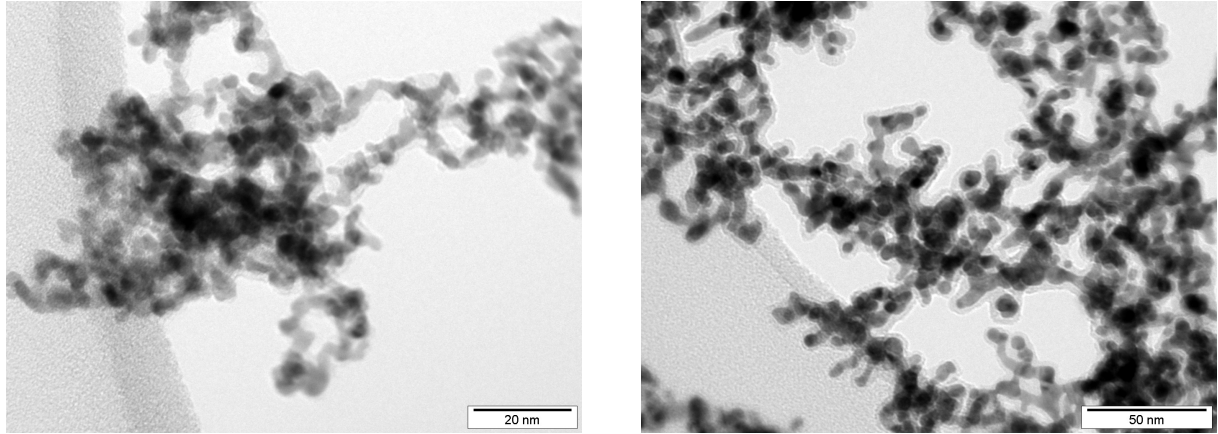
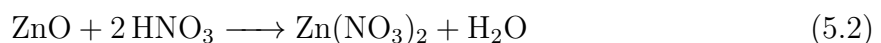
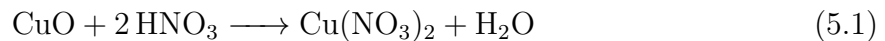


**Fig. 5.1:** Examples for silica coated metal particles. Left: Pt agglomerates with a very thin and incomplete coating, right: Au agglomerates with a thicker and more homogeneous coating. Both particles were coated with TEOS at ambient temperatures and a residence time of 4.2 min, but with 0.4 ppmv TEOS (Pt) or 3 ppmv (Au).

very thick coatings on these fractal agglomerates, the liquid seemed to compact some of the particles to more dense structures, which is an effect known from the literature [96].

Besides Platinum and Gold, the metals Copper, Zinc, Iron, Silver, Titanium and Nickel were produced in the SDG and introduced into the coating process. Since these materials are less noble, they oxidized in the carrier gas. In fact, due to the highly oxidizing environment with ozone in the system, it can be assumed that most metal particles get oxidized very quickly and are always coated as metal oxides. Fig. 5.2 shows four examples of SDG-synthesized nanoparticles coated with silica. Even though the particle geometries could be quite different, a successful coating was observed in all cases.

However, for Cu and Zn (oxide) particles, only certain discharge gases could be used in the coating system. When these particles were introduced into the post-discharge coating process with air from the institute supply, no coated particles were found. Instead, the sampling grid was covered with what seemed like bubbles, which burst when the electron beam of the TEM was moved over them. EDX measurements of such structures from Cu showed the elements Cu, O and Si, as expected for silica coated CuO particles. However, if the EDX measurements were started directly after moving the electron beam onto filled bubble structures, N was found and decreased simultaneously with the deflation of the bubbles. This indicates the formation of Zn or Cu nitrates with the  $\text{HNO}_3$  and  $\text{H}_2\text{O}$  present in the post-discharge environment (see section 4.2), a reaction well known from the liquid phase. For CuO and ZnO, the reactions might look like this:



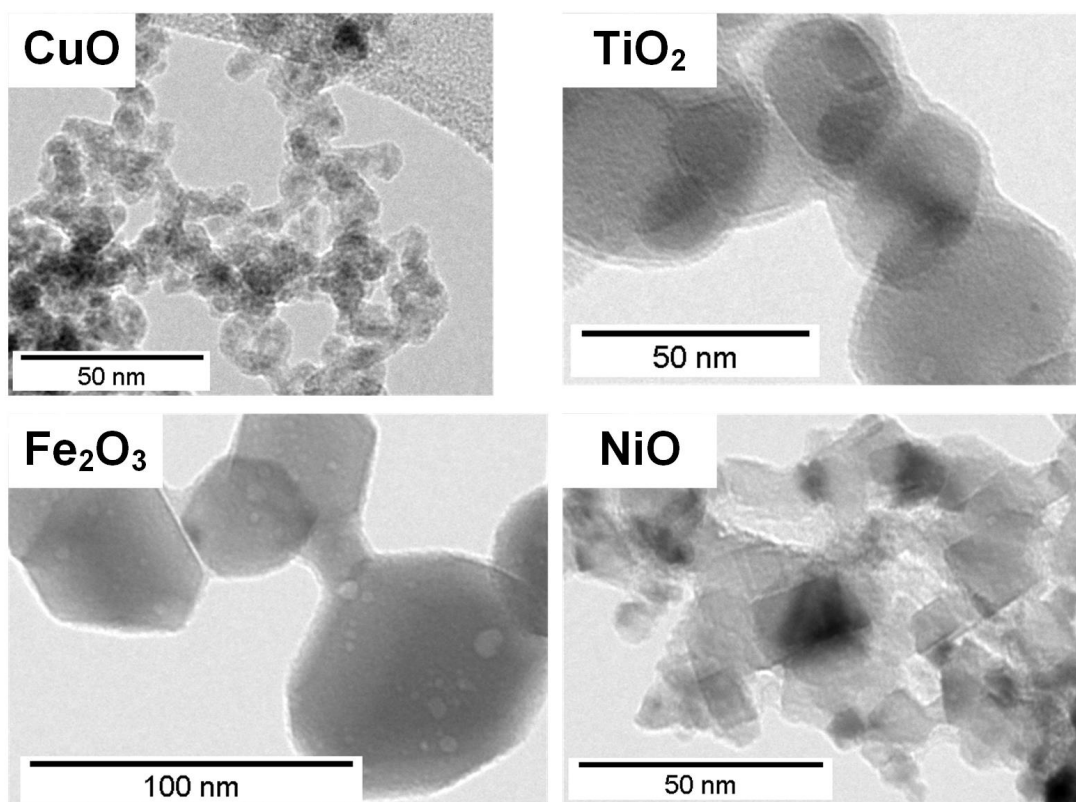


**Fig. 5.2:** Examples of sintered silica-coated metal oxides that were produced with the SDG and modified with TEOS. The identification of the coatings is difficult, due to the low contrast between these materials.

The reactions seemed to reverse back to the oxides in the TEM, due to the vaporization and removal of the acid and water. Obviously, these interactions are problematic for the formation of Cu or Zn based core-shell structures with the post-discharge process. However, it is relatively easy to circumvent the problems by removing or at least reducing the concentrations of HNO<sub>3</sub> and H<sub>2</sub>O in the system. This can be done by replacing the ambient air with a mixture of He and O<sub>2</sub>, which resulted in successful coatings. As discussed before, the use of these discharge gases necessitates the heating of the post-discharge environment to produce oxygen radicals (section 4.2). Similar results could be obtained if synthetic air was used instead of He and O<sub>2</sub> or if the pressurized air was diluted with pure N<sub>2</sub>, as in Publication 1.

The chemical composition of the coatings produced with TEOS was analyzed with FTIR, EDX and XPS. For FTIR and XPS, powder was collected on a membrane filter at the end of the process. The powder was pressed with KBr powder for measurement with the FTIR or analyzed directly on the membrane in XPS. Since the powder mass was low, due to the lab-scale core particle synthesis methods, a collection time of up to 6 h was required. Hence, the measurements give an average of the composition produced in this time interval and cannot provide information about eventual changes during this

time. The coatings might also have changed further after deposition on the filter, but the residence time in the aerosol still showed an influence on the measurements, even though it is small compared to the total time in the system. The influence of different process parameter combinations on the chemical composition of the coatings with TEOS were examined in detail in Publication 3 for ambient and elevated temperatures. Fig. 5.3 shows three examples of FTIR spectra of coated powders. The spectra were normalized to their maximum absorption to remove the influence of the measured powder mass and to make them more easily comparable. Since metal particles were used as the cores, which show no infrared absorption bands, all observed signals can be assigned to the coating.

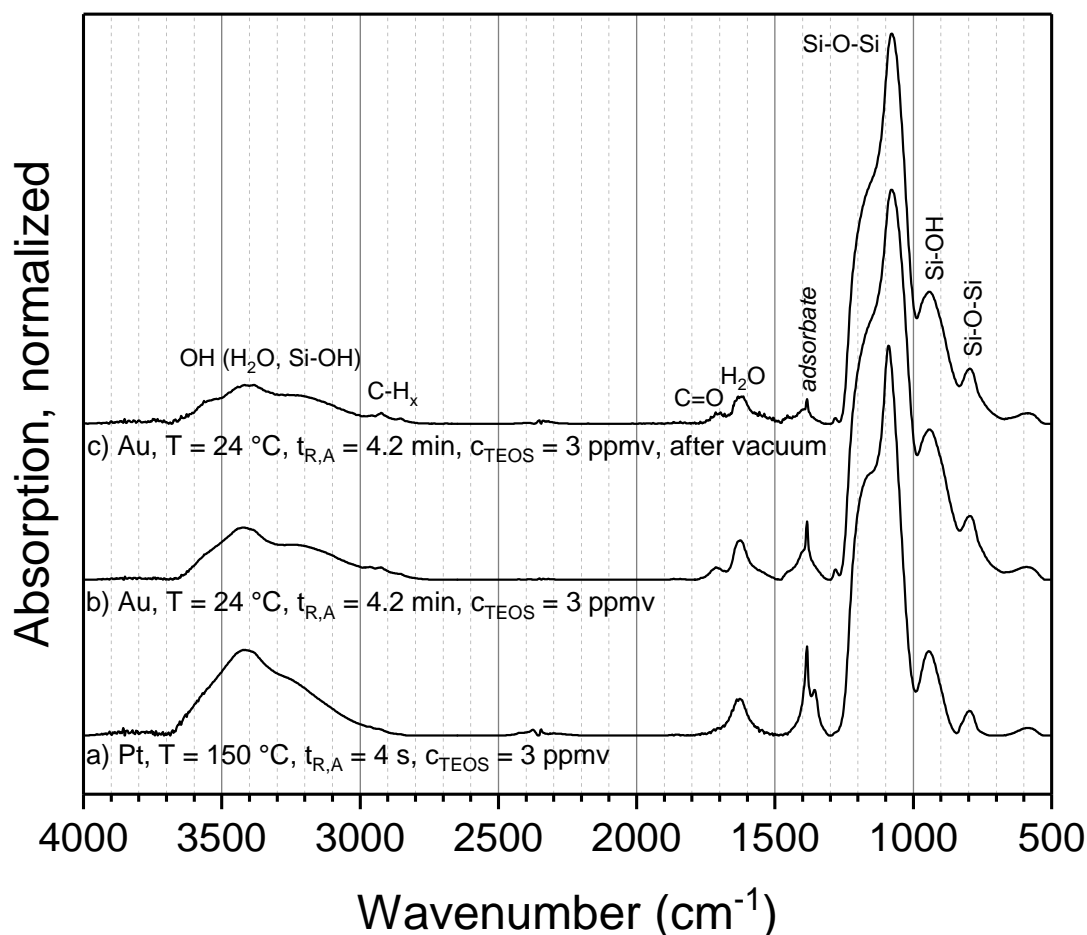


**Fig. 5.3:** Examples of FTIR spectra of metal particles coated with TEOS with different conditions. More spectra can be found in Publication 3.

All spectra exhibit a strong vibration band at  $1080\text{ cm}^{-1}$  with a shoulder at about  $1170\text{ cm}^{-1}$ , which can be assigned to the asymmetric stretching of Si–O–Si. The bending vibration of Si–O–Si is present at about  $800\text{ cm}^{-1}$ . All samples show evidence of silanol groups in the form of Si–OH bending vibrations at about  $950\text{ cm}^{-1}$  and OH stretching modes around  $3400\text{ cm}^{-1}$  that can be assigned to Si–OH and adsorbed water. Furthermore, adsorbed H<sub>2</sub>O on or in the sample is indicated by OH bending of water around

1630  $\text{cm}^{-1}$ . The samples coated at 24 °C exhibit a further vibration band at 1720  $\text{cm}^{-1}$ , which can be assigned to C=O. This band is not present in the samples at elevated temperatures. All samples showed an additional band at 1380  $\text{cm}^{-1}$ , which exhibited two peaks for the samples at elevated temperatures. The assignment of this band is unclear, but could relate to methyl groups.

The presence of these organic groups might indicate an organic character of the coatings (silica-organic), which would result in product properties different from pure inorganic silica. However, the organic bands found in the samples might also originate from by-products adsorbed on the sample surfaces. This hypothesis is supported by the C=O groups, which might be expected in possible by-products such as aldehydes or carbon acids, but seem less likely as part of the coating. Adsorbed species should be removable by either heating the powder or by lowering the pressure in the environment. Since higher temperatures might influence the coating, some samples were introduced into a vacuum (e.g., Fig. 5.3c). The respective bands were indeed reduced, indicating adsorbed species. The effect was especially pronounced for the particles coated at elevated temperatures, where larger peaks of these adsorbed species were found. Hence, the coatings produced with TEOS at different temperatures seem to be mostly pure inorganic silica. This was corroborated by EDX measurements, which showed atomic ratios close to those in  $\text{SiO}_2$ .

Additional information about the coating can possibly be acquired from the position and form of the Si–O–Si stretching mode between 1000 and 1300  $\text{cm}^{-1}$ . In the experiments, the position of the peak maximum was between 1078 and 1094  $\text{cm}^{-1}$ . This can be related to the angle and resulting strain of the Si–O–Si bonds, with a smaller wave number indicating a higher strain [90]. However, this can be the result of multiple effects, such as the film thickness, oxygen deficiency, densification or carbon admixture [97]. Here, samples with the biggest coating thicknesses exhibited the highest wave numbers. Furthermore, for coatings on nanoparticles, a generally higher strain might be expected compared to films on bulk substrates, due to the surface curvature and high contact area with the core particles. Concerning the form of the Si–O–Si peak, it typically exhibits a shoulder at slightly higher wavenumbers. A higher ratio of the peak shoulder intensity to the main peak intensity can be related to a higher disorder of the silica network [90]. For the present results, this is further corroborated by the distinctive silanol (Si–OH) signals in the samples. Massines et al. [90] found that a higher number of silica particles in films on bulk substrates increased both the ratio of the intensities as well as the intensity of the silanol peak. Hence, the here observed peak form is probably not unexpected for particle coatings.

In addition to the FTIR and EDX measurements, XPS was used to analyze the chemical composition of TEOS-coated metal particles. The detail spectra of coated Au particles are shown in Fig. 5.4. The Si and O peaks were fitted with literature values to get more

information about the bonds in the sample.

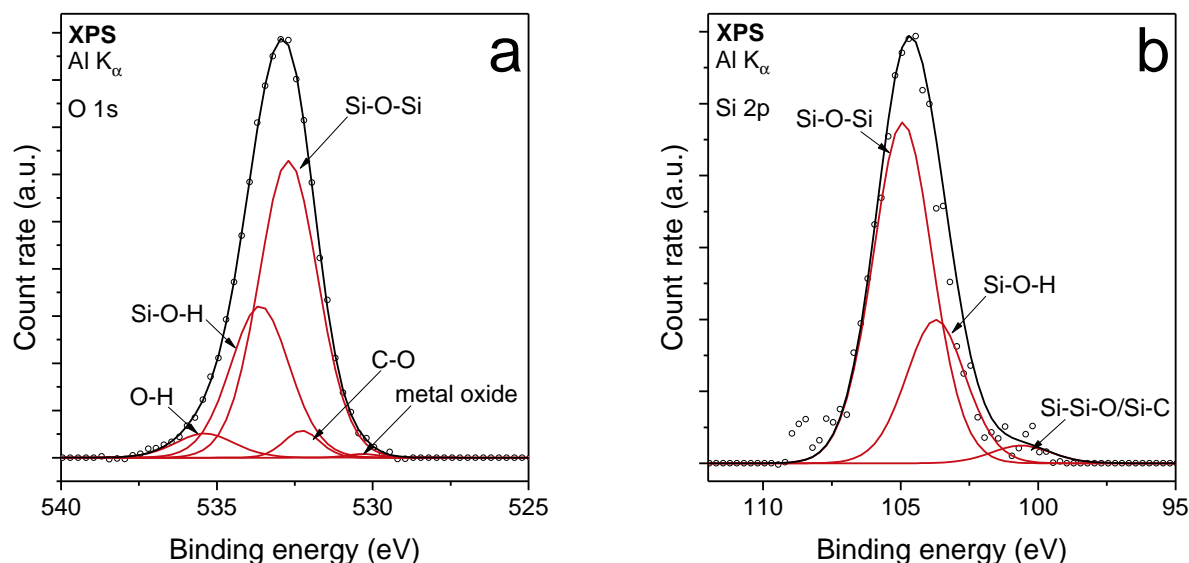


**Fig. 5.4:** XPS detail spectra of Au particles coated with TEOS at 24 °C. (a) O 1s and (b) Si 2p. The measurements and fits were done by the Institute of Energy Research and Physical Technologies, TU Clausthal.

Confirming the FTIR measurements, Si–O–Si as well as Si–OH bonds can be identified both in the O 1s and Si 2p peaks. Furthermore, the detail spectra give evidence of adsorbed water (O–H) and some organic groups (C–O) that were also found in FTIR. The Si 2p spectrum shows some evidence of Si–Si–O or Si–C bonding, which could indicate some small amount of organic parts of the coating or an incomplete polymerization. The metal oxide in the O 1s spectrum originates from the sample holder. The spectra showed no evidence of chemical bonding between the core particles and the coating, indicating a purely physical connection between core and shell. More spectra can be found in Publication 3.

### 5.1.2 AEROXIDE P25 titania

Titania particles are one of the most interesting nanopowders for many applications. A defining property of these particles is their photocatalytic activity, which results from the formation of free radicals on the particle surface upon radiation with UV light. This allows the particles to be used for the removal of pollutants, for example for water treatment [98, 99]. However, in other applications such as pigments in wall paints or as UV absorber in sun cremes, photocatalysis is an undesired effect and instead titania is used because of its other properties such as its high refractive index or UV absorption capabilities. Hence, it is common to apply a coating of an inert material, such as silica or alumina, to the particles to restrict the photocatalytic effects [1, 2]. Coatings can also be used to improve the dispersibility of the particles in liquids. Commercial titania nanoparticles

(e.g., AEROXIDE P25 by Degussa (Evonik)) are typically produced by flame synthesis and have a high amount of hydroxyl (Ti–OH) groups on the surface, which results in a hydrophilic behavior. By applying an organic or inorganic-organic coating to the powder, the surface can be changed to become hydrophobic.

Commercial titania powder was introduced into the post-discharge coating process by atomization of an aqueous suspension of 1 mg/mL AEROXIDE P25 particles (section 3.2.2). Due to the industrial production of the titania particles by flame synthesis, the primary particles were aggregated. The particles were introduced into the coating system and coated with TEOS at different temperatures and initial precursor concentrations. Fig. 5.5 shows two examples of particles coated at ambient temperature and at 200 °C. In both cases, a silica coating was acquired on the particles. However, in the case of the process variant at ambient temperature, the coatings were not entirely homogeneous around the particles. The coating material was focused in the inner parts of the aggregates, while outer primary particles showed only a thin coating or even uncoated surfaces. In contrast, the coating process at 200 °C resulted in a more uniform distribution of the silica around the core particles. This might be related to the rate of solidification of the coatings on the particles and the accompanying mobility on the surfaces. It might help explain the differences observed in the photocatalytic activity (section 6.3).

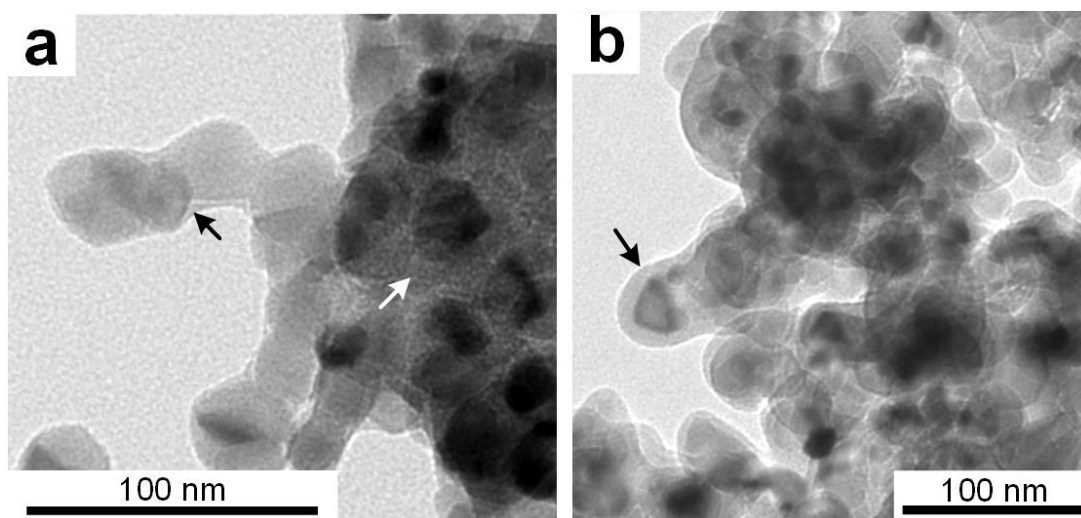


**Fig. 5.5:** Silica coated commercial titania (Degussa/Evonik P25). (a) coated with 9 ppmv TEOS at ambient temperature, (b) coated with 9 ppmv TEOS at 200 °C.

As done for the SDG-produced particles, the chemical composition of the TEOS-coated titania particles was analyzed by FTIR and XPS. The FTIR spectrum showed the same peaks observed for the coated metals, but exhibited additional bands associated with Ti–O–Ti from the core particles. Additionally, the band previously assigned to Si–OH could also be indicative of Si–O–Ti, which is expected at the same wavenumber. The

XPS detail spectra provided more information in this regard (Fig. 5.6).

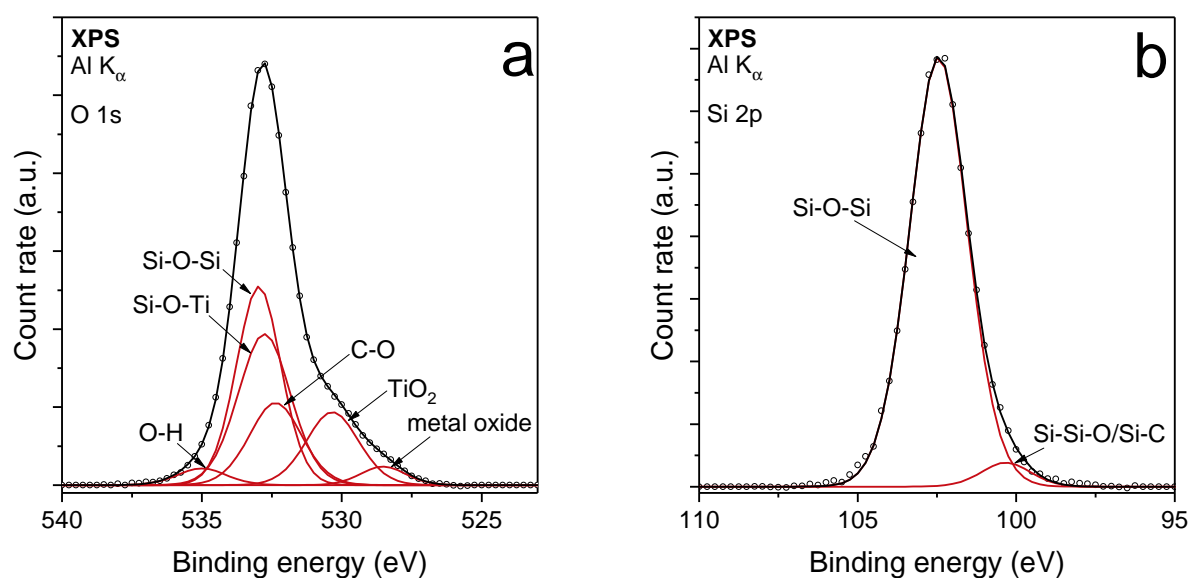


**Fig. 5.6:** XPS detail spectra of TiO<sub>2</sub> particles coated with TEOS at 24 °C. (a) O 1s and (b) Si 2p. The measurements and fits were done by the Institute of Energy Research and Physical Technologies, TU Clausthal.

The comparison of the detail spectra with those of the metal particles (Fig. 5.4) shows significant differences. In particular, there seems to be no evidence of Si–OH in the sample and instead Si–O–Ti bonding is found. This indicates that the P25 titania particles might participate chemically in the coating formation, which is different from the Pt and Au particles shown before. Again, the details of the mechanisms leading to this behavior are beyond the scope of this thesis. The interaction could be caused by specific surface groups on the titania, interactions of plasma species with the core particles or an influence of the titania on the formation of coating intermediates. These chemical bonds could be part of the reason for the photocatalytic behavior of the coated particles (section 6.3).

### 5.1.3 Salts and others

Ammonium sulfate ((NH<sub>4</sub>)<sub>2</sub>SO<sub>4</sub>) and sodium chloride (NaCl) were used as core particle examples for salts. Ammonium sulfate is known for its uses as fertilizer or food additive, while sodium chloride is known as table salt. Both salts are soluble in water. Nanoparticles were produced by atomization of aqueous salt solutions as described in section 3.2.2. The removal of the water in the denuder resulted in the formation of solid salt particles in the gas phase.

Ammonium sulfate exhibits a relatively low thermal stability and decomposes above 200 °C. Hence, higher temperatures need to be avoided during the coating. Since the post-discharge process with TEOS can be operated at ambient temperature, it was suitable to

coat this salt. The  $(\text{NH}_4)_2\text{SO}_4$  particles were produced from a 1 mg/mL salt solution and introduced into the coating system. The particles were coated with 3 ppmv TEOS and a residence time of 8.3 min, which led to dark structures on TEM micrographs. However, these structures were not thermally stable and the salt was decomposed in the electron beam, resulting in empty silica shells. Alternatively, the salt could be removed directly in the gas phase, by passing the aerosol through a tube furnace at 200 °C after the formation of the coatings. This allowed the continuous production of hollow silica structures (Fig. 5.7).

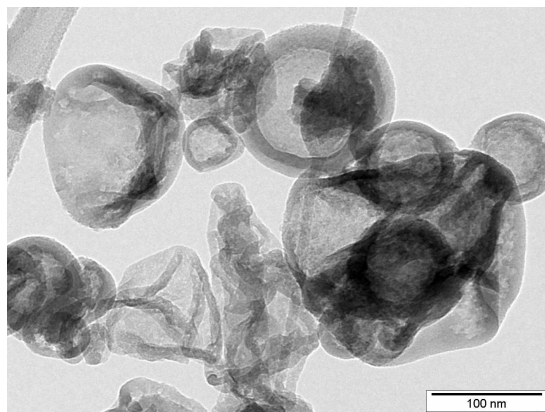


**Fig. 5.7:** Hollow silica structures produced by coating ammonium sulfate  $(\text{NH}_4)_2\text{SO}_4$  and removing the core material in a furnace.

The removal of the salt was confirmed by EDX measurements. While the dark and filled particles showed nitrogen, sulfur and large amounts of oxygen beside the silicon, the empty shells showed only Si and O with a ratio of about 1:2. Interestingly, many of the silica shells seemed to shrink and deflate when the salt was removed (Fig. 5.7). For rigid structures, one would normally expect the formation of holes in an otherwise spherical shell. While this was the case for a part of the silica shells, many deflated without visible damage to the hull. This behavior could be caused by different phenomena. One explanation are incompletely hardened shells that might still be flexible and unable to support themselves without the core particles. However, holes should still be required for the decomposition products to leave the shell. This might indicate a porosity of the shells, which could also contribute to the reduced structural stability. An increase in the TEOS concentration to 17 ppmv allowed the production of thicker shells. Many of these thicker shells kept their spherical structure even after passing through the furnace and EDX showed that they contained significant amounts of sulfur. However, EDX measurements found no residual nitrogen from the ammonium or unexpectedly high oxygen concentrations from the sulfate, indicating that some decomposition took place.

The second salt tested as core particle was sodium chloride (NaCl). The particles were produced from a 3.9 mg/mL solution of NaCl in water, which was atomized and

the solvent removed with a denuder. The coating was done with 9 ppmv TEOS and a residence time of 8.3 min. As shown in Fig. 5.8 (left), the particles were successfully coated with silica. Hollow silica structure could also be produced by removing the NaCl after the coating formation. This was done by dispersing the particles in water, which solved and removed the salt. The resulting shells are shown in Fig. 5.8 (right). This further reinforces the hypothesis of the formation of porous coatings in the TEOS process at ambient temperature, at least for these two salts.

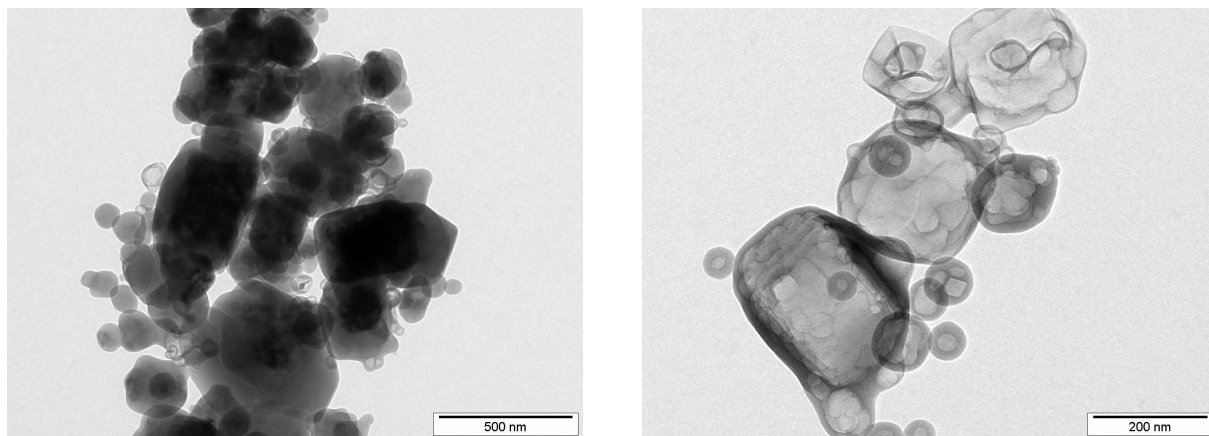


**Fig. 5.8:** Silica coated sodium chloride (NaCl). Left: the coated salt particles, right: silica shells after removal of NaCl by water.

Another core particle material used for coating was the polymer polystyrene. The particles could be coated with silica at ambient temperature, using TEOS. However, the coatings were not very homogeneous and often eccentric. This is probably related to the wettability of the coating or its intermediates on the hydrophobic polymer surfaces.

## 5.2 Silica-organic coatings with HMDSO

While the use of TEOS resulted in homogeneous and inorganic silica coatings on most studied substrates, HMDSO led to a different coating morphology and composition. HMDSO is a silicon organic compound like TEOS, but differs in the way the different atoms (Si, O, C) are connected (Tab. 3.1). This often results in more organic coatings that contain Si–C bonds [100, 101]. In contrast to TEOS, the experiments with HMDSO in the post-discharge environment showed that no coating could be achieved at ambient temperature. However, the use of a tube furnace to increase the temperature of the aerosol after mixing allowed the reactions to start, which might indicate the importance of oxygen radicals. Similar to TEOS, HMDSO does not react in the range usable with the available tube furnace (up to 500 °C) if no plasma species are present. It is known from the literature that the oxygen content in the discharge during plasma coating has a big influence on the percentage of organic bonds in the finished film [52, 101]. Experiments

with a He/O<sub>2</sub> mixture, which resulted in inorganic silica films, seemed to confirm this for the present system. However, since TEOS already provides a method to produce inorganic silica coatings, the focus of this section will be on the production of silica-organic (SiO<sub>x</sub>C<sub>y</sub>H<sub>z</sub>) coatings by using air as the discharge gas.

Coatings on Au particles with HMDSO were acquired at temperatures between 100 and 300 °C (Fig. 5.9). Based on the TEM micrographs of HMDSO-coated sphere-like metal particles, the formation of homogeneously nucleated particles seemed more probable in comparison to the TEOS-based coatings (Fig. 5.9a). Furthermore, most particles were coated with an eccentric coating instead of the concentric one observed for TEOS-based coatings. The particle formation can be explained in part by the higher vapor pressure of HMDSO compared to TEOS, which complicated the dosing of small enough precursor concentrations. However, the eccentric coating indicates an insufficient wettability of the condensing compounds on the metal particles. This could be caused by a hydrophobic character of the condensing species in contrast to the presumably hydrophilic species during TEOS coating. However, a good homogeneity of the films was found for thin coatings on metal agglomerates (Fig. 5.9b). This could be related to surface reactions that might dominate for thin coatings.

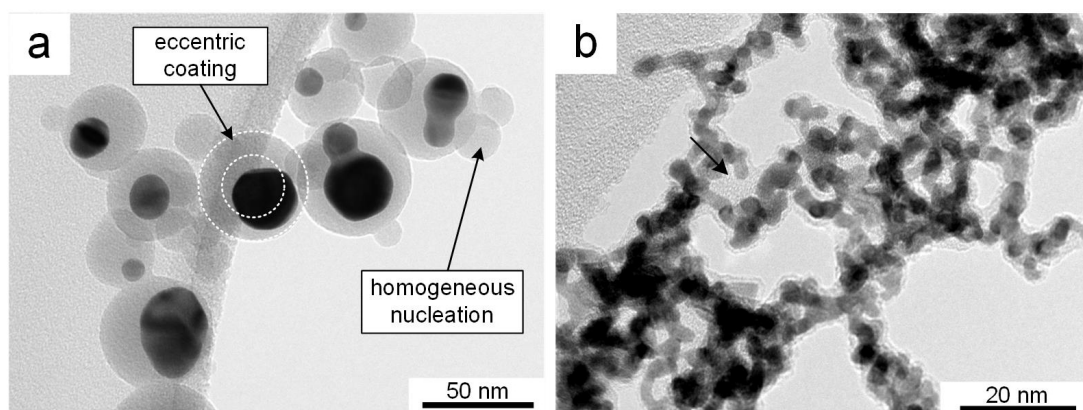


**Fig. 5.9:** TEM micrographs of metal particles coated with HMDSO. (a) sintered sphere-like Au particles, (b) Pt agglomerates.

The particles coated with HMDSO were analyzed with FTIR, EDX and XPS as well. EDX measurements showed Si and O atoms in the samples, but could not be used to quantify the C content, since the TEM grid background contained large amount of this element. Hence, powder samples were acquired from the system for FTIR and XPS. Fig. 5.10 shows FTIR spectra of HMDSO-coated metal particles.

The spectra show most of the vibration bands seen already in the TEOS-based coatings. In addition, however, Si-(CH<sub>3</sub>)<sub>y</sub> (y = 1...3) vibration bands are found at wavenumbers 1275, 850 and 800 cm<sup>-1</sup>. These organic bonds remained after the introduction of a sample into a vacuum environment (Fig. 5.10b), which indicates that they are part of the

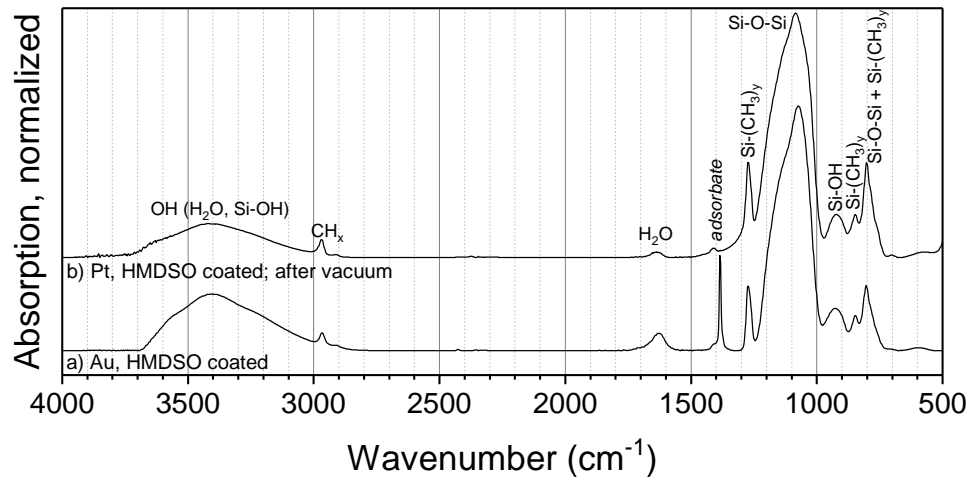


**Fig. 5.10:** FTIR spectra of metal particles coated with HMDSO at 250 °C.

coating itself. The form of the Si–O–Si peak changed somewhat compared to the silica coatings. In particular, the shoulder at higher wavenumbers seems to be larger, which might indicate a higher disorder of the silica network as discussed before. This could be caused by the introduction of the Si–(CH<sub>3</sub>)<sub>y</sub> bonds into the coating. XPS measurements also showed evidence of Si–CH<sub>3</sub> bonding in the C 1s detail peak. However, the Si 2p detail peak did not support this and only showed Si–O–Si. A possible explanation is the focusing of the Si–CH<sub>3</sub> groups in a very thin layer on the surface of the particles, where they have a relatively small influence on the total signal.

The coating with HMDSO changed the macroscopic properties of the particles significantly. As already indicated by the wetting behavior of the coating intermediates, these silica-organic (or organosilica) coatings (SiO<sub>x</sub>C<sub>y</sub>H<sub>z</sub>) exhibited a hydrophobic character. Fig. 5.11 compares the contact angle of water droplets on different surfaces. The left picture shows the background used for the experiments (membrane filter). In the middle image titania particles were atomized and collected on the filter. The water droplet placed on this sample seeped into the particles, wetting them completely and indicating a hydrophilic behavior of the particles, which was expected due to the Ti–OH groups typically found on flame generated titania. The same behavior was observed when silica-coated particles (TEOS-based) were used. However, if the particles were coated with HMDSO, the water droplet did not wet the surface and rolled off if the sample was tilted. This indicates a highly hydrophobic surface produced by the coating, which remained even after outgassing in the vacuum.

Such hydrophobic surfaces can be interesting for applications, where the particles need to be dispersed in an organic matrix, e.g. in composite materials. Hydrophobic polymer coatings on particles can be created in plasma processes (e.g., [102]). However, a disadvantage of these purely organic coatings is their often low thermal stability. In contrast, it was found that the hydrophobic HMDSO-based coatings seem to be relatively

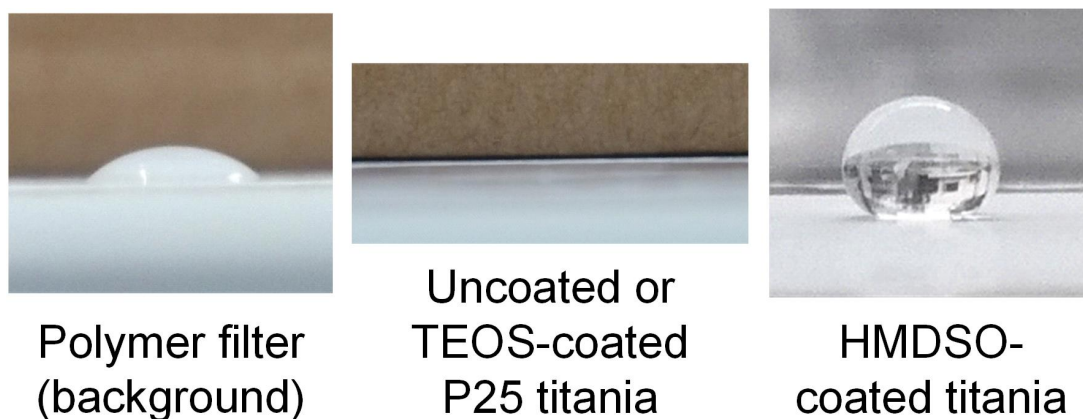


**Fig. 5.11:** Photographs of water droplets on different surfaces.

stable at higher temperatures. As shown in Fig. 5.12 (left), HMDSO-coated Pt particles could not be dispersed in water and instead swam on the liquid surface or stuck to the walls, whereas the hydrophilic uncoated Pt particles were dispersed (right). Interestingly, this hydrophobic character of the coated particles remained after 1 h of tempering at 250 °C, as shown in the middle. This further indicates that the hydrophobicity is an integral part of the coating and not just an effect of some adsorbed species.

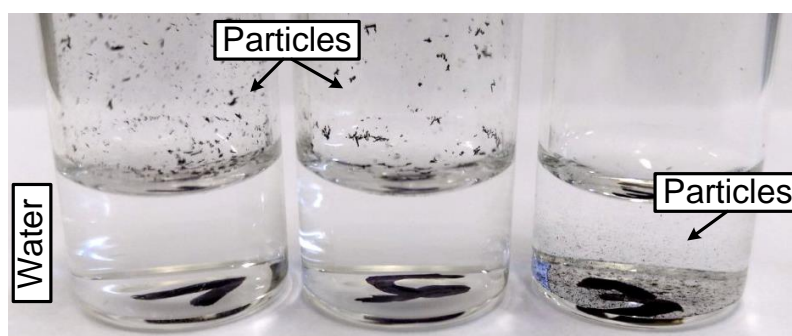


**Fig. 5.12:** Photographs of Pt particles modified with HMDSO in water after shaking. Left: HMDSO-coated Pt, middle: HMDSO-coated Pt after 1 h at 250 °C, right: uncoated Pt. Only the uncoated particles could be suspended in the water.

# CHAPTER 6

---

## Applications of the coated particles

---

### 6.1 Improvement of the mechanical stability of metal agglomerates

The mechanical stability of nanoparticle agglomerates can be relevant in different scenarios. For example, in medical [103] or food [104] applications it is often required to deagglomerate particles to achieve the desired product properties. In other applications a strong connection between particles is essential for the product. An example for this is the work of a Finnish group, who developed a process to deposit layers of titania particles on paperboard surfaces [105, 106]. While the particles can be connected well with the paper through the use of polymers, the interparticle connection strength is also essential for the long-term wear resistance. The stability of an agglomerate depends on multiple factors such as the primary particle size, the type of bonds between the particles (e.g., van-der-Waals vs. solid), the cross-section of the particle contacts and the overall structure of the agglomerate (e.g., open vs. compact) as well as the angle of impact on the surface in the case of inertial impaction [107, 108, 109]. Some of these properties can be modified, for example by changing the cross-section of particle connections through sintering [110]. Since a coating modifies interparticle connections as well, it would be interesting to study the effect of the coatings applied with the plasma process on the mechanical stability of particles. This was done in Publication 4 for TEOS and HMDSO-coated spark discharge generated Pt agglomerates.

To accomplish this, a low pressure impactor was used. The LPI setup consisted of a critical orifice for the introduction of the aerosol into the low pressure environment, a subsequent tube to obtain defined flow conditions and the impactor itself, which consisted of an acceleration nozzle and an impaction target. Faraday cup electrometers were used to measure the aerosol concentration before and after the impaction, which provided infor-

mation about the particle penetration (i.e. the particles not deposited on the impaction target). If particles impact on a surface, some of them might rebound back into the gas flow. This effect can be suppressed by increasing the energy dissipation through adhesion and deformation, e.g. by applying a sticky grease film on the target surface. In that case, basically all particles that impact on the target will be deposited. This allowed the measurement of the so-called deposition curves with the FCEs (Fig. 6.1).

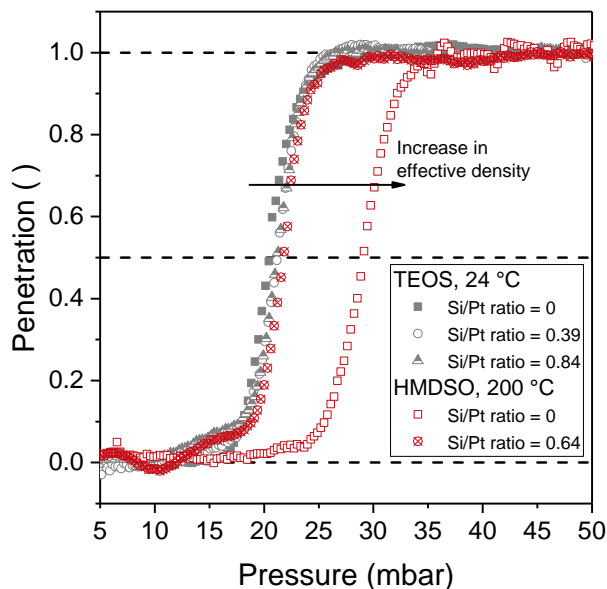


**Fig. 6.1:** Deposition curves of Pt agglomerates with different modifications in the LPI. The y-axis shows the ratio of the FCE signals before and after the impactor and the x-axis is the pressure in the impactor. The coating amount on the particles is described by the ratio of Si to Pt atoms in the sample (from EDX measurements).

The particles were either coated with TEOS at ambient temperature for 4.2 min or with HMDSO at 200 °C for 4 s and an additional residence time of 4.2 min at ambient temperature. The amount of coating (silica or silica-organic) was determined by EDX and is given by the ratio of Si to Pt atoms. The particles denoted Si/Pt = 0 were passed through the system at the respective temperatures, but were not coated. All curves showed the expected form with no penetration at low pressures and a complete penetration at higher pressures. A lower pressure results in a higher impaction velocity and hence a larger inertial force. The deposition curves can be described by the  $p_{50}$  value, which is the pressure where 50 % of the particles deposit on the target. For a given particles size (i.e. due to size classification of the particles before the LPI), a shift to a higher  $p_{50}$  indicates an increase in effective density of the agglomerates. In comparison to the unmodified particles (Si/Pt = 0, 24 °C), all coated agglomerates showed only a small shift to slightly higher  $p_{50}$  values. This indicates thin coatings that caused no structural changes to the Pt agglomerates. However, the uncoated particles that passed the furnace (Si/Pt = 0,

200 °C), showed a more significant shift to higher pressures, which indicates structural changes caused by the tempering. Interestingly, the HMDSO-coated particles that passed the same furnace (Si/Pt = 0.64, 200 °C), behaved instead similar to the particles at 24 °C. This indicates that the coating, which formed simultaneously to the tempering, seemed to hamper structural changes and improved the thermal stability of the Pt agglomerates.

To obtain more information about the mechanical stability of the particles during impaction, the size and structure of the inertially deposited particles was analyzed. This was done by placing a TEM grid on the impaction plate instead of using the grease film. The particles collected on the TEM grid at a certain impaction velocity were then studied with image analysis software to determine their projection area distributions, which is a measure for the degree of fragmentation. A smaller projection area compared to the original distribution indicates a higher degree of fragmentation. The projection areas were converted to area equivalent diameters and fitted with a fragmentation distribution function to obtain median values and corresponding broadnesses of the distributions (see Publication 4). In theory, a more stable agglomerate should require a higher impaction velocity to fragment than a less stable one. The results are presented as projection area equivalent diameters in dependence on the impaction velocity, which relates to the forces acting on the agglomerates (Fig. 6.2). The velocity was calculated with a model from Rennecke and Weber [111]. For a given impactor geometry, the velocity depends primarily on the pressure in the LPI and the particle density.

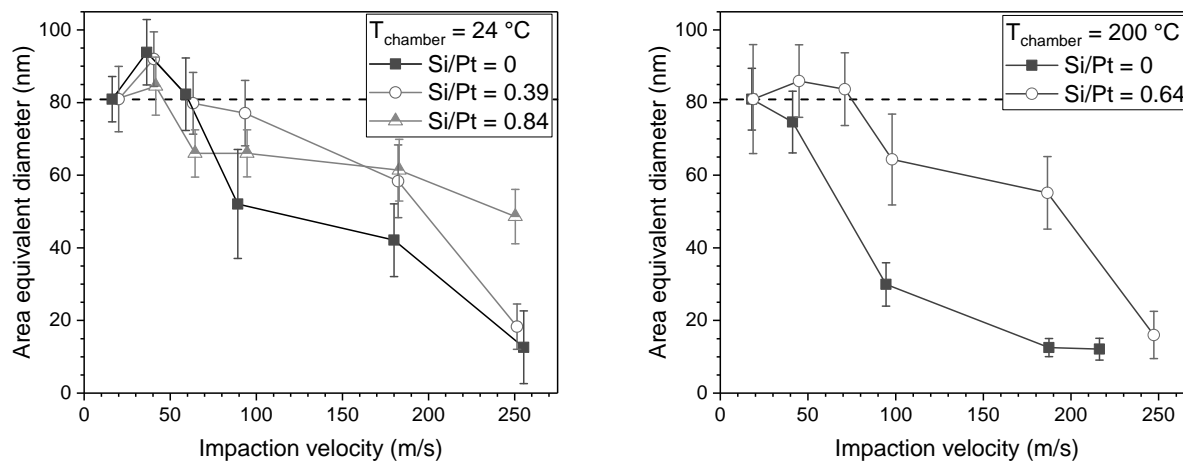


**Fig. 6.2:** Changes in the median area equivalent diameter of deposited agglomerates in dependence on the impaction velocity. (a) Particles coated with TEOS at 24 °C and (b) HMDSO-coated particles (200 °C). The coating thickness is characterized by the atomic ratio of Si to Pt. Si/Pt = 0 indicates no coating.

The comparison between the uncoated particles (Si/Pt = 0) after 4.2 min at ambient temperature (Fig. 6.2, left) and after an additional 4 s at 200 °C (Fig. 6.2, right), shows differences in the fragmentation behavior. The agglomerates not introduced into the tube

furnace (left) exhibited first an increase of the projection area with increasing velocity, before the area was reduced, while the tempered particles (right) quickly started to show a reduced area. This indicates a reduced stability of the tempered particles, which is probably related to the structural changes observed in the deposition curves (Fig. 6.1). All other particles showed at least a small increase in area equivalent diameter compared to the initial diameter. This can be explained with a flattening of agglomerate branches onto the TEM grid. The spark generated Pt agglomerates were very open structures with thin branches sticking out in all directions. On TEM samples acquired by diffusional sampling or low impaction velocities, these branches tended to remain upright and vibrated strongly under the electron beam of the TEM, which indicates a certain fragility. On samples acquired at higher impaction velocities, these branches lay flatly on the surface, and hence exhibited a higher projection area. The uncoated particles introduced into the tube furnace did not show this behavior, which again indicates structural changes.

The effects believed to lead to the observed impaction behavior of the Pt agglomerates are summarized in Fig. 6.3. The agglomerates approach the target surface with the impaction velocity (a). During the impaction event, deceleration forces strain the structures and, depending on the ratio of interparticle forces to counteracting forces, result in a deposition without structural changes, a flattening of the branches to the surface and/or a fragmentation of agglomerate parts (b). The flattening causes an increase in projection area, while fragmentation causes a decrease. Fragments of the agglomerates might either deposit on the sample grid or rebound back from the surface into the gas flow (c). In parallel to these structural effects, some agglomerates might also rebound from the surface back into the gas flow. Measurements of the particle penetration through the LPI have shown that this rebound happened in parallel to the other effects (see Publication 4).

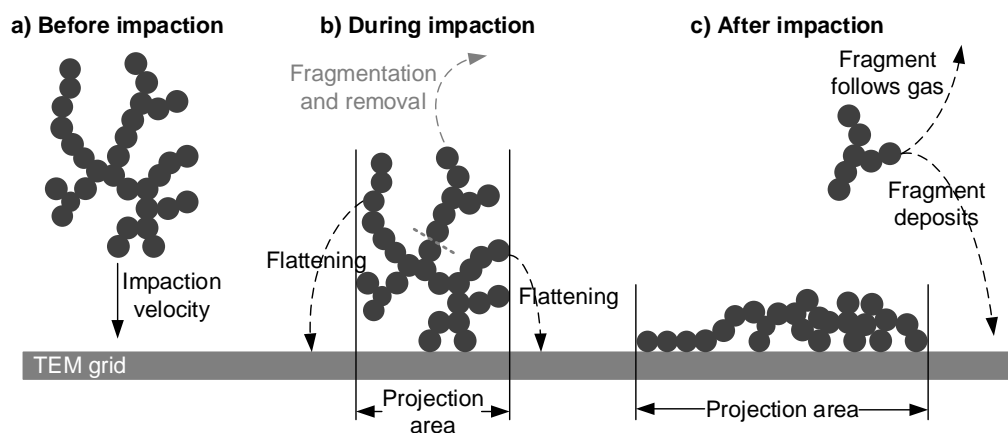


**Fig. 6.3:** Schematic visualization of the impaction behavior of nanoparticle agglomerates in the LPI.

The structural effects could be modified with the coatings, as shown for silica in Fig. 6.2 (left). With increasing coating on the particles, the first increase in equivalent diameter became less pronounced, while the subsequent decrease in diameter was smaller. This shows both a reduced restructuring of agglomerate branches to the TEM grid as well as less fragmentation at higher velocities. Hence, the coating did indeed stabilize the agglomerates against mechanical restructuring. The flattening of the branches onto the TEM grid was probably reduced because they became less flexible and the fragmentation might have been reduced due to stronger interparticle connections. These effects seemed to improve with a thicker coating ( $\text{Si/Pt} = 0.84$ ), but even the thinner coating ( $\text{Si/Pt} = 0.39$ ) reduced the fragmentation compared to the uncoated particles.

The differences between the uncoated tempered particles and the coated ones were even more prominent for the silica-organic coatings at 200 °C (Fig. 6.2, right). The coating caused a significantly reduced fragmentation that required higher velocities than the uncoated sample. Furthermore, the coated particles exhibited an increase in area equivalent diameter in the range where flattening is expected, which the uncoated did not. In fact, the HMDSO-coated particles showed a fragmentation behavior very similar to the particles at 24 °C. This fits well with the results from the deposition curves (Fig. 6.1) and indicates that the coatings hampered the temperature related structural changes.

In conclusion, it was indeed possible to improve the mechanical stability of Pt agglomerates with coatings formed in the plasma process. A direct comparison between the TEOS and HMDSO-based coating is difficult, because of several parameters being changed at the same time (e.g., precursor, coating composition, temperature). However, both types of coating clearly improved the stability during inertia impaction. Furthermore, the silica-organic coating seemed to also improve the thermal stability of the particles, which is an effect observed for silica coatings as well, as shown in the next section.

## 6.2 Improvement of the thermal stability of metal agglomerates

Metal nanoparticles such as Pd, Pt or Au can be used as catalysts. One of the main advantages of nanoscale catalyst particles over larger ones is their much higher mass specific surface area that directly influences the activity. However, such small catalyst particles are often in danger of being deactivated by multiple effects. An important one is the growth of particles due to sintering and the resulting loss in surface area [112]. This is especially relevant if the particles are used to catalyze a reaction at higher temperatures. Sintering could be prevented by encapsulating the whole catalyst particle in a shell of a more thermally stable material, such as silica. However, this would result

in a deactivation of the catalyst due to the complete coverage of the active metal surface, unless the coating were permeable for the reactants. While such a porous coating results in an improvement of the catalytic activity of certain particles at higher temperatures [18], it requires a comparatively large amount of coating material. Hence, an arguably better way to stabilize a nanoparticle would be the partial coverage of the agglomerate. In particular, parts that should have a bigger influence on the stability, such as the spaces between primary particles, need to be covered, while most of the metal surface should remain uncovered. Since the post-discharge coating process is able to produce very thin coatings that also tend to accumulate in inner particle parts, it might be promising for such applications.

As a simple example for the thermal stabilization of particles in the post-discharge process, Pt agglomerates were produced in the SDG and thermally restructured in a tube furnace between 300 and 500 °C. The particles were either introduced into the tube furnace uncoated or coated with 0.3 ppmv TEOS and 1.4 min residence time at ambient temperature (cylindrical DBD). This resulted in a very thin and incomplete coating that was focused primarily in interparticle spaces. EDX measurements showed an atomic ratio of Pt/Si = 0.22. The particles were classified with a RDMA prior to their entry into the furnace to ensure identical agglomerate sizes. The residence time in the furnace was kept constant at about 8 s (24 °C) for all particles. After the furnace, the particles were sampled onto a Lacey TEM grid and analyzed. The primary particle size was assessed with ImageJ from these TEM micrographs. As shown in Fig. 6.4, the TEM micrographs exhibit visible differences between the structures of the uncoated and coated particles. While the coated particles more or less retained their original structure, the uncoated particles sintered visibly to more compact structures. This is also apparent in the evolution of the primary particle size that was more than twice as large for the uncoated particles at 300 °C and nearly three times at 500 °C (Fig. 6.4). However, even the coated particles started to visibly restructure at 500 °C, but to a lesser degree than the uncoated ones. This is probably related to the incompleteness of the coating that allows the core material to move around the silica spots if the temperatures are high enough. Nevertheless, the results indicate that the process is capable to improve the sintering resistance of metal particles.

### 6.3 Photocatalysis effects of coated titania

Titania nanoparticles are known for their photocatalytic activity. However, in applications, where TiO<sub>2</sub> nanoparticles are used for their other properties such as their UV absorption and colorlessness (e.g., sun screens), the photocatalytic activity of the particles is unwanted and needs to be suppressed [1, 2]. This is most commonly achieved with a

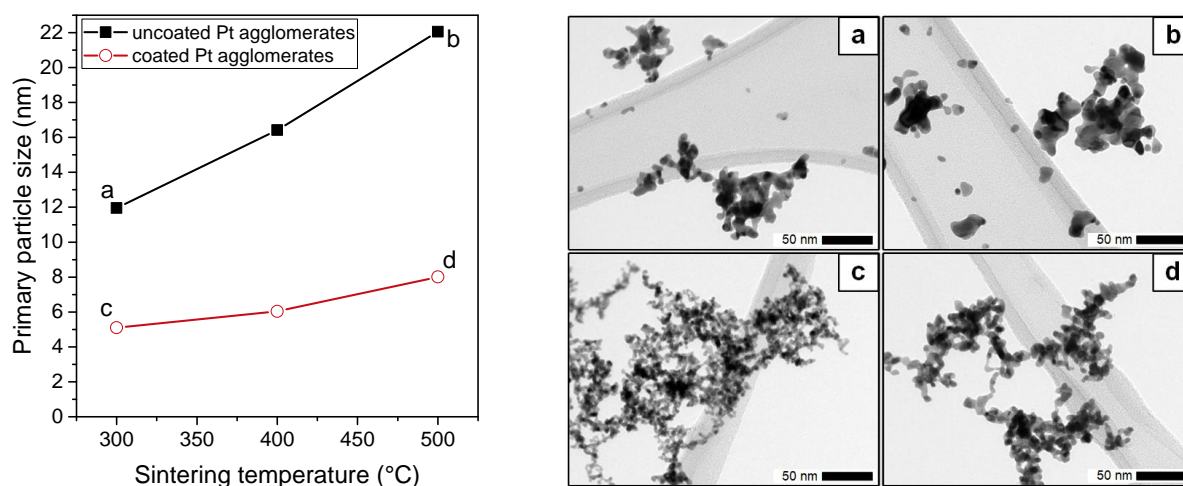


**Fig. 6.4:** Influence of silica coating on the thermal restructuring of Pt agglomerates, characterized by the primary particle size in dependence on the temperature.

coating of an inert material such as silica that acts as a barrier between the titania and the environment. The effect of the silica coating applied with the TEOS process to titania particles was shown in Publication 3.

The particles were introduced into the system with the atomizer setup (section 3.2.2) and then coated with TEOS as the precursor at either 24 or 200 °C. The powder was sampled from the system with a filter and the photocatalytic activity was quantified with the decomposition of methylene blue (MB) on  $\text{TiO}_2$  under 1 h of UV radiation. Since the small sample sizes did not allow the measurement of the temporal MB concentration, the samples were analyzed together with a reference sample of uncoated P25 at a constant radiation time. The MB concentration was measured with light absorption at 690 nm. Since the coating reduced the effective mass of titania in the sample in comparison to the reference of the same total mass, the results were corrected with the mass percentages of titania in the sample, which was acquired from EDX measurements. The results are presented as the ratio of the conversions of coated and uncoated sample in Fig. 6.5. A ratio above 1 indicates an improvement of the photocatalytic activity in the coated sample, while one below 1 indicates a decrease in activity.

The particles coated at 200 °C behaved more or less as expected. Even at a relatively low coating amount on the samples, the application of the coating reduced the activity significantly. Here, the silica seems to act as an effective barrier between the photo-generated species on the titania surfaces and the MB in the surrounding liquid. This observation fits with the TEM micrographs shown earlier in Fig. 5.5 that exhibited a relatively homogeneous coating on nearly all particles. Particles covered with thick coatings at ambient temperature also showed a decrease in activity. This also fits with TEM micrographs, where the thick coating was not very homogeneous, but nevertheless cov-

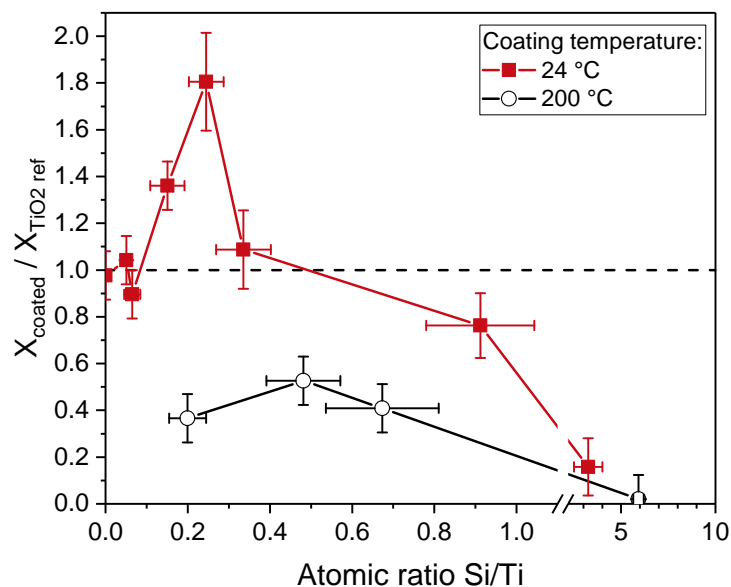


**Fig. 6.5:** Conversion of silica coated P25 titania particles in comparison to an uncoated reference and in dependence on the amount of coating.

ered all visible surfaces. However, when smaller amounts of silica were applied at 24 °C, an increase of photocatalytic activity with a maximum at about 0.2 Si:Ti atomic ratio was observed. This behavior could not be explained conclusively in this work. While the coatings at these conditions were significantly less homogeneous on TiO<sub>2</sub> than those acquired at 200 °C (Fig. 5.5), this should result in less of a reduction of activity than for the homogeneous coatings, but not in an increase. However, possible explanations can be formulated from the literature, such as a reduced recombination rate of photogenerated electron-hole pairs [113, 114], an improved adsorption rate of reactants and desorption of products [115, 116] or the formation of TiO<sub>2</sub>-SiO<sub>2</sub> mixed oxides [117], which was hinted at by the XPS measurements (section 5.1.2). In conclusion, the results shown in this section are promising, because they indicate that the coating process can be used to control the photocatalytic activity of titania particles to not only hamper photocatalysis, but also to improve it significantly (up to 80 % improvement).

# CHAPTER 7

---

## Summary and outlook

---

In this PhD thesis, a post-discharge process for the in-flight coating of nanoparticles was presented. It was operated at atmospheric pressure and low temperatures of either 24 °C or between 100 and 300 °C. A chemically reactive environment containing ozone and nitrogen oxides amongst others was created with a dielectric barrier discharge. The exhaust of the discharge reactor was mixed with different core particles and TEOS or HMDSO vapors to start the reactions. The coating took place in the so-called coating chamber, which was one of several quartz glass tubes. The chamber could be heated with a tube furnace to change the chemical environment. Even though the lab-scale setup was comparatively simple, it was possible to continuously coat virtually any particles or even produce silica particles without cores.

The feasibility of the process was demonstrated with the controlled coating of nanoparticles. The primary factor for a successful coating formation seemed to be the temperature of the discharge and the related produced species. Two distinct ways of operation could be identified, which were the coating at ambient temperature and that at elevated temperatures. It was shown that the differences between these two modes, such as the significantly shorter residence time above 100 °C, was not only a kinetic effect, but changed the coating environment. While TEOS could be used as the precursor in both modes, HMDSO required the higher temperatures to form coatings. The coating thickness on the core particles could be controlled with the initial precursor concentration, the residence time, the core particle surface area and the temperature. Especially important was the interplay of concentration and time, since this controlled whether the coatings were solidified after removal from the system. In general, the homogeneity of the coatings was found to be quite good, but it seemed to depend on the wettability of the core material with the coating or its intermediates. For the long residence times of a few minutes during the coating at ambient temperatures, a significant reduction in particle size number concentration and an accompanying shift of the size distribution to larger diameters was observed. Calculations

lations with different models indicated that this was primarily caused by agglomeration and less by losses to walls.

The process was used to realize different combinations of core particles and coating material. It was demonstrated by FTIR, XPS and EDX that the coating with TEOS as the precursor resulted in mostly inorganic silica shells, which could be applied to metals, metal oxides, salts or even polymers. While the connection of the coatings to metals seemed to be purely physical, XPS measurements indicated the formation of chemical bonds between the silica coating and titania particles in the form of Si–O–Ti mixed oxides. HMDSO could be used to modify the surface wettability of core particles to become very hydrophobic. This was related to the appearance of Si–CH<sub>x</sub> bonds in the measurements. These groups were found to be part of the silica-organic coating and could not be removed by a reduction in environmental pressure, which was possible for adsorbed by-products in the TEOS-based coatings. The hydrophobic characteristic of the coated particles could be preserved during tempering.

Finally, some applications of the coated particles were demonstrated. As shown in Publication 4, dendritic Pt agglomerates were modified with thin coatings and introduced into a low pressure impaction setup to study their fragmentation behavior during inertial impaction, which was related to the mechanical stability of the particles. It was found that both silica and silica-organic coatings improved the stability of the particles, which was apparent in a reduced restructuring of agglomerate branches and a lower degree of fragmentation. A thicker coating improved the effect, but a very thin coating already showed improvements in comparison to the uncoated particles. The coating with HMDSO at 200 °C seemed to hamper the thermal restructuring of the agglomerates, which had caused a reduced stability of the uncoated particles. The thermal stability of particles could also be improved by the coating with silica. This was shown for Pt agglomerates introduced into a tube furnace in Publication 1 and it was found that the particles with a thin coating sintered less than those without any coating. Last but not least, in Publication 3, P25 titania particles were coated with silica using TEOS at ambient and elevated temperatures and the effect of the coating on the photocatalytic activity studied. It was found that the coating at 200 °C reduced the activity even for relatively small coating thicknesses, which was related to a homogeneous coverage of almost all titania surfaces. However, coatings applied at 24 °C showed this behavior only at higher coating amounts and instead even improved the activity in some experiments. This was related to the less homogeneous coatings that left significant portions of the core particles uncovered and an interaction between the coating and the titania, resulting in improvements in adsorption or reaction behavior.

In conclusion, during this thesis, the process could be studied enough to acquire at least a basic understanding of the important process parameters that allow the formation

of a multitude of core-shell materials with some interesting applications. However, there are certain areas requiring additional work. One of the key problems with the setup was the very low amount of powder mass that could be collected for analysis. This was primarily related to the used core particle sources, but also to the way the residence time in the coating chamber was controlled, with only a part of the total aerosol even entering the chamber. Hence, the first step for further research would probably be the development of an upscaled version of the process that can produce more coated particles, since this would open up a lot of new analysis methods. This might even be accomplished in a fluidized bed reactor, similar to what is outlined in the literature. While this would obviously defeat the idea of a continuous in-flight coating, it could drastically increase the produced powder mass and furthermore simplify the control of the residence time. Certain promising effects such as the photocatalytic behavior of the coated titania particles could then be studied in much more detail.

---

## References

---

- [1] T. Egerton. “The Modification of Fine Powders by Inorganic Coatings”. In: *KONA Powder and Particle Journal* 16.0 (1998), pp. 46–59. DOI: [10.14356/kona.1998008](https://doi.org/10.14356/kona.1998008).
- [2] D. M. King et al. “Passivation of pigment-grade TiO<sub>2</sub> particles by nanothick atomic layer deposited SiO<sub>2</sub> films”. In: *Nanotechnology* 19.25 (2008), p. 255604. DOI: [10.1088/0957-4484/19/25/255604](https://doi.org/10.1088/0957-4484/19/25/255604).
- [3] R. Jansen et al. “Photoprotection”. In: *Journal of the American Academy of Dermatology* 69.6 (2013), 867.e1–867.e14. DOI: [10.1016/j.jaad.2013.08.022](https://doi.org/10.1016/j.jaad.2013.08.022).
- [4] R. Ghosh Chaudhuri and S. Paria. “Core/Shell Nanoparticles: Classes, Properties, Synthesis Mechanisms, Characterization, and Applications”. In: *Chemical Reviews* 112.4 (2012), pp. 2373–2433. DOI: [10.1021/cr100449n](https://doi.org/10.1021/cr100449n).
- [5] A. P. Weber, M. Seipenbusch, and G. Kasper. “Application of Aerosol Techniques to Study the Catalytic Formation of Methane on Gasborne Nickel Nanoparticles”. In: *The Journal of Physical Chemistry A* 105.39 (2001), pp. 8958–8963. DOI: [10.1021/jp0115594](https://doi.org/10.1021/jp0115594).
- [6] F. Massines et al. “Atmospheric Pressure Low Temperature Direct Plasma Technology: Status and Challenges for Thin Film Deposition”. In: *Plasma Processes and Polymers* 9.11-12 (2012), pp. 1041–1073. DOI: [10.1002/ppap.201200029](https://doi.org/10.1002/ppap.201200029).
- [7] J.-P. Borra et al. “Atmospheric Pressure Deposition of Thin Functional Coatings: Polymer Surface Patterning by DBD and Post-Discharge Polymerization of Liquid Vinyl Monomer from Surface Radicals”. In: *Plasma Processes and Polymers* 9.11-12 (2012), pp. 1104–1115. DOI: [10.1002/ppap.201100210](https://doi.org/10.1002/ppap.201100210).
- [8] S. E. Alexandrov and M. L. Hitchman. “Chemical Vapor Deposition Enhanced by Atmospheric Pressure Non-thermal Non-equilibrium Plasmas”. In: *Chemical Vapor Deposition* 11.11-12 (2005), pp. 457–468. DOI: [10.1002/cvde.200500026](https://doi.org/10.1002/cvde.200500026).
- [9] J.-P. Borra. “Nucleation and aerosol processing in atmospheric pressure electrical discharges: powders production, coatings and filtration”. In: *Journal of Physics D: Applied Physics* 39.2 (2006), R19–R54. DOI: [10.1088/0022-3727/39/2/R01](https://doi.org/10.1088/0022-3727/39/2/R01).
- [10] U. Kogelschatz. “Dielectric-barrier discharges: Their history, discharge physics, and industrial applications”. In: *Plasma Chemistry and Plasma Processing* 23.1 (2003), pp. 1–46. DOI: [10.1023/A:1022470901385](https://doi.org/10.1023/A:1022470901385).
- [11] K. H. Becker et al., eds. *Non-equilibrium air plasmas at atmospheric pressure*. Series in plasma physics. OCLC: ocm56807399. Bristol ; Philadelphia: Institute of Physics, 2005.
- [12] J. Meichsner et al. *Nonthermal plasma chemistry and physics*. OCLC: 945109501. 2013.
- [13] L. L. Hench and J. K. West. “The sol-gel process”. In: *Chemical Reviews* 90.1 (1990), pp. 33–72. DOI: [10.1021/cr00099a003](https://doi.org/10.1021/cr00099a003).
- [14] M. B. Gawande et al. “Core-shell nanoparticles: synthesis and applications in catalysis and electrocatalysis”. In: *Chemical Society Reviews* 44.21 (2015), pp. 7540–7590. DOI: [10.1039/C5CS00343A](https://doi.org/10.1039/C5CS00343A).
- [15] V. V. Hardikar and E. Matijević. “Coating of Nanosize Silver Particles with Silica”. In: *Journal of Colloid and Interface Science* 221.1 (2000), pp. 133–136. DOI: [10.1006/jcis.1999.6579](https://doi.org/10.1006/jcis.1999.6579).

- [16] I. A. Siddiquey et al. “Microwave-assisted silica coating and photocatalytic activities of ZnO nanoparticles”. In: *Materials Research Bulletin* 43.12 (2008), pp. 3416–3424. DOI: [10.1016/j.materresbull.2008.02.002](https://doi.org/10.1016/j.materresbull.2008.02.002).
- [17] A. M. El-Toni, S. Yin, and T. Sato. “Control of silica shell thickness and microporosity of titania–silica core–shell type nanoparticles to depress the photocatalytic activity of titania”. In: *Journal of Colloid and Interface Science* 300.1 (2006), pp. 123–130. DOI: [10.1016/j.jcis.2006.03.073](https://doi.org/10.1016/j.jcis.2006.03.073).
- [18] J.-N. Park et al. “Highly Active and Sinter-Resistant Pd-Nanoparticle Catalysts Encapsulated in Silica”. In: *Small* 4.10 (2008), pp. 1694–1697. DOI: [10.1002/smll.200800895](https://doi.org/10.1002/smll.200800895).
- [19] J. G. Croissant et al. “Mesoporous Silica and Organosilica Nanoparticles: Physical Chemistry, Biosafety, Delivery Strategies, and Biomedical Applications”. In: *Advanced Healthcare Materials* 7.4 (2018), p. 1700831. DOI: [10.1002/adhm.201700831](https://doi.org/10.1002/adhm.201700831).
- [20] H. K. Kammler, L. Mädler, and S. E. Pratsinis. “Flame Synthesis of Nanoparticles”. In: *Chemical Engineering & Technology* 24.6 (2001), pp. 583–596. DOI: [10.1002/1521-4125\(200106\)24:6<583::AID-CEAT583>3.0.CO;2-H](https://doi.org/10.1002/1521-4125(200106)24:6<583::AID-CEAT583>3.0.CO;2-H).
- [21] S. E. Pratsinis. “Flame aerosol synthesis of ceramic powders”. In: *Progress in Energy and Combustion Science* 24.3 (1998), pp. 197–219. DOI: [10.1016/S0360-1285\(97\)00028-2](https://doi.org/10.1016/S0360-1285(97)00028-2).
- [22] F. Kruis, H. Fissan, and A. Peled. “Synthesis of nanoparticles in the gas phase for electronic, optical and magnetic applications—a review”. In: *Journal of Aerosol Science* 29.5-6 (1998), pp. 511–535. DOI: [10.1016/S0021-8502\(97\)10032-5](https://doi.org/10.1016/S0021-8502(97)10032-5).
- [23] A. Teleki et al. “In Situ Coating of Flame-Made TiO<sub>2</sub> Particles with Nanothin SiO<sub>2</sub> Films”. In: *Langmuir* 24.21 (2008), pp. 12553–12558. DOI: [10.1021/la801630z](https://doi.org/10.1021/la801630z).
- [24] A. Teleki et al. “Role of Gas-Aerosol Mixing during in Situ Coating of Flame-Made Titania Particles”. In: *Industrial & Engineering Chemistry Research* 48.1 (2009), pp. 85–92. DOI: [10.1021/ie800226d](https://doi.org/10.1021/ie800226d).
- [25] F. Qi et al. “Thermostable photocatalytically active TiO<sub>2</sub> anatase nanoparticles”. In: *Journal of Nanoparticle Research* 13.3 (2011), pp. 1325–1334. DOI: [10.1007/s11051-010-0211-0](https://doi.org/10.1007/s11051-010-0211-0).
- [26] B. Buesser and S. E. Pratsinis. “Design of aerosol particle coating: Thickness, texture and efficiency”. In: *Chemical Engineering Science* 65.20 (2010), pp. 5471–5481. DOI: [10.1016/j.ces.2010.07.011](https://doi.org/10.1016/j.ces.2010.07.011).
- [27] B. Buesser and S. E. Pratsinis. “Design of Aerosol Coating Reactors: Precursor Injection”. In: *Industrial & Engineering Chemistry Research* 50.24 (2011), pp. 13831–13839. DOI: [10.1021/ie201575a](https://doi.org/10.1021/ie201575a).
- [28] C. Vahlas et al. “Principles and applications of CVD powder technology”. In: *Materials Science and Engineering: R: Reports* 53.1-2 (2006), pp. 1–72. DOI: [10.1016/j.mser.2006.05.001](https://doi.org/10.1016/j.mser.2006.05.001).
- [29] Q. H. Powell et al. “Gas-phase coating of TiO<sub>2</sub> with SiO<sub>2</sub> in a continuous flow hot-wall aerosol reactor”. In: *Journal of materials research* 12.02 (1997), pp. 552–559. DOI: [10.1557/JMR.1997.0079](https://doi.org/10.1557/JMR.1997.0079).
- [30] G. P. Fotou and T. T. Kodas. “Sequential gas-phase formation of Al<sub>2</sub>O<sub>3</sub> and SiO<sub>2</sub> layers on aerosol-made TiO<sub>2</sub> Particles”. In: *Advanced Materials* 9.5 (1997), pp. 420–423. DOI: [10.1002/adma.19970090513](https://doi.org/10.1002/adma.19970090513).
- [31] D. J. Simpson et al. “SiO<sub>2</sub> coated pure and doped titania pigments: low temperature CVD deposition and quantum chemical study”. In: *Physical Chemistry Chemical Physics* 13.47 (2011), pp. 21132–21138. DOI: [10.1039/C1CP22681A](https://doi.org/10.1039/C1CP22681A).
- [32] S. M. George. “Atomic Layer Deposition: An Overview”. In: *Chemical Reviews* 110.1 (2010), pp. 111–131. DOI: [10.1021/cr900056b](https://doi.org/10.1021/cr900056b).
- [33] A. M. Boies et al. “SiO<sub>2</sub> coating of silver nanoparticles by photoinduced chemical vapor deposition”. In: *Nanotechnology* 20.29 (2009), p. 295604. DOI: [10.1088/0957-4484/20/29/295604](https://doi.org/10.1088/0957-4484/20/29/295604).

- [34] A. M. Boies et al. “Chemical Kinetics of Photoinduced Chemical Vapor Deposition: Silica Coating of Gas-Phase Nanoparticles”. In: *The Journal of Physical Chemistry C* 116.1 (2012), pp. 104–114. DOI: [10.1021/jp2071716](https://doi.org/10.1021/jp2071716).
- [35] S. Kim and S. H. Ehrman. “Capillary Condensation onto Titania (TiO<sub>2</sub>) Nanoparticle Agglomerates”. In: *Langmuir* 23.5 (2007), pp. 2497–2504. DOI: [10.1021/la0624561](https://doi.org/10.1021/la0624561).
- [36] Y. Zhu, C. Li, and Q. Wu. “The process of coating on ultrafine particles by surface hydrolysis reaction in a fluidized bed reactor”. In: *Surface and Coatings Technology* 135.1 (2000), pp. 14–17. DOI: [10.1016/S0257-8972\(00\)00686-1](https://doi.org/10.1016/S0257-8972(00)00686-1).
- [37] K. Okuyama et al. “Gas-phase nucleation in the tetraethylorthosilicate (TEOS) / O<sub>3</sub> APCVD process”. In: *AIChE journal* 43.S11 (1997), pp. 2688–2697. DOI: [10.1002/aic.690431313](https://doi.org/10.1002/aic.690431313).
- [38] K. Fujino et al. “Silicon Dioxide Deposition by Atmospheric Pressure and Low-Temperature CVD Using TEOS and Ozone”. In: *Journal of The Electrochemical Society* 137.9 (1990), pp. 2883–2887. DOI: [10.1149/1.2087093](https://doi.org/10.1149/1.2087093).
- [39] M. Matsuura et al. “Film Characteristics of APCVD Oxide Using Organic Silicon and Ozone”. In: *Japanese Journal of Applied Physics* 30.Part 1, No. 7 (1991), pp. 1530–1538. DOI: [10.1143/JJAP.30.1530](https://doi.org/10.1143/JJAP.30.1530).
- [40] M. Adachi et al. “Gas-Phase Nucleation in an Atmospheric Pressure Chemical Vapor Deposition Process for SiO<sub>2</sub> Films Using Tetraethylorthosilicate (TEOS)”. In: *Japanese Journal of Applied Physics* 31.10A (1992), p. L1439. DOI: [10.1143/JJAP.31.L1439](https://doi.org/10.1143/JJAP.31.L1439).
- [41] M. Adachi et al. “Particle Generation and Film Formation in an Atmospheric-Pressure Chemical Vapor Deposition Reactor Using the Tetraethylorthosilicate (TEOS) / He, TEOS / O<sub>2</sub> / He, and TEOS / O<sub>3</sub> / He Systems”. In: *Japanese Journal of Applied Physics* 32.Part 2, No. 5B (1993), pp. L748–L751. DOI: [10.1143/JJAP.32.L748](https://doi.org/10.1143/JJAP.32.L748).
- [42] M. Adachi, K. Okuyama, and N. Tohge. “Particle generation and film formation in an atmospheric-pressure chemical vapour deposition process using tetraethylorthosilicate”. In: *Journal of materials science* 30.4 (1995), pp. 932–937. DOI: [10.1007/BF01178427](https://doi.org/10.1007/BF01178427).
- [43] M. Adachi et al. “Precursors in Atmospheric-Pressure Chemical Vapor Deposition of Silica Films from Tetraethylorthosilicate/Ozone System”. In: *Japanese Journal of Applied Physics* 33.Part 2, No. 3B (1994), pp. L447–L450. DOI: [10.1143/JJAP.33.L447](https://doi.org/10.1143/JJAP.33.L447).
- [44] M. Yoshimaru and T. Yoshie. “Effects of Substrate on the Growth Characteristics of Silicon Oxide Films Deposited by Atmospheric Pressure Chemical Vapor Deposition Using Si(OC<sub>2</sub>H<sub>5</sub>)<sub>4</sub> and O<sub>3</sub>”. In: *Journal of The Electrochemical Society* 145.8 (1998), pp. 2847–2853. DOI: [10.1149/1.1838724](https://doi.org/10.1149/1.1838724).
- [45] T. Kawahara, A. Yuuki, and Y. Matsui. “Reaction Mechanism of Chemical Vapor Deposition Using Tetraethylorthosilicate and Ozone at Atmospheric Pressure”. In: *Japanese Journal of Applied Physics* 31.9R (1992), p. 2925. DOI: [10.1143/JJAP.31.2925](https://doi.org/10.1143/JJAP.31.2925).
- [46] J. Arnó, Z. Yuan, and S. Murphy. “Fourier Transform Infrared Characterization of Downstream Gas-Phase Species Generated by Tetraethylorthosilicate/Ozone Atmospheric Pressure Reactions”. In: *Journal of The Electrochemical Society* 146.1 (1999), pp. 276–280. DOI: [10.1149/1.1391599](https://doi.org/10.1149/1.1391599).
- [47] T. K. Whidden and S. Y. Lee. “In situ Fourier transform infrared spectroscopy near the substrate in tetraethoxysilane/ozone chemical vapor deposition”. In: *Electrochemical and solid-state letters* 2.10 (1999), pp. 527–530. DOI: [10.1149/1.1390892](https://doi.org/10.1149/1.1390892).
- [48] S. Romet, M. F. Couturier, and T. K. Whidden. “Modeling of silicon dioxide chemical vapor deposition from tetraethoxysilane and ozone”. In: *Journal of the Electrochemical Society* 148.2 (2001), G82–G90. DOI: [10.1149/1.1342186](https://doi.org/10.1149/1.1342186).
- [49] H. Juárez et al. “Low temperature deposition: Properties of SiO<sub>2</sub> films from TEOS and ozone by APCVD system”. In: *Journal of Physics: Conference Series* 167.1 (2009), p. 012020. DOI: [10.1088/1742-6596/167/1/012020](https://doi.org/10.1088/1742-6596/167/1/012020).
- [50] J. Kim, S. Hwang, and J. Yi. “SiO<sub>2</sub> Films Deposited at Low Temperature by Using APCVD with TEOS/O<sub>3</sub> for TFT Applications”. In: *Journal of the Korean Physical Society* 49.3 (2006), pp. 1121–1125.

- [51] S. E. Alexandrov, N. McSporran, and M. L. Hitchman. “Remote AP-PECVD of Silicon Dioxide Films from Hexamethyldisiloxane (HMDSO)”. In: *Chemical Vapor Deposition* 11.11-12 (2005), pp. 481–490. DOI: [10.1002/cvde.200506385](https://doi.org/10.1002/cvde.200506385).
- [52] F. Fanelli et al. “Ar/HMDSO/O<sub>2</sub> Fed Atmospheric Pressure DBDs: Thin Film Deposition and GC-MS Investigation of By-Products”. In: *Plasma Processes and Polymers* 7.7 (2010), pp. 535–543. DOI: [10.1002/ppap.200900159](https://doi.org/10.1002/ppap.200900159).
- [53] I. Vinogradov and A. Lunk. “Film Deposition in the Dielectric Barrier Discharge at Atmospheric Pressure in He/O<sub>2</sub>/HMDSO and He/N<sub>2</sub>O/HMDSO mixtures”. In: *Plasma Processes and Polymers* 6.S1 (2009), S514–S518. DOI: [10.1002/ppap.200931102](https://doi.org/10.1002/ppap.200931102).
- [54] D. Trunec et al. “Deposition of thin organosilicon polymer films in atmospheric pressure glow discharge”. In: *Journal of Physics D: Applied Physics* 37.15 (2004), pp. 2112–2120. DOI: [10.1088/0022-3727/37/15/010](https://doi.org/10.1088/0022-3727/37/15/010).
- [55] J.-P. Borra et al. “Vaporization of bulk metals into single-digit nanoparticles by non-thermal plasma filaments in atmospheric pressure dielectric barrier discharges”. In: *Journal of Aerosol Science* 79 (2015), pp. 109–125. DOI: [10.1016/j.jaerosci.2014.09.002](https://doi.org/10.1016/j.jaerosci.2014.09.002).
- [56] J.-P. Borra et al. “Nano-droplet ejection and nucleation of materials submitted to non-thermal plasma filaments”. In: *The European Physical Journal Applied Physics* 56.2 (2011), p. 24019. DOI: [10.1051/epjap/2011110201](https://doi.org/10.1051/epjap/2011110201).
- [57] C. Bayer et al. “PECVD-Partikelbeschichtungen in einer Plasma-Wirbelschicht”. In: *Chemie Ingenieur Technik* 70.6 (1998), pp. 727–730. DOI: [10.1002/cite.330700611](https://doi.org/10.1002/cite.330700611).
- [58] H. Hody et al. “Plasma functionalization of silicon carbide crystalline nanoparticles in a novel low pressure powder reactor”. In: *Surface and Coatings Technology* 205.1 (2010), pp. 22–29. DOI: [10.1016/j.surfcoat.2010.05.045](https://doi.org/10.1016/j.surfcoat.2010.05.045).
- [59] K. Tsugeki et al. “Silica coating of aluminium nitride particles by radio-frequency plasma chemical vapour deposition”. In: *Journal of Materials Science Letters* 13.1 (1994), pp. 43–45. DOI: [10.1007/BF00680269](https://doi.org/10.1007/BF00680269).
- [60] D. Shi et al. “Uniform deposition of ultrathin polymer films on the surfaces of Al<sub>2</sub>O<sub>3</sub> nanoparticles by a plasma treatment”. In: *Applied Physics Letters* 78.9 (2001), pp. 1243–1245. DOI: [10.1063/1.1352700](https://doi.org/10.1063/1.1352700).
- [61] D. Shi et al. “Plasma deposition of Ultrathin polymer films on carbon nanotubes”. In: *Applied Physics Letters* 81.27 (2002), pp. 5216–5218. DOI: [10.1063/1.1527702](https://doi.org/10.1063/1.1527702).
- [62] A. U. Oksuz et al. “Plasma Nanocoating of Thiophene onto TiO<sub>2</sub> Nanoparticles”. In: *Industrial & Engineering Chemistry Research* 52.19 (2013), pp. 6610–6616. DOI: [10.1021/ie303176j](https://doi.org/10.1021/ie303176j).
- [63] T. Mori et al. “Development of silica coating methods for powdered pigments with atmospheric pressure glow plasma”. In: *Thin solid films* 316.1 (1998), pp. 89–92. DOI: [10.1016/S0040-6090\(98\)00395-2](https://doi.org/10.1016/S0040-6090(98)00395-2).
- [64] M. Kogoma, K. Tanaka, and A. Takeda. “Powder Treatments using Atmospheric Pressure Glow Plasma (Silica Coating of TiO<sub>2</sub> Fine Powder)”. In: *Journal of Photopolymer Science and Technology* 18.2 (2005), pp. 277–280. DOI: [10.2494/photopolymer.18.277](https://doi.org/10.2494/photopolymer.18.277).
- [65] S. H. Jung et al. “Surface Modification of Fine Powders by Atmospheric Pressure Plasma in a Circulating Fluidized Bed Reactor”. In: *Industrial & Engineering Chemistry Research* 43.18 (2004), pp. 5483–5488. DOI: [10.1021/ie034216w](https://doi.org/10.1021/ie034216w).
- [66] M. Karches, C. Bayer, and P. Rudolf von Rohr. “A circulating fluidised bed for plasma-enhanced chemical vapor deposition on powders at low temperatures”. In: *Surface and Coatings Technology* 116-119 (1999), pp. 879–885. DOI: [10.1016/S0257-8972\(99\)00194-2](https://doi.org/10.1016/S0257-8972(99)00194-2).
- [67] H. Caquineau et al. “Low temperature silicon oxide deposition on polymer powders in a fluidized bed coupled to a cold remote plasma”. In: *Surface and Coatings Technology* 206.23 (2012), pp. 4814–4821. DOI: [10.1016/j.surfcoat.2012.04.091](https://doi.org/10.1016/j.surfcoat.2012.04.091).
- [68] W. He et al. “Polymer coating on the surface of zirconia nanoparticles by inductively coupled plasma polymerization”. In: *Applied Physics Letters* 85.6 (2004), pp. 896–898. DOI: [10.1063/1.1778470](https://doi.org/10.1063/1.1778470).

- [69] V. Brueser, M. Hahnel, and H. Kersten. “Thin film deposition on powder surfaces using atmospheric pressure discharge”. In: *New Vistas in Dusty Plasmas*. Vol. 799. Citeseer, 2005, pp. 343–346.
- [70] S. Dahle et al. “Silicon Dioxide Coating of Titanium Dioxide Nanoparticles from Dielectric Barrier Discharge in a Gaseous Mixture of Silane and Nitrogen”. In: *Plasma Chemistry and Plasma Processing* 33.5 (2013), pp. 839–853. DOI: [10.1007/s11090-013-9472-6](https://doi.org/10.1007/s11090-013-9472-6).
- [71] J. C. Shearer et al. “Composite SiO<sub>2</sub>/TiO<sub>2</sub> and amine polymer/TiO<sub>2</sub> nanoparticles produced using plasma-enhanced chemical vapor deposition”. In: *Applied Surface Science* 256.7 (2010), pp. 2081–2091. DOI: [10.1016/j.apsusc.2009.09.052](https://doi.org/10.1016/j.apsusc.2009.09.052).
- [72] A. Kouprine et al. “Polymer-like C: H thin film coating of nanopowders in capacitively coupled RF discharge”. In: *Plasma chemistry and plasma processing* 24.2 (2004), pp. 189–215. DOI: [10.1023/B:PCPP.0000013198.39742.38](https://doi.org/10.1023/B:PCPP.0000013198.39742.38).
- [73] J. Tavares, E. J. Swanson, and S. Coulombe. “Plasma Synthesis of Coated Metal Nanoparticles with Surface Properties Tailored for Dispersion”. In: *Plasma Processes and Polymers* 5.8 (2008), pp. 759–769. DOI: [10.1002/ppap.200800074](https://doi.org/10.1002/ppap.200800074).
- [74] E. Marino et al. “Synthesis and coating of copper oxide nanoparticles using atmospheric pressure plasmas”. In: *Surface and Coatings Technology* 201.22-23 (2007), pp. 9205–9208. DOI: [10.1016/j.surfcoat.2007.04.091](https://doi.org/10.1016/j.surfcoat.2007.04.091).
- [75] H. Lei et al. “In situ encapsulation of copper nanoparticles by the dielectric barrier discharge”. In: *Applied Physics Letters* 91.11 (2007), p. 113119. DOI: [10.1063/1.2785950](https://doi.org/10.1063/1.2785950).
- [76] V. Vons, Y. Creighton, and A. Schmidt-Ott. “Nanoparticle production using atmospheric pressure cold plasma”. In: *Journal of Nanoparticle Research* 8.5 (2006), pp. 721–728. DOI: [10.1007/s11051-006-9133-2](https://doi.org/10.1007/s11051-006-9133-2).
- [77] D. Vollath and D. V. Szabo. “Coated nanoparticles: a new way to improved nanocomposites”. In: *Journal of Nanoparticle Research* 1.2 (1999), pp. 235–242. DOI: [10.1023/A:1010060701507](https://doi.org/10.1023/A:1010060701507).
- [78] D. Vollath and D. V. Szabó. “The Microwave plasma process – a versatile process to synthesise nanoparticulate materials”. In: *Journal of Nanoparticle Research* 8.3-4 (2006), pp. 417–428. DOI: [10.1007/s11051-005-9014-0](https://doi.org/10.1007/s11051-005-9014-0).
- [79] A. Münzer et al. “Inline coating of silicon nanoparticles in a plasma reactor: Reactor design, simulation and experiment”. In: *Materials Today: Proceedings*. 7th NRW Nano-Conference 4 (2017), S118–S127. DOI: [10.1016/j.matpr.2017.09.176](https://doi.org/10.1016/j.matpr.2017.09.176).
- [80] C. Nessim. “Surface modification of powders using dielectric barrier discharges”. PhD thesis. Sherbrooke: Université de Sherbrooke, 2008.
- [81] C. Nessim, M. Boulos, and U. Kogelschatz. “In-flight coating of nanoparticles in atmospheric-pressure DBD torch plasmas”. In: *The European Physical Journal Applied Physics* 47.2 (2009), p. 22819. DOI: [10.1051/epjap/2009076](https://doi.org/10.1051/epjap/2009076).
- [82] N. S. Tabrizi et al. “Generation of nanoparticles by spark discharge”. In: *Journal of Nanoparticle Research* 11.2 (2009), pp. 315–332. DOI: [10.1007/s11051-008-9407-y](https://doi.org/10.1007/s11051-008-9407-y).
- [83] B. O. Meuller et al. “Review of Spark Discharge Generators for Production of Nanoparticle Aerosols”. In: *Aerosol Science and Technology* 46.11 (2012), pp. 1256–1270. DOI: [10.1080/02786826.2012.705448](https://doi.org/10.1080/02786826.2012.705448).
- [84] W. C. Hinds. *Aerosol technology: properties, behavior, and measurement of airborne particles*. 2nd ed. New York: Wiley, 1999.
- [85] K. Okuyama et al. “Production of ultrafine metal oxide aerosol particles by thermal decomposition of metal alkoxide vapors”. In: *AIChE Journal* 32.12 (1986), pp. 2010–2019. DOI: [10.1002/aic.690321211](https://doi.org/10.1002/aic.690321211).
- [86] O. L. Flaningam. “Vapor pressures of poly(dimethylsiloxane) oligomers”. In: *Journal of Chemical & Engineering Data* 31.3 (1986), pp. 266–272. DOI: [10.1021/je00045a002](https://doi.org/10.1021/je00045a002).
- [87] P. Larkin. *Infrared and raman spectroscopy: principles and spectral interpretation*. Amsterdam ; Boston: Elsevier, 2011.

- [88] J. Soria et al. “FTIR and NMR Study of the Adsorbed Water on Nanocrystalline Anatase”. In: *The Journal of Physical Chemistry C* 111.28 (2007), pp. 10590–10596. DOI: [10.1021/jp071440g](https://doi.org/10.1021/jp071440g).
- [89] M. Moravej and R. F. Hicks. “Atmospheric Plasma Deposition of Coatings Using a Capacitive Discharge Source”. In: *Chemical Vapor Deposition* 11.11-12 (2005), pp. 469–476. DOI: [10.1002/cvde.200400022](https://doi.org/10.1002/cvde.200400022).
- [90] F. Massines et al. “Atmospheric pressure plasma deposition of thin films by Townsend dielectric barrier discharge”. In: *Surface and Coatings Technology* 200.5-6 (2005), pp. 1855–1861. DOI: [10.1016/j.surfcoat.2005.08.010](https://doi.org/10.1016/j.surfcoat.2005.08.010).
- [91] G. M. Sverdrup, C. W. Spicer, and G. F. Ward. “Investigation of the gas phase reaction of dinitrogen pentoxide with water vapor”. In: *International Journal of Chemical Kinetics* 19.3 (1987), pp. 191–205. DOI: [10.1002/kin.550190304](https://doi.org/10.1002/kin.550190304).
- [92] S. W. Benson and A. E. Axworthy. “Mechanism of the Gas Phase, Thermal Decomposition of Ozone”. In: *The Journal of Chemical Physics* 26.6 (1957), pp. 1718–1726. DOI: [10.1063/1.1743610](https://doi.org/10.1063/1.1743610).
- [93] C.-Y. Wu and P. Biswas. “Particle Growth by Condensation in a System with Limited Vapor”. In: *Aerosol Science and Technology* 28.1 (1998), pp. 1–20. DOI: [10.1080/02786829808965508](https://doi.org/10.1080/02786829808965508).
- [94] P. G. Gormley and M. Kennedy. “Diffusion from a Stream Flowing through a Cylindrical Tube”. In: *Proceedings of the Royal Irish Academy. Section A: Mathematical and Physical Sciences* 52 (1949), pp. 163–169.
- [95] K. W. Bewig and W. A. Zisman. “The wetting of gold and platinum by water”. In: *The Journal of Physical Chemistry* 69.12 (1965), pp. 4238–4242. DOI: [10.1021/j100782a029](https://doi.org/10.1021/j100782a029).
- [96] B. Miljevic et al. “Restructuring of carbonaceous particles upon exposure to organic and water vapours”. In: *Journal of Aerosol Science* 47 (2012), pp. 48–57. DOI: [10.1016/j.jaerosci.2011.12.005](https://doi.org/10.1016/j.jaerosci.2011.12.005).
- [97] D. Trunec et al. “Deposition of hard thin films from HMDSO in atmospheric pressure dielectric barrier discharge”. In: *Journal of Physics D: Applied Physics* 43.22 (2010), p. 225403. DOI: [10.1088/0022-3727/43/22/225403](https://doi.org/10.1088/0022-3727/43/22/225403).
- [98] S.-Y. Lee and S.-J. Park. “TiO<sub>2</sub> photocatalyst for water treatment applications”. In: *Journal of Industrial and Engineering Chemistry* 19.6 (2013), pp. 1761–1769. DOI: [10.1016/j.jiec.2013.07.012](https://doi.org/10.1016/j.jiec.2013.07.012).
- [99] K. Nakata and A. Fujishima. “TiO<sub>2</sub> photocatalysis: Design and applications”. In: *Journal of Photochemistry and Photobiology C: Photochemistry Reviews* 13.3 (2012), pp. 169–189. DOI: [10.1016/j.jphotochemrev.2012.06.001](https://doi.org/10.1016/j.jphotochemrev.2012.06.001).
- [100] S. Lee et al. “Plasma-Deposited SiO<sub>x</sub>CyHz Barrier Coatings for Organic Device Encapsulation”. In: *Japanese Journal of Applied Physics* 52.7R (2013), p. 076001. DOI: [10.7567/JJAP.52.076001](https://doi.org/10.7567/JJAP.52.076001).
- [101] R. Reuter et al. “The Role of Oxygen and Surface Reactions in the Deposition of Silicon Oxide like Films from HMDSO at Atmospheric Pressure”. In: *Plasma Processes and Polymers* 9.11-12 (2012), pp. 1116–1124. DOI: [10.1002/ppap.201100146](https://doi.org/10.1002/ppap.201100146).
- [102] B. Akhavan, K. Jarvis, and P. Majewski. “Hydrophobic Plasma Polymer Coated Silica Particles for Petroleum Hydrocarbon Removal”. In: *ACS Applied Materials & Interfaces* 5.17 (2013), pp. 8563–8571. DOI: [10.1021/am4020154](https://doi.org/10.1021/am4020154).
- [103] A. Voss and W. H. Finlay. “Deagglomeration of dry powder pharmaceutical aerosols”. In: *International journal of pharmaceuticals* 248.1-2 (2002), pp. 39–50. DOI: [10.1016/S0378-5173\(02\)00319-8](https://doi.org/10.1016/S0378-5173(02)00319-8).
- [104] H. S. Guraya and C. James. “Deagglomeration of Rice Starch-Protein Aggregates by High-Pressure Homogenization”. In: *Starch - Stärke* 54.3-4 (2002), pp. 108–116. DOI: [10.1002/1521-379X\(200204\)54:3/4<108::AID-STAR108>3.0.CO;2-2](https://doi.org/10.1002/1521-379X(200204)54:3/4<108::AID-STAR108>3.0.CO;2-2).
- [105] H. Teisala et al. “Development of superhydrophobic coating on paperboard surface using the Liquid Flame Spray”. In: *Surface and Coatings Technology* 205.2 (2010), pp. 436–445. DOI: [10.1016/j.surfcoat.2010.07.003](https://doi.org/10.1016/j.surfcoat.2010.07.003).

- [106] M. Stepien et al. “Wear resistance of nanoparticle coatings on paperboard”. In: *Wear* 307.1-2 (2013), pp. 112–118. DOI: [10.1016/j.wear.2013.08.022](https://doi.org/10.1016/j.wear.2013.08.022).
- [107] M. Gensch and A. P. Weber. “Fragmentierung von gasgetragenen Nanopartikel-Agglomeraten bei schräger Impaktion”. In: *Chemie Ingenieur Technik* 86.3 (2014), pp. 270–279. DOI: [10.1002/cite.201300134](https://doi.org/10.1002/cite.201300134).
- [108] S. Froeschke et al. “Impact fragmentation of nanoparticle agglomerates”. In: *Journal of Aerosol Science* 34.3 (2003), pp. 275–287. DOI: [10.1016/S0021-8502\(02\)00185-4](https://doi.org/10.1016/S0021-8502(02)00185-4).
- [109] M. Ihalainen et al. “Break-Up and Bounce of TiO<sub>2</sub> Agglomerates by Impaction”. In: *Aerosol Science and Technology* 48.1 (2014), pp. 31–41. DOI: [10.1080/02786826.2013.852155](https://doi.org/10.1080/02786826.2013.852155).
- [110] M. Seipenbusch et al. “Interparticle forces in silica nanoparticle agglomerates”. In: *Journal of Nanoparticle Research* 12.6 (2010), pp. 2037–2044. DOI: [10.1007/s11051-009-9760-5](https://doi.org/10.1007/s11051-009-9760-5).
- [111] S. Rennecke and A. Weber. “A novel model for the determination of nanoparticle impact velocity in low pressure impactors”. In: *Journal of Aerosol Science* 55 (2013), pp. 89–103. DOI: [10.1016/j.jaerosci.2012.07.014](https://doi.org/10.1016/j.jaerosci.2012.07.014).
- [112] P. Albers, J. Pietsch, and S. F. Parker. “Poisoning and deactivation of palladium catalysts”. In: *Journal of Molecular Catalysis A: Chemical* 173.1-2 (2001), pp. 275–286. DOI: [10.1016/S1381-1169\(01\)00154-6](https://doi.org/10.1016/S1381-1169(01)00154-6).
- [113] S. Hu, F. Li, and Z. Fan. “Preparation of SiO<sub>2</sub>-Coated TiO<sub>2</sub> Composite Materials with Enhanced Photocatalytic Activity Under UV Light”. In: *Bulletin of the Korean Chemical Society* 33.6 (2012), pp. 1895–1899. DOI: [10.5012/bkcs.2012.33.6.1895](https://doi.org/10.5012/bkcs.2012.33.6.1895).
- [114] T. Gholami et al. “Photocatalytic degradation of methylene blue on TiO<sub>2</sub>@SiO<sub>2</sub> core/shell nanoparticles: synthesis and characterization”. In: *Journal of Materials Science: Materials in Electronics* 26.8 (2015), pp. 6170–6177. DOI: [10.1007/s10854-015-3198-6](https://doi.org/10.1007/s10854-015-3198-6).
- [115] C. Minero, F. Catozzo, and E. Pelizzetti. “Role of adsorption in photocatalyzed reactions of organic molecules in aqueous titania suspensions”. In: *Langmuir* 8.2 (1992), pp. 481–486. DOI: [10.1021/la00038a029](https://doi.org/10.1021/la00038a029).
- [116] M. Nussbaum and Y. Paz. “Ultra-thin SiO<sub>2</sub> layers on TiO<sub>2</sub>: improved photocatalysis by enhancing products’ desorption”. In: *Physical Chemistry Chemical Physics* 14.10 (2012), p. 3392. DOI: [10.1039/c2cp23202b](https://doi.org/10.1039/c2cp23202b).
- [117] X. Gao and I. E. Wachs. “Titania–silica as catalysts: molecular structural characteristics and physico-chemical properties”. In: *Catalysis Today* 51.2 (1999), pp. 233–254. DOI: [10.1016/S0920-5861\(99\)00048-6](https://doi.org/10.1016/S0920-5861(99)00048-6).